COMPUTATIONAL MODELING OF THE IL-4 PATHWAY TO UNDERSTAND PRINCIPLES OF SYSTEMIC REDOX REGULATION IN CELL SIGNALING

A Thesis
Presented to
The Academic Faculty

by

Gaurav Dwivedi

In Partial Fulfillment
of the Requirements for the Degree
Doctor of Philosophy in the
Department of Biomedical Engineering

Georgia Institute of Technology
May 2014

COMPUTATIONAL MODELING OF THE IL-4 PATHWAY TO UNDERSTAND PRINCIPLES OF SYSTEMIC REDOX REGULATION IN CELL SIGNALING

Approved by:

Melissa L. Kemp, Advisor
Department of Biomedical Engineering
Georgia Institute of Technology

Jeffrey Skolnick
School of Biology
Georgia Institute of Technology

Eberhard O. Voit
Department of Biomedical Engineering
Georgia Institute of Technology

Manu O. Platt
Department of Biomedical Engineering
Georgia Institute of Technology

Gregory C. Gibson
School of Biology
Georgia Institute of Technology

Date Approved: March 6, 2014

I dedicate this dissertation to my parents, who are my inpiration, and to my grandfather, who still teaches me the meaning of curiosity.

ACKNOWLEDGEMENTS

I must foremost acknowledge the immense debt of gratitude I owe to my PhD advisor, Dr. Melissa L. Kemp. Not only has Melissa successfully guided me towards accomplishing this work, but she has done it in a way that now defines the meaning of guidance to me. In the several years of my association with Melissa, she has always managed to point me in the right direction without feeling the need to sermonize and without ever losing her extremely pleasant demeanor. Melissa has the ability to lead by setting the right examples and inspires great trust as a leader and mentor. It is because of this trust that I have had little hesitation in seeking her help at times of difficulty within or outside the lab, and in return I have invariably found unreserved support and confidence. Even though Melissa's scientific aptitude and knowledge far exceed my limited abilities, I am truly grateful for her willingness and patience in letting me bumble along with my sometimes silly ideas and then gently nudging me on to the right path just before I strayed too far. Melissa's genuine concern for the well-being and advancement of her students, the respect she accords to them, the readiness she shows in giving credit where it is due, and the creative and intellectual freedom she carefully inculcates in her trainees are only some of the factors that make her a great mentor. I feel very fortunate to have had the chance to work with Melissa. I will think myself even more fortunate if I have succeeded at imbibing even a small fraction of all that she has tried to teach me.

It would have been very difficult, indeed impossible, to finish a large portion of this work without the company and help of my talented peers in the Kemp lab. I would like to thank Catherine Rivet for being a wonderful friend and for inspiring me with her dazzling brilliance at everything she did. To me the lab lost a lot of its joy when she graduated. I thank Linda Kippner for teaching me the ways of the wet-lab, for allowing me to often

interrupt her work with my demands for stuff and for taking time out of her research to make sure those demands were met in time. By laughing at all my unfunny jokes Linda has always acted as a great morale booster and I thank her for that. During my time in the group I have had the opportunity to work and interact with a group of immensely gifted individuals. Maggie's eye for scientific detail and her ability to connect with people, Saheli's perseverance and Pritha's erudition are great examples for me to emulate. I have come to associate Adam with a well thought out and methodical way of working, Ariel with the ability to learn a lot very quickly, Nnenna with a pragmatic and confident attitude, Doug with prodigious programming skills and white dogs, and young Chad with his tongue-in-cheek humor. My lab mates have saved me a lot of time and embarrassment by complementing my insufficiencies and have been great founts of inspiration throughout my time in the lab. I thank them for everything and hope that my long association with them has allowed some of their abilities to silently seep into me.

I would like to thank Dr. Greg Gibson, Dr. Manu Platt, Dr. Jeffrey Skolnick and Dr. Eberhard Voit for being on my PhD thesis committee and for their insightful suggestions that greatly helped to improve the quality of my work. I also thank Dr. Voit for his wonderful book that inspired and taught me to think about biology in a quantitative way. I thank Dr. Mark Borodovsky for his valuable advice, for his immeasurable patience in dealing with me, and for graciously facilitating my progress through the Bioinformatics PhD program.

The support of my family has been indispensable in my journey towards the PhD degree. With their intellect and scholarship, both my parents have always been great examples for me to follow in my academic endeavors. It is also their example that made the decision to pursue a PhD appear extremely natural and obvious to me. Their unstinting support has allowed me to focus on my graduate studies without having to worry about numerous other issues of life. All my attempts to thank my parents can never match their love and generosity. I thank my sister, Aayushi, for the really enjoyable online sessions of Scrabble

and trivia. Although I first introduced her to Harry Potter, she is also now my ultimate resource of Potter-lore and has helped settle many arguments with her deep knowledge. I thank my sister for her affection and also for acting in both our steads at home while I have been away. I thank my girlfriend, Srishti, whose care and devotion gave me the ability to carry on with my work, especially at times of increased stress. By placing more faith in my abilities than I ever could myself, she has many a time restored my flagging confidence. Her company and friendship have made the experience a lot more easy and enjoyable than it would have been otherwise.

TABLE OF CONTENTS

LIST OF TABLES

LIST OF FIGURES

LIST OF SYMBOLS OR ABBREVIATIONS

ATM Ataxia telangiectasia mutated protein kinase.

CHX Cycloheximide.

CM-H_2DCFDA Carboxymethyl dichlorofluorescein diacetate.

CMA Covariance matrix adaptation.

DCF Dichlorofluorescein diacetate.

DPI Diphenyleneiodonium chloride.

DUOX Dual oxidase.

DUSP Dual specificiy phosphatase.

EGFR Epidermal growth factor receptor.

Epo Erythropoietin.

EpoR Erythropoietin receptor.

ERK Extracellular signal-regulated kinase.

ES Evolutionary strategy.

ES-HM Evolutionary strategy with hyper-mutation.

γC Common gamma chain.

Grx Glutaredoxin.

GSH Glutathione.

HLE B3 Human lens epithelial B3 cell line.

HRG Heregulin.

IL-4 Interleukin-4.

IL-4R Interleukin-4 receptor.

ITIM Immunoreceptor tyrosine-based inhibitory motif.

JAK Janus kinase.

MAPK Mitogen activated protein kinase.

MAPKK MAPK kinase.

MAPKKK MAPKK kinase.

MC Monte Carlo.

MEK MAPK/Erk kinase.

MFI Mean fluorescence intensity.

MKP3 MAP kinase phosphatase 3.

NADPH Nicotinamide adenine dinucleotide phosphate (reduced).

NOX NADPH oxidase.

ODE Ordinary differential equations.

PDGF Platelet-derived growth factor.

PTP Protein tyrosine phosphatase.

ROS Reactive oxygen species.

SHP-2 Src homology domain containing PTP 2.

SOCS Suppressor of cytokine signaling.

SOD Superoxide dismutase.

STAT Signal transducer and activator of signaling.

TCPTP T cell protein tyrosine phosphatase.

Trx Thioredoxin.

T_H2 Type 2 helper T cells.

LIST OF LISTINGS

SUMMARY

Elevated levels of reactive oxygen species (ROS) cause or aggravate a variety of pathological conditions such as cardiovascular disease, cancer and rheumatoid arthritis. Despite known links between oxidative stress and disease, years of clinical studies have failed to show clear benefits of antioxidant therapy. It is now recognized that ROS such as hydrogen peroxide can act as signaling molecules and are required for physiological functioning of a number of signaling pathways. Therefore, a mechanistic basis of ROS-mediated regulation of cell signaling must be established to enable rational design of antioxidant-based therapies.

The challenges in quantification of transient changes mediated by ROS during cell signaling have impeded investigation of redox-regulated signaling. In the present work, computational modeling is used to circumvent these technical challenges and to test competing hypotheses of redox regulation. Using a quantitative, systems level approach to study interactions between ROS dependent and independent regulatory mechanisms, the most comprehensive model of the IL-4 signaling pathway to date has been developed and validated with experimental data. The model is capable of predicting kinase phosphorylation dynamics under new oxidative conditions, and our analyses suggest that reversible oxidation of tyrosine phosphatases is the primary mechanism of redox regulation in this pathway. Additional computational methods have been developed to study ROS as mediators of crosstalk between signaling pathways, to optimize model parameters, and to interrogate model dynamics for the purpose of model selection. Collectively, these modeling tools provide a new systems-level perspective for investigating reversible protein oxidation as a means of control over cellular signal transduction.

CHAPTER I

INTRODUCTION

Even though it is recognized that reactive oxygen species (ROS) can regulate intracellular signaling in both health and disease [23], the details of this regulation remain to be determined. Binding of several types of extracellular ligands to their receptors can lead to enzymatic production of ROS. A pertinent example is IL-4, a cytokine that transduces its signal through the JAK/STAT pathway [130, 97]. The ability of ROS to influence the course of cell signaling arises from their potential to oxidize thiol groups in cysteine residues of proteins, leading to altered protein properties [62]. Several classes of proteins, including kinases and phosphatases, have been identified as targets for reversible oxidation by ROS with different sensitivities to oxidation [111]. Although several hypotheses are proposed to explain ROS modulated signaling, their relative importance and systemic consequences remain to be determined.

Technical limitations of experimental methods in reliably and sensitively measuring ROS and their effects in cells have been an impediment in evolving a systemic framework of redox signaling. Even though experimental methods for quantifying intracellular ROS and oxidation of proteins are quickly developing, quantitative measurement of oxidative changes in proteins remains a challenge [166, 104, 43]. The present work circumvents these limitations of experimental techniques with the help of computational modeling based on experimental data that can be reliably acquired, even though such data may not be directly indicative of oxidative modifications of proteins. This work addresses the lack of systems level understanding of redox signaling and helps establish principles of ROS-mediated regulation of signal transduction.

1.1 Research objective and specific aims

The overall *objective* of this study is to develop a systems level understanding of ROS-mediated regulatory mechanisms in signal transduction using the IL-4 pathway as a model signaling system. The overarching *hypothesis* of this dissertation is that *in the absence of direct measurements on all redox regulatory mechanisms operating in IL-4 signaling, computational modeling can be used to infer the importance of postulated mechanisms and to discover the principles of redox regulation in the signaling pathway*. Computational modeling and experimental methods are used in synergy towards the following specific aims.

Aim 1. Develop a systems model of redox regulation in the IL-4 signaling pathway. The working hypothesis for this aim is that redox sensitivities at different points in a signaling network produce non-identical effects, and interactions between redox sensitive and redox independent mechanisms determine the systemic outcome. This hypothesis is first tested using a computational model of the mitogen activated protein kinase (MAPK) pathway with ROS dependent and independent regulatory mechanisms built into it [30]. Hypothetical scenarios with alternative regulatory mechanisms are explored using mathematical models. The results suggest that the interplay of ROS dependent and independent mechanisms is crucial in determining signaling dynamics (Chapter 2).

Computational modeling is next used to examine putative redox regulatory mechanisms in the IL-4 pathway (Chapter 3). Time series data on feasibly measurable components of the IL-4 signaling system have been acquired. The data are used to test alternative models of redox regulation and the primary mode of redox regulation in the IL-4 pathway is identified. The most comprehensive model of IL-4 signaling as yet has been developed and validated as part of this aim.

Aim 2. Develop an optimization algorithm to estimate parameters of the IL-4 model. Since the model envisaged under aim 1 is novel by including mechanisms of regulation not studied before, a number of parameters of the model are not available in the

literature. To estimate such parameters an optimization algorithm based on evolutionary strategies (ES) has been designed and implemented. The purpose of this aim is to improve the optimum searching capabilities of ES (Chapter 4). A variant of ES called ES-HM (ES with hyper-mutation) has been developed to accomplish this aim, and the algorithm was used to estimate the parameters of the IL-4 pathway model. This algorithm can be applied more generally to other parameter estimation problems in systems biology models.

Aim 3. Study ROS mediated crosstalk of IL-4 pathway with other cytokine signaling pathways. The working hypothesis for this aim is that the non-specificity of ROS enables them to act as integrators of otherwise distinct signaling modules. Crosstalk between IL-4 and erythropoietin (Epo) pathways is studied using theoretical tools previously developed to study degeneracy in biological networks represented by differential systems [78]. The ability of ROS to integrate separate signaling modules is examined and functional consequences of this potential function of ROS are discussed (Chapter 5).

1.2 Motivation and significance

Aerobic life forms require molecular oxygen (O_2) as the ultimate electron acceptor in the process of generating energy from nutrients. A side effect of mitochondrial respiration is the low-level flux of reactive derivatives of O_2 known as reactive oxygen species (ROS), generated because the electron transport chain may allow "leakage" of electrons to oxygen [146]. One electron reduction of O_2 generates the superoxide anion radical ($O_2^{-\bullet}$) which can be converted to other forms of ROS through a series of reactions. Dismutation of superoxide, which may be spontaneous or catalyzed by superoxide dismutase (SOD) converts the radical into O_2 and hydrogen peroxide (H_2O_2). H_2O_2 is an uncharged molecule and is not a highly active ROS. However, reaction of H_2O_2 with transition metal ions can generate the hydroxyl radical ($^\bullet OH$), which is a very strong oxidizing agent [29]. Other reactive radical and non-radical forms such as hydroperoxyl ($HO_2^\bullet$) and hypochlorous acid (HOCl) may also be generated. Uncontrolled levels of these oxidants can be toxic to the cell because

of their reactivity with DNA, proteins, lipids and carbohydrates [23]. Antioxidant enzymes like catalases, SODs and peroxidases have evolved to keep the toxic effects of ROS under control.

Oxidative stress is defined as a condition in which ROS generation overwhelms the antioxidant machinery of the cell and can lead to damage of cellular components. Oxidative stress is known to be linked with a number of diseases including cancer, cardiovascular diseases, rheumatoid arthritis and neurological disorders [114, 92, 160, 60]. Clearly established association between oxidative stress and disease states, combined with some early studies showing inverse relation between dietary consumption of antioxidants and heart disease [37, 54] garnered support for the use of antioxidants as therapeutic agents with potential to prevent or cure these diseases. However, to date, results from a number of clinical studies using various types (e.g., vitamin E, vitamin C, β-carotene), combinations and doses of antioxidants have not shown clear benefits in terms of primary or secondary prevention of oxidative stress related diseases [92, 148, 12]. A small number of studies have even found antioxidants to cause adverse effects in some groups of patients [71]. The current status of antioxidant therapy is partly reflected in the American Heart Association's recommendation discouraging the use of antioxidant supplements for prevention of cardiovascular disease [71].

The lack of success of antioxidants seems surprising, considering that the connection between oxidative stress and a number of diseases is well established; especially so, if one were to look at ROS through a more traditional lens and perceive them as essentially deleterious byproducts of aerobic respiration and other enzymatic and non-enzymatic processes [36]. This picture of ROS, however, is no longer thought to be complete. The NADPH oxidase (NOX) family of enzymes with specialized subcellular localization patterns and activation mechanisms, serving the lone purpose of ROS generation, has come to light [75]. Although other enzymes like xanthine oxidase and cyclooxygenase are also known to produce ROS, it is not the primary function of these enzymes. For instance, the

main function of xanthine oxidase is purine catabolism, while that of cyclooxygenase is prostaglandin synthesis; ROS are only produced as byproducts of reactions catalyzed by these enxymes [63]. Contrary to the incidental production of ROS by these enzymes or by leakage through the respiratory chain, the superoxide anion radical, a form of ROS, is the primary product of NOX enzymes. The existence of these enzymes specializing in the production of ROS is unlikely to be a mere evolutionary accident.

Indeed, it is now well known that controlled enzymatic production of ROS is a feature of many signaling pathways and ROS, such as hydrogen peroxide, act as signaling molecules essential in determining the dynamics of these pathways [111, 115, 39]. Because of its relatively mild reactivity, longer half-life and charge neutrality, H_2O_2 is considered to be an important second messenger molecule [115]. Seen in this light, it is perhaps not so astounding that untargeted use of general oxidant inhibitors should not yield specific benefits in diseases. The clear role of oxidative stress in disease and the importance of ROS in normal cell signaling are facts that need to be reconciled before antioxidant therapy can be successfully utilized.

A major reason for the lack of understanding of redox signaling is the limitation placed by experimental techniques available for measuring oxidative changes in proteins. While new methods continue to be developed, currently available techniques are not absolutely quantitative and are affected by many factors in unpredictable ways [64, 43]. Even if methods that could quantitatively measure temporal changes in protein oxidation were to be available, the inherent complexity of signaling pathways would make it difficult to infer how redox regulation is integrated into the rest of the pathway. Protein phosphorylation serves as an illustration of this point – even though phosphorylation of many proteins in a signaling pathway can be measured with good quantitative precision, the underlying regulatory mechanisms of the pathway are not obvious from the observables alone [124, 123]. Therefore, experimental insight must be complemented by other approaches like biological systems modeling, that can help to discover design and operation principles and provide

directions for future experimental work [38].

With this motivation, the present work is an effort towards developing the current understanding of the mechanisms by which ROS regulate cell signaling. Not only will this clarify the role of ROS in physiological signaling, but will also shed light on how oxidative stress contributes to disease. Furthermore, instead of qualitative generalizations that classify ROS as more or less "evil" [115], or in the same vein, as a class of molecules with split personalities of Dr. Jekyll and Mr. Hyde [39], a systemic and quantitative view of the role of ROS in cell signaling is desirable. The term "systemic" is used here in the sense that instead of focusing on individual components of a signaling pathway that could be affected by ROS, a more holistic understanding should be sought wherein the emergent effects of ROS mediated regulation of multiple redox-sensitive components and their interactions with the rest of the signaling pathway are studied. Such a view, apart from being descriptive and explanatory, could be predictive and enable design of rational intervention strategies to prevent and cure oxidative stress related diseases. However, even though some attention has recently been directed towards developing quantitative models of ROS generation and consumption in the cellular context [1], the understanding of the effects of ROS on cell signaling remains qualitative in nature.

Mathematical modeling can be an extremely effective method to identify the underlying principles of operation in biological systems [2]. Time series measurements of some components of biological networks can be very useful for determining the underlying structure and parameters of the network [19, 149]. Inherent in the construction of mathematical models is a quantitative description of the modeled biological processes. Additionally, by appropriately choosing the levels of abstraction and detail to be incorporated in a model, interactions between elements considered to be important and their emergent properties can be studied. In the context of redox regulation in cell signaling, where some dynamic changes such as protein phosphorylation can be reliably measured and others like protein

oxidation cannot, mathematical modeling promises to be a very useful tool for understanding the mechanistic basis of redox regulation.

Recognizing the need to understand the mechanisms by which ROS regulate cell signaling and the importance of the integrative approach in studying complex biological phenomena, the overall goal of the present work is *to enhance a quantitative, systems level understanding of redox regulation in cell signaling*. Giving due consideration to the limitations on the types of experimental data that can be reliably acquired as relates to redox regulated processes, mathematical and computational approaches are heavily relied on to fill the gaps in knowledge left behind by intuitive interpretation of observables of the signaling pathway. It is hypothesized that computational models informed by feasibly measurable experimental data will be effective at filling these gaps and identifying the mechanisms of redox regulation in signaling.

As an empirically observable phenomenon, the dependence of a variety of signaling pathways on ROS has been established [137, 151, 88, 26]. With the assumption that there must be some common principles of redox regulation applicable across a significant number, if not all, of these ROS sensitive pathways, the attention in this work has been focused on select examples. In particular, the mitogen activated protein kinase (MAPK) cascade and the IL-4 signaling pathway, with greater effort spent on the latter, were chosen. These choices were driven by two determining factors: i) both these pathways have been shown to depend on intracellular ROS [137, 130]; and, ii) the ROS-independent layers of regulation in both these pathways are well characterized [98, 66]. While the first point is an absolute requirement to study redox regulation of the pathways, the second is based on practical considerations and is an attempt to minimize the number of unknowns. The presence of other as yet undetermined regulatory mechanisms would only add confounding factors making it difficult to isolate the effects of ROS on the signaling pathway. It should be noted that both these pathways are typical examples of larger "families" of signaling pathways; whereas

the MAPK cascade is commonly activated by growth factor and stress signaling [59], IL-4 uses the JAK/STAT signaling pathway which is a common theme in cytokine signaling [100]. Therefore, it is reasonable to expect that mechanisms found to be important in the MAPK and IL-4 pathways will be applicable across a number of signaling systems.

The following sections cover the background pertinent to redox regulation of cell signaling with focus on the IL-4 and MAPK pathways, and the biological and mathematical points examined in the rest of this dissertation are highlighted.

1.3 ROS regulate protein function by cysteine modification

Activation of a variety of cell surface receptors including growth factor receptors [137, 99, 27], cytokine receptors [86, 159, 151, 136], hormone receptors [40, 88], B and T cell receptor [26, 73, 132] among others, causes increase in intracellular ROS. The production of ROS following activation of signaling receptors is mediated by various enzymes of the NADPH oxidase (NOX) family [17, 85, 95, 40, 122] . Seven members of the NOX family (NOX1-5, DUOX1-2) are known[75]. The phagocytic NOX2 was the first NOX enzyme to be discovered and is known to mediate the "respiratory burst" in phagocytes. It is a multisubunit enzyme made of the oxidase gp91phox and several cytosolic regulatory subunits. Phosphorylation of the cytosolic units is required for the assembly of NOX2 [75]. NOX2 and NOX1 activation is also dependent on RacGTP [75, 18]. NOX5, DUOX1 and 2 on the other hand, are dependent on Ca^{2+} for activation [76]. NOX assembly and disassembly are complex process in themselves that are beyond the scope of this dissertation, but have been previously studied using mathematical modeling [164, 165]. Studies cited above have also shown that NOX mediated production of ROS in these signaling systems is functionally important as perturbing normal ROS levels results in altered cell signaling behavior.

That ROS can affect cell signaling has been known for a long time with the discovery of the ability of H_2O_2 to "mimick" the action of insulin [21]. Even before the components of the insulin pathway were discovered, it was hypothesized that this effect must be mediated

by oxidation of sulfhydryl functional groups on then unknown components of the pathway [22]. The biochemical basis of ROS mediated regulation of cell signaling is a lot more clear now and agrees in principle with this early hypothesis. It is now known that thiol (–SH, also sulfhydryl) groups present in cysteine residues of proteins can be oxidized by ROS to sulfenic acid form (–SOH) resulting in altered protein functions [166]. However, not all cysteine thiols are susceptible to oxidation by physiological ROS. The local electrostatic environment of some cysteine residues can lower their pKa from the typical value of more than 8 to under 7. Such cysteines are ionized to the thiolate form ($–S^-$) and are able react readily with ROS to form protein sulfenic acid [158]. Further oxidation of the sulfenic acid is possible generating the sulfinic acid (–SOOH) and subsequently the sulfonic acid (–SOOOH) forms [158, 32]. Oxidation to the sulfinic and sulfonic acid forms is irreversible, but the sulfenic acid can be reduced back to the thiol form by cellular oxidoreductase enzymes like thioredoxin and glutaredoxin [10]. Mechanisms to protect the sulfenic acid from further oxidation exist and the relatively unstable sulfenic acid is converted to intra- or inter-molecular disulfide (or in some cases sulfenyl amide), protecting the cysteine from further oxidation [141] (Fig. 1).

Based on the thiol chemistry described above, proteins with readily ionizable cysteines can act as sensors of the cellular redox state. A diverse array of proteins such as transmembrane receptors like the epidermal growth factor receptor (EGFR) [104], kinases such as ATM protein kinase [42], phosphatases like MAP kinase phosphatase 3 (MKP3) [127] and the GTPase Ras [53], among others, have been shown to be sensitive to cysteine oxidation. While oxidation of some proteins like MKP3 results in loss of catalytic function, in others like EGFR, oxidation could enhance activity. This illustrates that utilizing the basic template of cysteine oxidation allows ROS to influence the function of a diversity of proteins in very different ways.

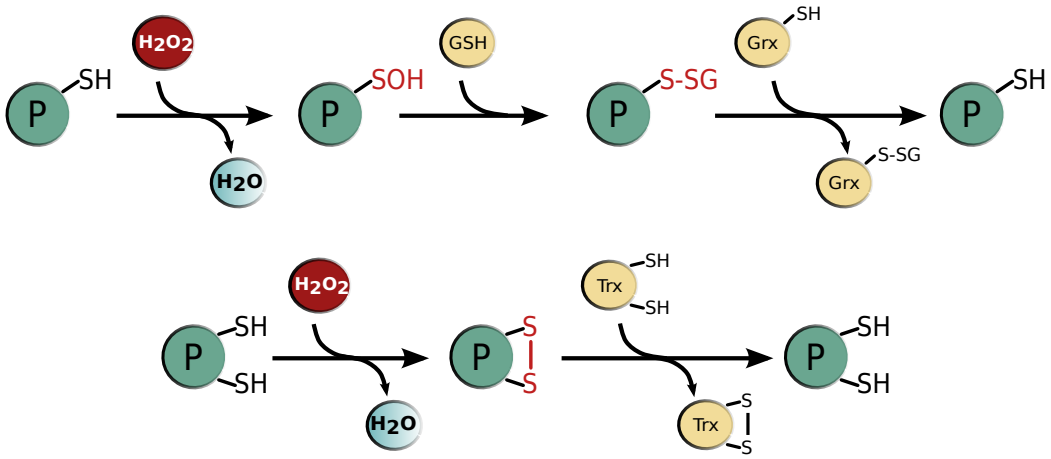

Figure 1: Thiol groups (-SH) of cysteine residues with low pKa are oxidized by physiological ROS like hydrogen peroxide to form sulfenic acid (-SOH). The sulfenic acid form may be protected from further oxidation by formation of intra- or inter-molecular disulfide bonds (-S–S-). Oxidoreductase enzymes glutaredoxin (Grx) or thioredoxin (Trx) can reduce the oxidized cysteine restoring the protein to its original reduced state. GSH, glutathione.

1.4 Redox sensitivity in the MAP kinase signaling pathway

MAP kinase cascade is a generalized term for a set of signaling pathways that possess a similar three-tiered structure. These pathways are characterized by a phosphorylation cascade in which a MAPK is activated through dual phosphorylation by MAPK kinase (MAPKK), which in turn is activated following dual phosphorylation by MAPKK kinase (MAPKKK) [109]. The pathways could be activated by a wide range of stimuli including growth factors, hormones and stresses to activate different types of MAPK, and could regulate processes like proliferation, differentiation or apoptosis [59]. Platelet derived growth factor (PDGF) is an activator of MAPK signaling and can activate the Raf/MEK/ERK cascade [167]. PDGF signaling is also one of the first signaling pathways whose activation was shown to be accompanied by heightened intracellular oxidation [137]. The specific example of PDGF activated Raf/MEK/ERK pathway has been examined in this dissertation to study redox regulation of this particular MAPK cascade.

The dephosphorylation of Raf/MEK/ERK pathway is regulated by a combination of

serine/threonine phosphatases, dual specificity phosphatases (DUSP) as well as protein tyrosine phosphatases (PTPs) [109]. Members of all three phosphatase families, with known roles in regulating the ERK signaling cascade, e.g. serine/threonine phosphatase PP2A [34], tyrosine phosphatase SHP-2 [89], and dual specificity phosphatase DUSP3 [154] have previously been shown to become inactivated by oxidation. It is likely that different phosphatases, especially those belonging to different families, have different rates of reactivity with ROS [25]. Additionally, each phosphatase targets a different kinase in the MAPK pathway. Different points of action of phosphatases combined with differential susceptibilities to oxidation could have important roles in determining the dynamics of the ERK signaling pathway. ROS independent processes, such as distribution of proteins across different subcellular compartments or crosstalk between pathways, when overlaid with phosphatase oxidation could affect system dynamics profoundly. These possibilities and their systemic outcomes have been investigated in Chapter 2.

1.5 Diverse putative mechanisms of redox regulation in the IL-4 signaling pathway

IL-4 is a pleiotropic cytokine with diverse roles in the immune system such as differentiation of antigen-stimulated naive T cells into the T_H2 type, immunoglobulin class switching to IgE isotype in B cells and in regulation of allergy response [97]. IL-4 signals through the IL-4 receptor α (IL-4Rα) and common γ chain (γC) complex. Receptor activation results in phosphorylation and activation of receptor-bound Janus Kinase 1 (JAK1) and JAK3 which then phosphorylate signal transducer and activator of transcription 6 (STAT6) [65]. Several PTPs including PTP1B, TCPTP, CD45 and SHP-1 have been suggested to be important for downregulation of IL-4 signaling [131].

The IL-4 pathway has been shown to activate NOX1 in the A549 cell line resulting in upregulation of intracellular ROS, and perturbation of normal ROS production resulted in altered STAT6 activation dynamics in these cells [130]. Three different mechanisms that could potentially be involved in ROS mediated regulation of IL-4 signaling can be

identified from a survey of the literature. The first of these mechanisms is reversible inactivation of PTP activity by oxidation. Phosphatases of the PTP family carry a conserved [I/V]HCXXGXXR[S/T] motif in the active site, and the invariant cysteine residue has an unusually low pKa in the range of 4-6 [143, 103]. As described in Section 1.3, the low pKa makes this cysteine highly susceptible to oxidation, and oxidation of the cysteine results in inactivation of the PTP. The oxidation of cysteine thiol can be reversed by oxidoreductase enzymes and the catalytic activity of the PTP restored (Fig. 1). Such cycles of ROS mediated inactivation and subsequent reactivation of PTPs can modulate the dynamics of protein phosphorylation. The second mechanism involves direct oxidation of receptor-associated JAK molecules. Previously published research has shown that oxidation of JAK can result in loss of catalytic activity [133], which can directly affect the dynamics of processes downstream of the JAK molecule. The third and final mechanism affects sub-cellular distribution of phosphatase activity. TCPTP, which is an important nuclear phosphatase of STAT6 normally distributes evenly between the nuclear and cytosolic compartments; however, under conditions of oxidative stress it has a tendency to preferentially accumulate in the cytosol [74]. Combined with the ability of STAT6 to shuttle between the nuclear and cytosolic compartments, redistribution of phosphatase activity is likely to affect the dynamics of STAT6 phosphorylation.

These three mechanisms, phosphatase oxidation, kinase oxidation and redistribution of phosphatase activity across sub-cellular compartments, can affect signaling dynamics in very distinct and profound ways. In Chapter 3 we investigate how the interaction of these mechanisms with other redox-sensitive or insensitive mechanisms determines system dynamics.

1.6 ROS mediated crosstalk and its consequences

An interesting feature of ROS mediated regulation of cell signaling is the relative non-specificity of the action of ROS. Enzymatic control of signaling pathways through, for

example, kinases and phosphatases has a great degree of specificity in the way an enzyme chooses its target. The action of ROS on the other hand, instead of being protein specific, is amino acid specific (see Section 1.3). This suggests that any protein accessible by ROS and containing amino acid residues reactive towards ROS could potentially be modified, irrespective of the source of ROS. In other words, ROS produced due to activation of one signaling pathway could act as facilitators of pathway crosstalk and influence the dynamics of another pathway. This type of crosstalk has indeed been observed before [94]. In relation to the IL-4 pathway, it has been shown that ROS produced by activation of some other cytokine signaling pathways can influence IL-4 signaling [130].

The potential of ROS to integrate otherwise distinct signaling modules has been given a brief theoretical examination in Chapter 5. Li et al. have developed a mathematical formalism to study functional integration (ROS mediated crosstalk in the present case) between structurally distinct modules (the crosstalking pathways) in the context of biological systems represented by differential equation systems [78]. This formalism has been applied to study ROS mediated crosstalk of IL-4 pathway with erythropoietin (Epo) signaling and its implications have been discussed.

1.7 Estimation of parameters of the computational model

The system model of the IL-4 pathway presented in this dissertation incorporates several novel regulatory mechanisms. The model parameters corresponding to these mechanisms have neither been determined experimentally, nor have they been estimated in other modeling studies. A variant of the evolutionary strategy ES algorithm [11] has been developed and utilized to estimate these unknown parameters. The algorithm is presented in Chapter 4, and its performance is compared against other algorithms. Although developed and applied as a tool to study the central question of redox regulation in cell signaling, this algorithm is generally applicable to other problems in parameter optimization.

CHAPTER II

SYSTEMIC REDOX REGULATION OF THE MAP KINASE CASCADE [1]

2.1 Introduction

With systems biology maturing as a discipline, it is natural that different approaches have emerged to study the complexity of biological systems. One sub-discipline that has arisen is known as cellular information processing. This approach borrows from engineering to treat the cell as a "black box" with a number of extracellular inputs (e.g. soluble ligands, matrix interactions) being interpreted, integrated and processed to elicit outputs (e.g. change in phenotype, apoptosis, transcription). This sub-discipline generally focuses on small to medium-sized network modeling to enrich understanding of regulatory mechanisms rather than large genome-wide or proteome-wide data analysis. Redox regulation of the MAP kinase cascade is studied here using this approach.

Oxidative modifications of protein thiols are emerging as important regulatory mechanisms, operating in combination with phosphorylation events to propagate signals. As more proteins are identified as redox-sensitive, it becomes imperative to ask how thiol oxidation within a signaling network modulates the interpretation of extracellular cues. We constructed and analyzed computational models of common kinase/phosphatase motifs in response to transient cellular oxidation in order to examine the systemic behavior that emerges due to redox sensitivity of signaling proteins. While we focus on redox control in the presence of hydrogen peroxide, the dynamic regulation of intracellular oxidants allow the principles to extend to other reactive oxygen species.

[1] Modified from [30]

2.2 *Reversible oxidative inactivation of phosphatases*

One of the most prevalent, conserved roles of protein thiol oxidation in signaling is the inactivation of active-site cysteines across the protein tyrosine phosphatase (PTP) family [24]. Although the consequences on enzymatic function are uniformly inhibitory, the susceptibility of PTP isoforms to oxidation varies, as shown by both in vitro kinetic experiments [119] and cellular studies [41, 105]. Furthermore, some serine/threonine phosphatases, such as calcineurin [134] and PP2A [35] have cysteine thiols susceptible to oxidation while other members of this protein family do not. Examination of signaling networks requires accounting for the different degrees of inhibition of phosphatases during receptor-initiated cellular oxidation.

We investigated general properties of systemic redox regulation through phosphatase inactivation during dynamic cellular oxidation using a computational model that can account for previously published data [14]. Chao-Wei Chen et al. reported that PDGF stimulation of human lens epithelial cells (HLE B3) activates the ERK signaling cascade with concomitant production of hydrogen peroxide [14]. Catalase-mediated scavenging of hydrogen peroxide resulted in severely ablated ERK signaling. Furthermore, exogenous addition of H_2O_2 was sufficient to activate ERK signaling. We hypothesized that these observations can be explained by a model of ERK signaling that takes into account ROS-mediated, reversible oxidative inactivation of phosphatases. The opposing activities of kinases and phosphatases counterbalance each other in the basal state. When the cells are stimulated with PDGF, the ERK pathway receives an upstream activating signal originating from the receptor. Simultaneously, ROS-mediated inactivation of phosphatases skews the enzymatic balance in favor of the kinases thereby activating the signaling cascade. Over time the input signal decays and ROS production ceases, allowing the phosphatases to be reduced back from their reversible inactive state. The signaling pathway is then restored to its basal state.

We adopted the three step Raf/MEK/ERK cascade from [124] and modified it by adding

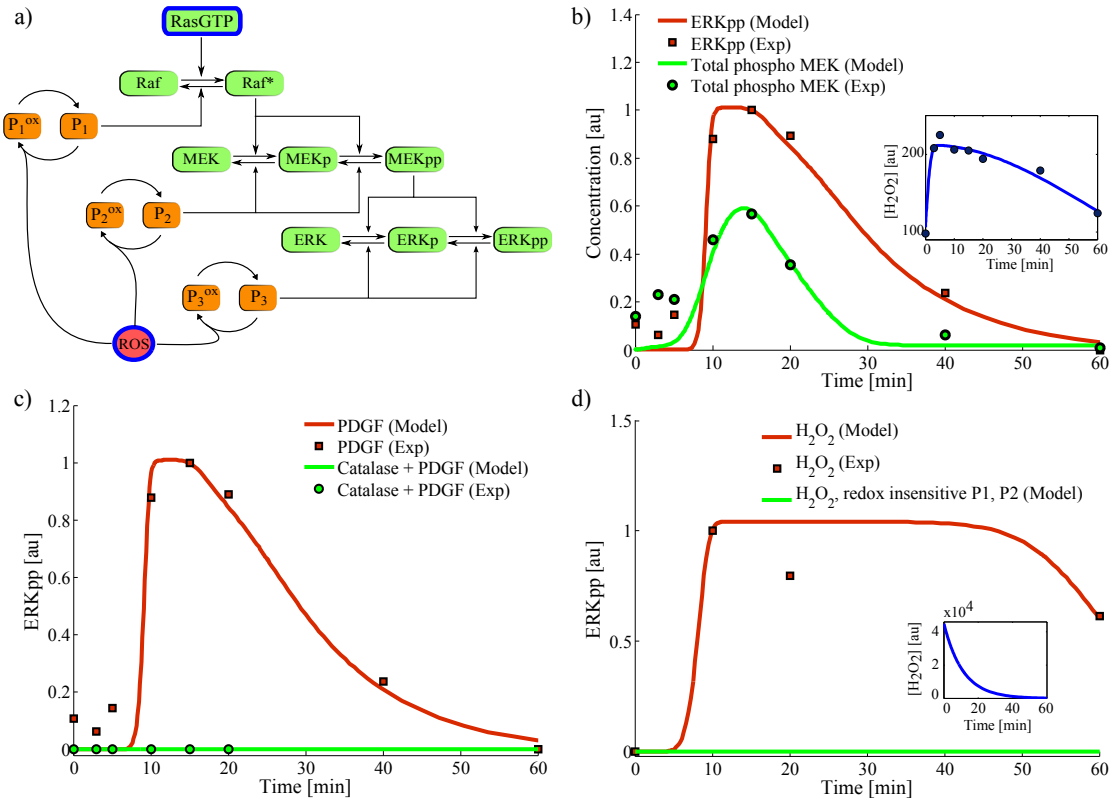

Figure 2: Computational model of redox regulation in MAPK cascade. (a) ERK signaling pathway with two step phosphorylation was modeled. Phosphatases were reversibly inhibited by oxidation. Species highlighted in blue (RasGTP and ROS) were supplied as input functions to the model. (b) Parameters of the model were optimized to fit experimental measurements of MEK and ERK phosphorylation following PDGF stimulation of HLE B3 cells. The ROS input function (inset) was obtained by fitting a curve to measured DCF fluorescence. P3 was the most susceptible to oxidation and all of it got oxidized very quickly and remained oxidized for the period of simulation. P2 had the slowest oxidation rate and less than 1% of total P2 was oxidized throughout the simulation. P1 was maximally oxidized at nearly 30 minutes with 16% of the protein in oxidized form which monotonically decreased subsequently. (c) Catalase pretreatment was simulated using the model fitted in b by setting ROS level to 0. The prediction was consistent with measured data. (d) Exogenous bolus addition of H_2O_2 was simulated using the fitted model in b with an exponentially decaying ROS curve (inset) and RasGTP was fixed at its basal level. Optimization of the ROS curve alone was sufficient to fit the experimental data. ERKpp levels failed to increase substantially if phosphatases P1 and P2 were assumed insensitive to oxidation. All experimental data were obtained from [14].

ROS mediated reversible inactivation of phosphatases (Fig. 2a). ROS dynamics were simulated using a curve fitted to PDGF induced H_2O_2 time course as measured in [14] (Fig. 2b inset). A transient RasGTP signal was used an input to the model and was optimized to fit the data. All three phosphatases (P1, P2, P3) were assumed to be susceptible to oxidation but with varying sensitivities (Fig. 2a). The oxidation rates were optimized to fit experimentally measured MEK and ERK phosphorylation time courses reported in [14] (Fig. 2b). The variation in oxidation across the cascade may be representative of a) differences in proximity to the ROS source and thus the effective concentration of H_2O_2; b) differences in oxidation rates of the proteins; c) differences in reduction rates due to structural differences in oxidized proteins [15] or d) the specificity for a reducing enzyme (glutaredoxin vs. thioredoxin). Although a prior modeling study demonstrated how inhibition of phosphatases is a means to influence MAPK dynamics through both duration and amplitude of signal [56], the authors considered a flat rate of dephosphorylation for dynamic simulations. Our added description of time-dependent variation in phosphatase activity due to dynamic oxidative modifications provides regulatory features for fine-tuning the response to a given input, depending on which phosphatases in a cascade are affected.

The model was able to reproduce experimentally measure ERK and MEK phosphorylation levels (Fig. 2b). Catalase pretreatment was simulated in the model by setting ROS levels to zero at all times. The model predicted attenuated ERK phosphorylation in good agreement with published data (Fig. 2c). An exogenous bolus addition of H_2O_2 was simulated using a high initial value followed by a first order decay (Fig. 2d inset). Optimization of two parameters, H_2O_2 initial value and decay rate, was enough to capture the experimental observations. We note that the fit in Fig. 2b was obtained with very low oxidation rates for P1 and P2 and a much higher rate for P3. Interestingly, the model suggests that the slow oxidation could be physiologically important since making P1 and P2 completely insensitive to oxidation resulted in no ERK phosphorylation even with exogenous addition of a large amount of H_2O_2 (Fig. 2d).

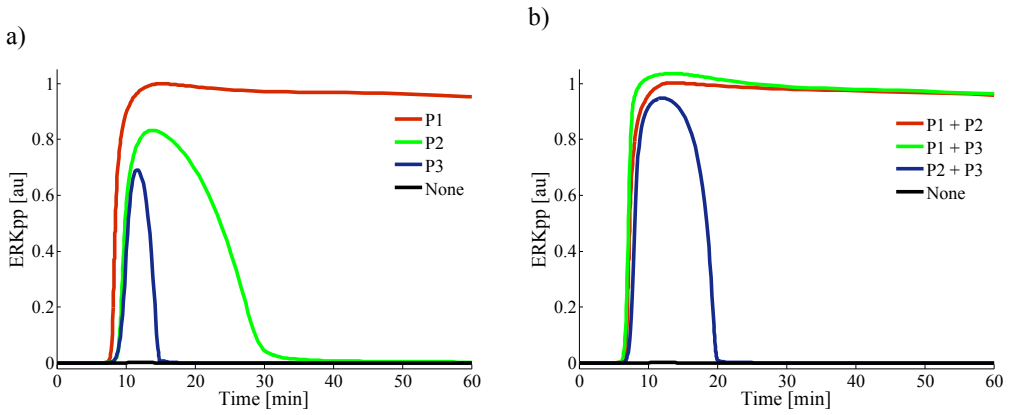

Figure 3: Topological features influence the contribution of phosphatases. Simulations were performed by setting different combinations of phosphatases as redox sensitive. (a) ERKpp levels when only a single phosphatase is redox sensitive. The same oxidation and reduction rates were assigned to each phosphatase for consistency. Oxidation of phosphatases with substrates further removed from ERK leads to greater amplification of the response. (b) ERKpp response when pairs of phosphatases are redox sensitive. The output for two phosphatases appears to be a qualitative sum of the outputs when individual phosphatases are redox sensitive.

This observation suggested that the location of P1 and P2 in the signaling network may have an important role in their ability to influence the signaling. To test this idea we performed computational experiments with the optimized model. Different sets of phosphatases were defined to be oxidation sensitive and dually-phosphorylated ERK (ERKpp) was monitored as the output. The results suggest that phosphatases with substrates further upstream of ERK are progressively more potent in influencing the signaling dynamics (Fig. 3a). Furthermore, when pairs of phosphatases are redox sensitive, their individual effects add up qualitatively (Fig. 3b). These results suggest that topologically conserved MAPK networks can produce a variety of outputs, perhaps even to the same input signal, as the dynamics of phosphatase oxidation/reduction change in a context-dependent manner.

2.3 Oxidative control through compartmentalization

Differences in redox potential in the cellular environment are created not only by punctate distribution of ROS sources, but also by organellar compartmentalization [62]. The redox microenvironment faced by proteins in a signaling cascade can be quite different as they

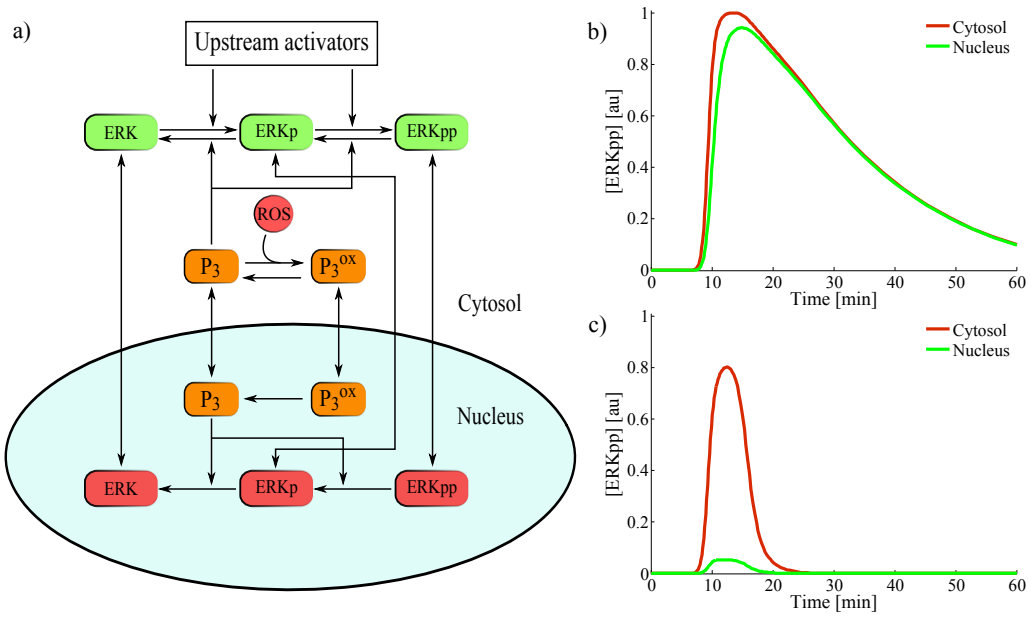

Figure 4: Compartmentalization of redox potential affects signaling. (a) The model optimized to HLE B3 cell data (Fig. 2) was modified to include nuclear-cytoplasmic shuttling of ERK and its phosphatase P3. Nuclear entry and exit were modeled as first order reactions with equal rate constants and were assumed to be the same for all proteins concerned. (b) The nucleus was assumed to be at an identical oxidative state as the cytosol. Cytosolic and nuclear levels of ERK were predicted to be similar. (c) The nucleus was modeled as a more reduced compartment with no protein oxidation occurring in the nucleus. Protein reduction rates were assumed to be the same in both compartments. Both the nuclear and cytosolic signals are attenuated compared to panel b.

move across compartments. In particular, the nucleus has a more reducing microenvironment than the cytosol by approximately a 20 mV difference in thioredoxin potential [46]. Oxidative modification can be reduced or enhanced by the transport process; consequently, the dynamic location of a protein can impact its oxidation state and hence catalytic activity.

We modeled the impact of translocation of a redox sensitive protein from cytosol to a relatively more reducing nucleus. MAP kinases can translocate to the nucleus to perform their functions as transcription factor regulators. Phosphatases of MAPKs present in the nucleus are exposed to a more reduced environment as compared to the cytosolic phosphatases and are hence likely to be more active. As a consequence, the cytosolic activity of MAPK may not correspond exactly with the nuclear activity of MAPK. To assess the effects

of compartmentalization of redox state between the cytosol and nucleus we used the optimized ERK signaling model shown in Fig. 2 and extended it to include nucleo-cytoplasmic shuttling of ERK and its phosphatase P3 (Fig. 4a). When the nucleus is assumed to be at the same redox state as the cytosol with protein oxidation and reduction occurring at the same rate in both compartments, the cytosolic and nuclear fractions of active MAPK follow each other very closely (Fig. 4b). However, when the nucleus is taken to be more reduced than the cytosol and free of ROS, then the nuclear fraction of active MAPK is significantly attenuated (Fig. 4c). Moreover, the overall signal strength is also reduced by the nuclear compartmentalization. Observations of ERK oscillations between the nucleus and cytosol have an unexplained mechanistic basis in signaling regulation [128, 129, 152]. The ability to regulate the active form of the kinase by redox regulation of its corresponding phosphatase may be an explanation for the shuttling process.

2.4 Oxidative control through kinases

Unlike the phosphatases, the reported examples of other signaling molecules are much more varied in the nature and consequences of their thiol modifications, ranging from affecting enzymatic activity, cellular location or binding in macromolecular complexes. Redox sensitivity of kinases can also profoundly influence cell signaling. There is recent evidence that the MAPK p38 can be reversibly oxidized [142]. It was found that under prostaglandin-stimulated oxidative conditions as well as with exogenous H_2O_2 addition, phosphorylation of p38 is maintained while its activity is reversibly inhibited by oxidation at multiple cysteine sites. To study this scenario we modified the model shown in Fig. 2 to include ROS mediated reversible oxidation of a dually phosphorylated MAPK (Fig. 5a). In the absence of kinase oxidation, most of the dually phosphorylated MAPK is available as free (i.e., unbound to other proteins) active MAPK, assuming that the dually phosphorylated form is the enzymatically active form (Fig. 5b). When the kinase is sensitive to oxidation, only a fraction of the phosphorylated MAPK is available in its active form, the

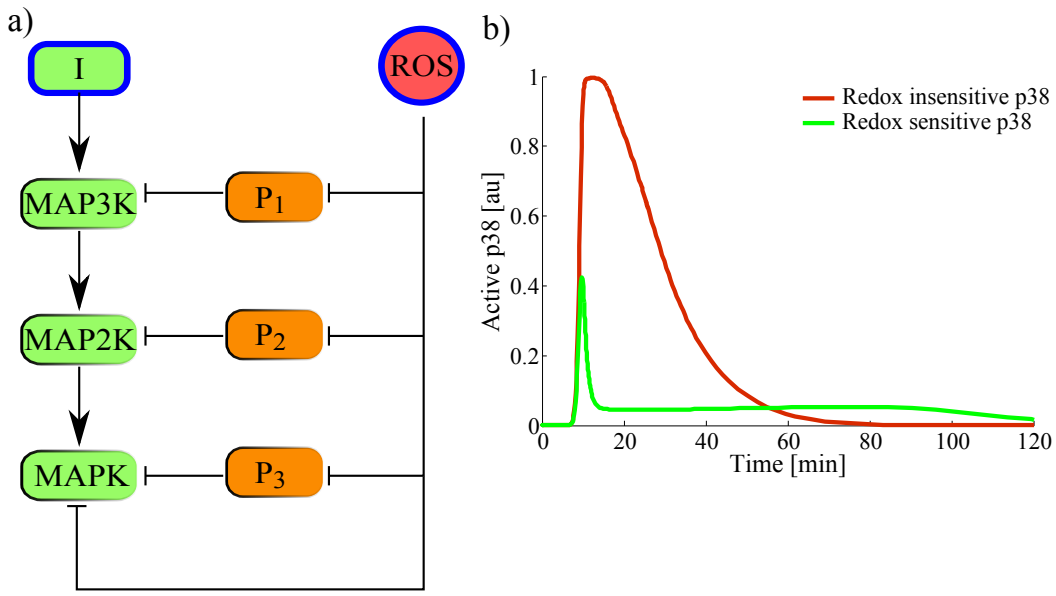

Figure 5: Oxidative inhibition of MAPK. (a) Reversible oxidative inhibition of MAPK was modeled by modifying the model in Fig. 2. The bis-phosphorylated form of MAPK (MAPKpp) was assumed to be redox sensitive and the oxidation was reversible. (b) Taking the MAPK cascade as corresponding to the p38 signaling pathway, simulations were performed with dually phosphorylated p38 being sensitive to oxidation or not. Reduced dually phosphorylated p38, unbound to other proteins was assumed to be the enzymatically active form and the oxidized form was catalytically inactive. Inclusion of reversible oxidation resulted in low p38 activity sustained over a longer period of time.

rest being in the oxidized state (Fig. 5b). These results agree qualitatively with the data reported in [142]. In addition, the oxidation of phosphorylated MAPK serves as a sequestration mechanism for the active kinase. The oxidized form is reduced slowly back to the active form allowing the active MAPK to be maintained at an almost steady, low level for a longer period of time. This suggests that oxidation of the kinase may be a mechanism to trap the rapidly generated active kinase and release it slowly over time.

2.5 Complexity in signaling networks

The relative contributions of different redox sensitive phosphatases can vary from those seen in the linear kinase cascade in Figure 1, depending on the complexity of the system. For example, heregulin (HRG) stimulation of ErbB receptor simultaneously activates the Ras/Raf/MEK/ERK and PI3K/Akt pathways [52]. Apart from a common activating input,

the two pathways are connected by two other links; i) cross-talk in the form of Raf inhibition by Akt ; and ii) a common serine/threonine phosphatase PP2A inhibiting the two pathways at Akt and MEK (Fig. 6a). As with PDGF, EGF receptor ligation has been reported to induce reactive oxygen species as a necessary component of the signal transduction [27]. A computational model of this system was adopted from [52] and was modified to include ROS mediated inactivation of phosphatases. This network presents the interesting feature of ROS playing an activating, as well as inhibitory role in the ERK pathway at the same time. ROS mediated inhibition of PP2A and MKP3 directly activates the ERK pathways. However, inhibition of PP2A allows greater activity of Akt which inhibits ERK signaling through Raf. Simulations show that with the same network structure, either of these effects can dominate depending on parameters of the model. The presence of ROS could amplify (Fig. 6b) or attenuate (Fig. 6c) ERK phosphorylation in a context dependent manner. This suggests that increased complexity of the network makes it more difficult to predict the role played by ROS in cell signaling. At the same time this shows that dynamic modification of phosphatase activity affects the outcome of signaling in ways that are hard to predict intuitively; therefore ignoring the dynamics of phosphatase modification in models of signal transduction may not always be prudent.

2.6 Conclusion

These simple models are instructive in demonstrating that the degree of cellular oxidation has the ability to modulate the amplitude and duration of signal transduction events in biochemical signaling networks. Furthermore, compartmentalization of redox potential in different cellular organelles can result in different interpretations of the same signaling molecule due to subcellular location. Redox regulation is a powerful mechanism for tuning the cellular response to a given input in a context-dependent manner; thus a cell may skew towards a particular phenotype based upon the interpretation of a cue through altered signaling dynamics. Importantly, hypo- and hyper-responsiveness to receptor ligation can

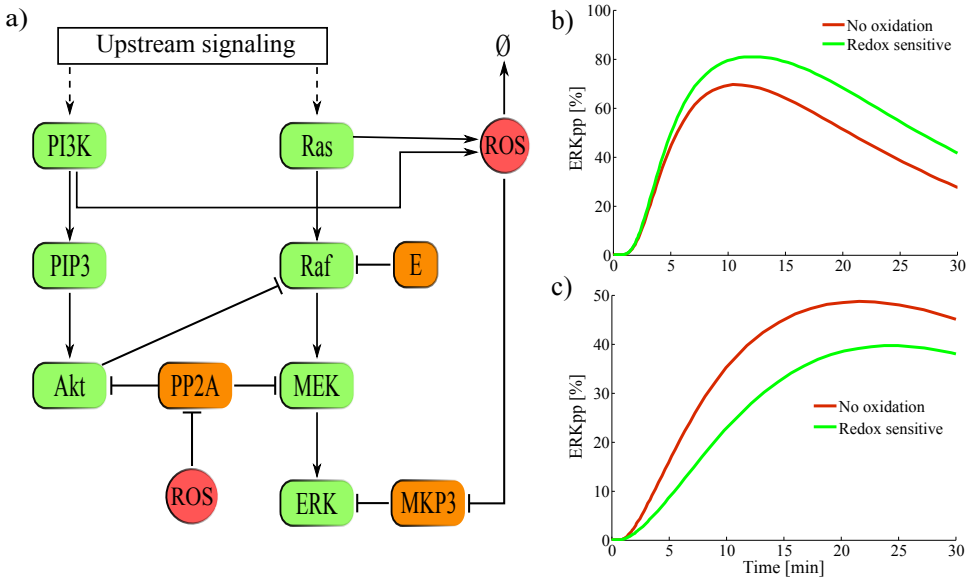

Figure 6: Increased complexity leads to variable effects of ROS regulation. (a) The Akt-ERK crosstalk model was adopted from [52] and modified to include oxidative inhibition of phosphatases MKP3 and PP2A. ROS production was assumed to be a NOX dependent process requiring the presence of active PI3K and RasGTP for Nox activation. ROS production was therefore modeled as a process driven by active PI3K and RasGTP and the decay was a first order process. (b) Redox sensitivity of phosphatases resulted in amplification of ERKpp compared to a condition where no protein was redox sensitive. (c) By strengthening the inhibitory effect of Akt on Raf, at the same time weakening the control of PP2A on MEK dephosphorylation (altering three parameters in all) the qualitative effect of ROS on ERKpp was reversed as compared to panel b. With the altered parameters the oxidation sensitive model resulted in signal attenuation compared to the redox insensitive model.

be achieved without changing the topology of a signaling network.

Computational modeling of protein oxidation networks is a promising avenue for interpreting the complex effects of cellular oxidation on cellular information processing. For the model presented in Fig. 2, the addition of transient phosphatase activity was all that was necessary in order to explain a number of experimental conditions in which altering redox state affects signaling. While there are numerous aspects of redox signaling ignored in these simulations (spatial gradients, mitochondrial vs. NOX mediated ROS production, additional feedback mechanisms etc.), we can still gain insights into principles of regulatory control by testing network topologies and differential sensitivities to reversible oxidation. As knowledge builds of redox control mechanisms within signaling networks, it is likely that common regulatory motifs will emerge across the varied receptor families in which oxidative bursts occur. A key question that improved proteomic tools [108, 112, 126] will help answer is whether redox-sensitive proteins are evenly distributed within receptor signaling networks, or clustered at specific nodes for influencing the relaying of information.

2.7 Methods

The model in Fig. 2 was derived from [124] by retaining only the three step Raf/MEK/ERK module. To mimic the shape of RasGTP profile in [124], a skewed Gaussian curve was used as RasGTP input. All parameters of the original model were used unchanged except initial value of P2 which was increased 10 fold to fit the experimental data. The experimental data were obtained from [14] and represent band intensities of Western blot experiments as quantified in the original publication. The intensities were normalized to loading controls for individual gels. The normalized ERKpp values were scaled and shifted so that the lowest signal has a value of 0 and the signal at 15 minute is 1. The same scaling factor was used for all experimental data in Fig. 2a and b. The scaled data for individual proteins were shifted so that the lowest value in each set reads 0. The model outputs were scaled by the computed value of ERKpp at 15 minute in Fig. 2a and b. Same method was used in Fig. 2d,

however, the scaling to unity was for the 10 minute time point for both experimental and model data. We used a curve fitted to experimentally measured H_2O_2 as ROS input to the models in Fig. 2 (see Fig. 2b inset) which should account for all cellular sources of ROS following receptor activation. The same input function was retained for models in figures 1-4. Since no reliable method was available to scale DCF fluorescence intensities to true H_2O_2 concentrations, we used DCF fluorescence values from Chen et al. [14] as a scaled representation of the concentration. The protein oxidation and reduction rates were defined in this context and do not represent true rates. The fitted phosphatase oxidation rates spanned a wide range with orders of magnitude from 10^{-6} to 10. All proteins were assigned the same reduction rate in Fig. 2. The reducing enzymes were assumed to remain constant for the sake of parsimony and were not explicitly modeled. This model was used as the basis for all models in figures 1-4 with appropriate modifications. Details of all models are provided in Appendix A.

CHAPTER III

COMPUTATIONAL MODELING PREDICTS PHOSPHATASE OXIDATION AS THE PRIMARY MECHANISM OF REDOX REGULATION IN IL-4 SIGNALING

3.1 Introduction

From initially being perceived as accidental and harmful byproducts of aerobic respiration, reactive oxygen species (ROS) have now emerged as important regulators of physiological cell signaling [32]. In particular, due its relatively milder reactivity and longer half-life, H_2O_2 is recognized as an important second messenger in signal transduction [115]. Activation of several types of cell surface receptors induces transient ROS production by activating NADPH oxidase (NOX) family enzymes, and the ROS so produced play a role in modulating downstream signaling [137, 27, 83]. ROS such as H_2O_2 react with the thiol functional group of susceptible cysteine residues in redox sensitive proteins converting the cysteine to sulfenic acid form [33]. While further oxidation is irreversible, the sulfenic acid form can be protected by formation of disulfides and sulfenyl amides which can be reduced back to the thiol form by oxidoreductases like thioredoxin and glutaredoxin [147, 121, 15]. This reversible cysteine oxidation can result in transient changes in protein function, such as gain or loss of catalytic activity, at several levels in a signal pathway resulting in systemic changes in cell signaling dynamics [30].

The IL-4 signaling pathway, which has important immunological roles like T_H2 differentiation and immunoglobulin E class switching [157], has been shown to be redox regulated [130] and is controlled by a number of proteins which are potentially redox sensitive. The pathway is initiated by binding of IL-4 to the IL-4 receptor (IL-4R) α chain and subsequent recruitment of the common gamma chain (γC) to form the type I receptor complex.

A type II receptor complex is also formed in some cell types where the γC is substituted by the IL-13Rα subunit [157, 97]. Jurkat T lymphoma cells, the cell line we have used in our study, does not signal through the type II receptor and the following discussion is limited to type I receptor [110]. Janus kinase (JAK) 1 and JAK3 are bound constitutively to IL-4Rα and γC, respectively [65]. Formation of the receptor complex activates the JAK molecules by trans-phosphorylation, which in turn phosphorylate several tyrosine residues on the cytosolic tails of the receptor chains. The phosphorylated receptor recruits cytosolic signal transducer and activator of transcription 6 (STAT6) which is phosphorylated by the active JAK molecules. Phosphorylated STAT6 (pSTAT6) forms a homodimer, which is the active form of STAT6 and can initiate transcription of target genes [157, 97]. A number of protein tyrosine phosphatases (PTPs) are involved in downregulation of IL-4 signaling. CD45 has been shown to inhibit phosphorylation of both JAK1 and JAK3 in response to IL-4 stimulation [57, 162]. SHP-1 is another negative regulator of IL-4 signaling and it binds an immunoreceptor tyrosine-based inhibitory motif (ITIM) in the cytoplasmic tail of IL-4Rα, possibly dephosphorylating the receptor or JAK molecules [65, 49, 50]. PTP1B and TCPTP dephosphorylate STAT6 and are involved in IL-4 signaling [80, 81]. The more abundant 45 kDa form of TCPTP can shuttle between the cytosolic and nuclear compartments making it an important nuclear regulator of STAT6 phosphorylation [80].

Multiple components of the IL-4 pathway described above can act as redox sensors. Members of the PTP family are particularly sensitive to oxidation due to a low pKa cysteine residue in their active sites [106, 141, 103]. ROS such as H_2O_2 reversibly oxidize several PTPs including PTP1B, TCPTP, CD45 and SHP-1 following activation of a variety of cell surface receptors or when ROS are added exogenously [88, 83, 117, 153, 15]. Along these lines, increased oxidation and inactivation of PTP1B was observed in IL-4 treated A549 cells [130]. It is very likely that the other PTPs involved in IL-4 regulation are also redox regulated in a manner similar to PTP1B. In addition to the PTPs, members of the JAK family have also been shown to possess a redox switch. JAK2 has been shown

to become inactive under conditions of exogenous as well physiological oxidative stress [133]. Structural homology between JAK1 and JAK2 [133] as well as indirect experimental evidence [72] suggest that JAK1 could also be inactivated by oxidation. Additionally, JAK3 has been shown to be catalytically most active when highly reduced, with increasing loss of activity with oxidation, independent of its phosphorylation state [28]. In addition to catalytic activities of the PTP and JAK proteins, the subcellular localization of TCPTP has also been shown to be affected by redox state of the cell with more oxidizing conditions favoring cytosolic accumulation of TCPTP [74]. All these lines of evidence suggest that IL-4 signaling could potentially be controlled by multiple mechanisms of redox regulation.

Along with redox sensitive control mechanisms, other equally important control systems are in place to ensure tight regulation of JAK/STAT signaling. A prior computational study of the JAK2/STAT5 signaling system found that phosphorylation-state dependent nuclear-cytosolic cycling of STAT5 was an important determinant of signaling dynamics [139]. In the case of the IL-4 pathway, the mechanism of nuclear cycling appears to be cell-type dependent. While there is evidence to indicate that STAT6 phosphorylation is required for nuclear translocation [4], the contrary has also been shown where STAT6 freely shuttles between nuclear and cytosolic compartments [16]. Along with phosphatases, proteasome dependent degradation and suppressor of cytokine signaling (SOCS) mediated downregulation are also common motifs in JAK/STAT signaling [107, 20, 131]. Role of proteasomal complexes in downregulating IL-4 induced STAT6 phosphorylation has been previously reported [150, 49]. SOCS1 and SOCS3 proteins have also been found to inhibit IL-4 signaling [79].

Given that multiple redox dependent and independent control points exist in the IL-4 signaling network, how do the various putative mechanisms interact to regulate signaling dynamics? This question is particularly challenging because the outcomes of some of the potential redox regulatory mechanisms are qualitatively opposite in nature. For instance, while PTP oxidation could increase signaling activity, JAK oxidation could suppress it.

Direct experimental measurements of protein oxidation changes during cell signaling are essential to answer these questions. Methods for detecting intracellular changes in protein sulfenic acids are developing but technical challenges remain to be addressed before quantitative, systems level measurements are possible [43]. Even if such data were to be available, inferring relative contributions and interactions between various regulatory mechanisms would not be straightforward due to the complexity of the signaling pathway. Computational modeling is a powerful tool that can harness available data to uncover underlying interactions in biological networks [68]. To answer the question posed above we have used computational modeling informed by quantitative experimental data, both directly and indirectly related to redox processes, to study redox regulation in IL-4 signaling. We conclude that PTP oxidation is the dominant mechanisms of redox regulation in IL-4 signaling and its interaction with redox independent mechanisms is critical in explaining IL-4 signaling dynamics. We have developed a systems model of the IL-4 pathway that successfully predicts IL-4 signaling dynamics over a wide range of redox conditions.

3.2 Methods

3.2.1 Cell culture and reagents

Jurkat T cells were cultured in complete media (RPMI-1640 containing 10% FBS, 1% HEPES, 1% MEM non-essential amino acids, 1% sodium pyruvate, 100 U/ml penicillin, and 100 g/ml streptomycin). For all experiments Jurkat cells were first serum starved at a concentration of 2×10^6 cells/ml in media containing 0.5% FBS for 4 hours. The length of serum starvation of selected to maximize observed change in STAT6 phospohrylation (Section B.3). Human recombinant IL-4 (R&D Systems, Minneapolis, MN) was used at 100 ng/ml to treat the cells. The inhibitors cycloheximide (CHX), diphenyleneiodonium chloride (DPI) and MG132 (all EMD Millipore, Billerica, MA) were administered at 20 μg/ml, 20 μM and 10 μM, respectively. Rabbit anti-STAT6 phosphotyrosine 641 antibody (Cell Signaling Technology, Danvers, MA) was used at 1:100 dilution. Rabbit anti-SOCS3

antibody (Abcam, Cambridge, MA) was used at 1:500 dilution. R-PE conjugated anti-rabbit IgG (Life Technologies, Carlsbad, CA) was used as secondary antibody for flow cytometry at 1:500 dilution. R-PE conjugated anti-STAT6 (BD, Franklin Lakes, NJ) was used per manufacturer's recommendation. CM-H_2DCFDA (Life Technologies, Carlsbad, CA) was used at 5 μM to measure intracellular oxidation.

3.2.2 Treatment with inhibitors and flow cytometry

Serum starved cells were suspended in PBS at 4×10^6 cells/ml. This cell density was chosen to get maximal change in STAT6 phosphorylation with IL-4 treatment (Section B.3). For each time point in an experiment, the appropriate inhibitor was added one hour before IL-4 stimulation. Cells were fixed in 1.5% paraformaldehyde for 10 min at room temperature and permeabilized in 90% methanol for 30 min at 4°C. After staining with suitable antibodies, the samples were analyzed on a BD LSR II flow cytometer (BD, Franklin Lakes, NJ). Fluorescence data were analyzed using in-house code written in Matlab; mean fluorescence intensity (MFI) was used to summarize the behavior of analyzed cell populations. For pSTAT6 and SOCS3 analysis, cells non-specifically labeled only with secondary antibody were used to acquire the background signal. For STAT6, unstained cells (because the primary Ab was fluorophore conjugated) were used as background. To enable comparison between experimental conditions, background corrected MFIs were normalized by dividing by the background corrected MFI of Jurkat cells not treated with inhibitors and IL-4 as follows:

$$\mathrm{MFI}_{\mathrm{norm}} = \frac{\mathrm{MFI}_{\mathrm{sample}} - \mathrm{MFI}_{\mathrm{bk}}}{\mathrm{MFI}_{\mathrm{untreat}} - \mathrm{MFI}_{\mathrm{bk}}}$$

where, $\mathrm{MFI}_{\mathrm{norm}}$ is the background corrected, normalized MFI, $\mathrm{MFI}_{\mathrm{sample}}$ is the experimentally measured MFI of the sample, $\mathrm{MFI}_{\mathrm{bk}}$ denotes the background MFI and $\mathrm{MFI}_{\mathrm{untreat}}$ is the measured MFI of untreated Jurkat cells.

To detect intracellular redox state, CM-H_2DCFDA was added 30 min prior to IL-4

stimulation. After adding IL-4, samples were analyzed on BD LSR II Flow Cytometer to measure CM-H_2DCFDA MFI. MFI time course of CM-H_2DCFDA stained cells not treated with IL-4 was subtracted as background from all other CM-H_2DCFDA time courses.

3.2.3 Computational modeling of the IL-4 pathway

All modeling, simulation and analysis was performed in Matlab. For Monte Carlo (MC) simulations, all the networks to be analyzed were coded as ordinary differential equation (ODE) systems assuming mass action kinetics and solved using numerical ODE solvers in Matlab. The ODE system representing the largest model with all regulatory mechanisms and the parameter bounds used for the MC simulations are shown in Appendix B.1. The systems model of the IL-4 pathway was implemented using the Simbiology toolbox in Matlab. Equations and parameters of the model are presented in Appendix B.2. Derivatives of Hill curves fitted to experimentally measured CM-H_2DCFDA fluorescence were taken to represent instantaneous intracellular ROS trends. The time derivative of the fitted Hill curve, $f(x)$ was modified to $a + bf(x)$, where a and b are model parameters representing baseline ROS level and a scaling factor, respectively. The modified curve was supplied to the model as an input. Simulated time course $x(t)$ of species x was also similarly scaled to $y(t) = \alpha_x + \beta_x x(t)$, where α_x and β_x are constants defined for species x and are independent of experimental conditions. Different scaling is required for different species because the antibody used to measure each protein has different characteristics and the measured MFI scales differently to actual amount.

Initial estimates of parameters were obtained from [161] and [1]. Evolutionary strategies with hyper mutation algorithm was then used (Chapter 4) to fit the model to experimental data using these initial estimates. The following error function was minimized to obtain the fit:

$$e = \sum_i \sum_j \sum_t \left(\frac{y_{ij}(t) - e_{ij}(t)}{e_{ij}(t)\sigma_{ij}(t)} \right)^2$$

where, $y_{ij}(t)$ is the scaled and shifted value (as described above) of the j^{th} species under the i^{th} experimental condition at time t; $e_{ij}(t)$ represents the experimentally measured value under the same circumstances and $\sigma_{ij}(t)$ is the standard error associated with the experimental measurement.

3.3 Results

3.3.1 ROS are necessary but not sufficient for STAT6 phosphorylation

Jurkat cells were stimulated with IL-4 and intracellular oxidation was monitored using flow cytometry by staining the cells with CM-H_2DCFDA. Fluorescence of the dye increased quickly after addition of IL-4 and showed a tendency to saturate 1 hour after IL-4 addition (Fig. 7a). Pretreating the cells with DPI, an inhibitor of phagocytic Nox and flavoprotein inhibitor, lowered the baseline oxidation of the dye and significantly reduced oxidation following stimulation with IL-4. Since the oxidation of CM-H_2DCFDA is an irreversible process, the fluorescence time courses shown in Fig. 7a represents cumulative oxidation of the dye as a function of time. In order to infer instantaneous levels of ROS from the cumulative dye oxidation time courses, Hill curves were fitted to the data points (Fig. 7a) and derivatives of these curves were obtained (Fig. 7b). The derivatives indicate that following IL-4 treatment of Jurkat cells, intracellular ROS concentration increased rapidly peaking at approximately 20 min and gradually returned to baseline level. In DPI pretreated cells the change in ROS level was observed to be much lower than that in untreated cells.

To study the effects of ROS on IL-4 signaling, time-dependent phosphorylation of total intracellular STAT6 (i.e, sum of nuclear and cytosolic pSTAT6, see Appendix B.4) was quantified under a variety of oxidative conditions. Treatment of Jurkat cells with IL-4 significantly increased STAT6 phosphorylation within 5 min and kept it elevated for 2 hours (Fig. 7c). Cells pretreated with DPI showed significantly lower baseline phosphorylation of STAT6 and responded very weakly to IL-4 stimulation. Addition of exogenous hydrogen peroxide (10 μM) in addition to IL-4 further increased STAT6 phosphorylation when

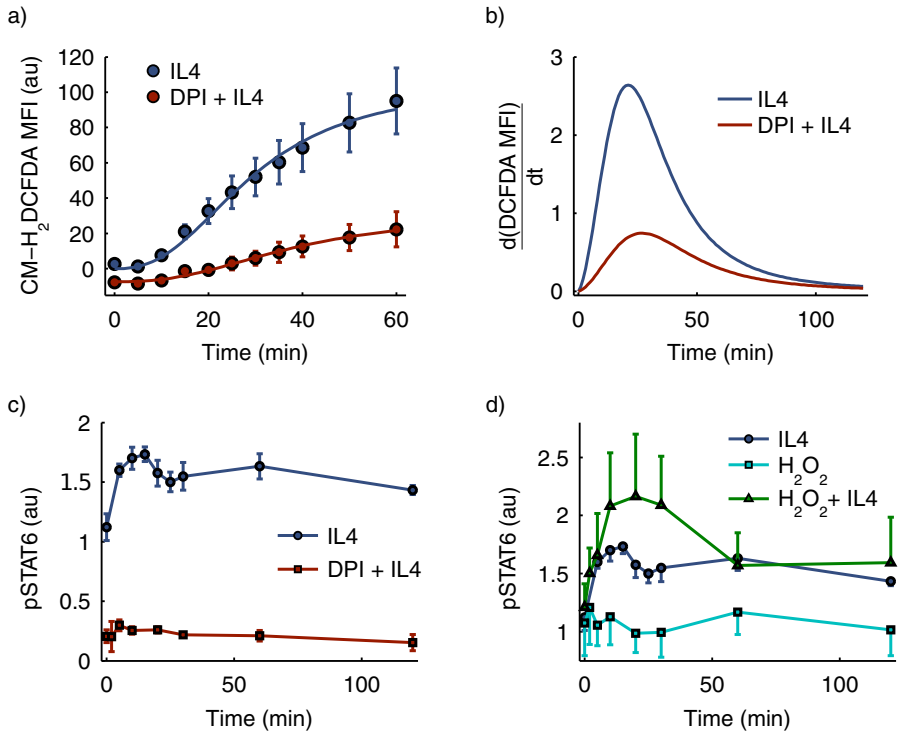

Figure 7: IL-4 induced ROS is required for STAT6 signaling. (a) Jurkat cells were pretreated or not with 20 μM DPI for one hour and stimulated with 100 ng/ml IL-4. Cells were incubated with 5 μM CM-H_2DCFDA for 30 min before IL-4 addition. Fluorescence intensity of oxidized dye was recorded for each time point using flow cytometry. The lines are hill curves fitted to the means. (b) Derivatives of the Hill curves shown in a. (c) Jurkat cells pretreated or not with 20 μM DPI for one hour were stimulated with 100 ng/ml IL-4 and pSTAT6 was quantified using flow cytometry. (d) Jurkat cells were treated with H_2O_2 (10 μM), IL4 (100 ng/ml) or both and pSTAT6 was measured. Values on y-axis represent background subtracted and normalized mean fluorescence intensities. Graphs represent mean ± standard error of mean. n = 6 for pSTAT6 under IL4 stimulation for all but the 4th (15 min) and 6th (25 min) time points where n = 3; n = 3 for all other experiments; au, arbitrary units.

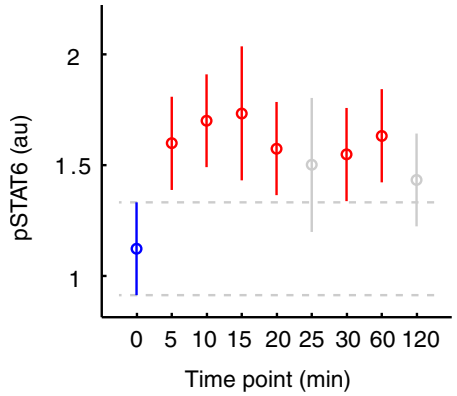

Figure 8: pSTAT6 shows oscillatory behavior. Tukey's HSD test was used for pairwise comparison of pSTAT6 from Fig. 7c across time points. Comparison of pSTAT6 at 0 min (blue bar) with all other time points is shown. The bars represent comparison intervals according to Tukey's HSD and non-overlapping intervals indicate significant difference at p = 0.05 level. Red bars, significantly different from pSTAT6 at 0 min; gray bars, not significantly different. X-axis is not to scale.

compared to IL-4 treatment alone (Fig. 7d). However, addition of the same concentration of H_2O_2 in the absence of IL-4 failed to alter STAT6 phosphorylation from its basal level.

3.3.2 Interplay of PTP oxidation with nuclear-cytosolic shuttling of proteins results in characteristic phosphorylation dynamics

The pSTAT6 time course in response to IL-4 stimulation of Jurkat cells shows oscillatory behavior attaining two local maxima over the two hour period (Fig. 7c). Statistical significance of differences in STAT6 phosphorylation between time points was tested using a one way ANOVA. STAT6 phosphorylation differed significantly across time points with $F(8, 39) = 3.71$, $p = 0.0026$. Tukey-post hoc comparison across the time points indicated that at $p = 0.05$ level, pSTAT6 at 0 min was significantly lower than pSTAT6 at all other time points except the 25 min and 120 minute time points (Fig. 8). This implies that the first peak of pSTAT6 occurs between 0 and 25 min and the second one between 25 and 120 min.

We hypothesized that the dynamic information contained in the STAT6 phosphorylation time course, especially the characteristic shape of the oscillating curve, could be used

to infer the regulatory mechanisms involved in IL-4 signaling. We sought to use this information to investigate the importance of 4 distinct regulatory mechanisms described in Section 3.1: i) reversible inactivation of PTPs by oxidation; ii) ROS mediated cytosolic accumulation of PTPs; iii) reversible inactivation of JAK by oxidation; and iv) dependence of nuclear-cytosolic shuttling of STAT6 on its phosphorylation state. While the first three are directly influenced by redox state of the cell, the fourth is not. To investigate the systemic effects of these mechanisms, we constructed a library of models of IL-4 signaling to represent various combinations of these four regulatory mechanisms. Next, we assessed these models based on their ability to produce an oscillating curve with characteristics similar to those seen in the experimental data. The details of this process are described below.

The IL-4 signaling network was divided into 5 regulatory modules and by taking different combinations of these modules, a library of 16 different models was constructed (details in Fig. 9). This library covers all possible combinations of the 4 mechanisms listed above. Next, simplified ODE representation of all 16 models were obtained using a rationale based approach to reduce model complexity. Specifically, linear chains of events such as sequential assembly of active receptor complex, or dimerization of phosphorylated STAT6 were collapsed into a single reaction. JAKs, which are constitutively bound to the receptor, were not modeled explicitly and were assumed to be implicit in the receptor. Different PTPs that can act on STAT6 were abstracted as a single generic PTP. The various network topologies obtained were coded into systems of ordinary differential equations assuming elementary mass action kinetics for all reactions. Parameters of the models were manually adjusted so that total pSTAT6 dynamics roughly matched the experimentally observed dynamics. For each model, 50,000 sets of parameters were randomly sampled in a fixed space spanning one order of magnitude around the estimated parameter vector, the model was simulated for all sampled parameter vectors and the dynamics of total pSTAT6 (i.e., nuclear and cytosolic pSTAT6) were recorded. The predicted pSTAT6 traces were qualitatively and quantitatively compared with the experimental results as described next to judge the fitness of the models.

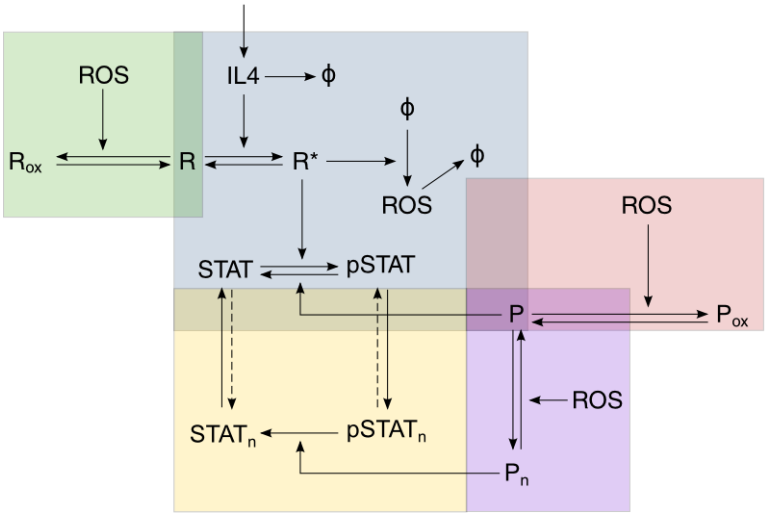

Figure 9: Creating a library of models of IL-4 signaling. Four regulatory modules were constructed around the core of IL-4 initiated STAT6 signaling. The core module (blue box) comprises IL-4 induced receptor (R) activation and subsequent STAT activation. Activated receptor upregulates ROS which can affect signaling through three different modules: reversible phosphatase (P) oxidation (red box), reversible JAK (assumed to be implicit in the receptor) oxidation (green box), or by modulating nuclear-cytosolic shuttling of the phosphatase (purple box). The last module (yellow box) relates to nuclear-cytosolic translocation of STAT6. This module represents two possible variations: i) the dashed arrows are absent and STAT6 trafficking is unidirectional and dependent on its phosphorylation state; ii) the dashed arrow are present and STAT6 translocation is independent of its phosphorylation state. Keeping the blue module in place, the red, green and purple modules were added or not and the dashed arrow in the yellow module were included or not. This results in a total of 16 different models representing all possible combinations of the 4 regulatory modules.

The models were first tested qualitatively based on their ability to reproduce the oscillatory behavior observed in the experimental data. This was done by counting the number of local maxima in each pSTAT6 trace produced by the models. All simulations produced two or fewer peaks, and traces that could produce exactly two distinct local maxima were taken to qualitatively match the oscillations observed in the experimental data. Among the 16 models, 7 failed to produce any oscillating traces for total pSTAT6. Of the remaining 9 models which generated one or more oscillating traces, 5 models produced fewer than 50 instances (0.1% of total number of MC simulations) of oscillating pSTAT6 (Fig. 10). Using this threshold of 0.1%, 12 configurations were rejected as likely models on a purely qualitative basis. Notably, all the 8 models in which STAT6 translocation was independent of its phosphorylation state consistently produced none or extremely small numbers of oscillating pSTAT6 traces. This strongly suggests that cycling of STAT6 between nucleus and cytosol is phosphorylation dependent. Only 4 models demonstrated the occurrence of two distinct peaks for more than 0.1% of the 50,000 MC simulations (Fig. 10). All 4 of these models included PTP oxidation as a redox regulatory mechanism. The model that had PTP oxidation as the only ROS mediated mechanism (first bar in Fig. 10) generated the most instances of oscillating pSTAT6 traces. The other two redox regulated mechanism, JAK oxidation and ROS mediated nuclear translocation of PTP, could not cross the 0.1% threshold when acting alone; however, combining one or both of these mechanisms with PTP oxidation allowed oscillation to occur. Nevertheless, fewer instances of oscillating traces were generated when either one of these mechanisms was combined with PTP oxidation, and even fewer when both were added in together (Fig. 10).

Quantitative comparison of features of the oscillating curves generated from the simulations with the experimental data provides further support to PTP oxidation as the prime mechanism of redox regulation in IL-4 signaling. A smoothing spline was fitted to the mean pSTAT6 data and features of the curve including heights of the two peaks, separation between them and the value at the final time point were extracted (Fig. 11a). Simulations

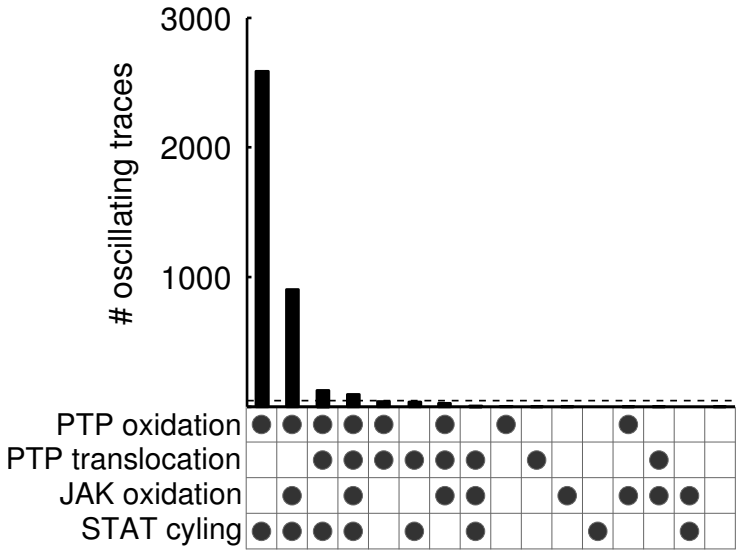

Figure 10: Models that reproduce oscillating pSTAT6 dynamics. For each model 50,000 MC simulations were run and dynamics of total phosphorylated STAT6 were analyzed. Counts of simulations that produced oscillatory pSTAT6 dynamics are shown. The dot matrix under the x-axis indicates the regulatory mechanisms included in each model. Dots in the first three rows mark inclusion of the following redox regulatory mechanisms: row 1, PTP oxidation (red module in Fig. 9); row 2, ROS mediated PTP translocation (purple module in Fig. 9); row 3, JAK oxidation (green module in Fig. 9). A dot in the fourth row means STAT6 cycling between nucleus and cytosol was dependent on its phosphorylation state (dashed arrows excluded from the yellow module in Fig. 9), whereas a blank means that cycling was phosphorylation independent (dashed arrow included in the yellow module). Bars below the dashed line correspond to models for which under 0.1% of all MC simulations produced oscillatory behavior.

that produced two distinct local maxima for the total pSTAT6 trace were identified for each model. The features indicated in Fig. 11a, were extracted from the simulated curves. Ratio of peak heights, separation between the peaks and ratio of final value to first peak were computed and compared with the experimental results. Representative results are shown for two models in Fig. 11(b, c, d and e). When only PTP oxidation was included as a mechanism of redox regulation, not only did the model produce most instances of oscillating curves, but the shapes of these curves also conformed well with the measured dynamics (Fig. 11b and d). However, when other ROS dependent mechanisms were added on to the model, both the number of oscillating curves and their similarity with experimental data worsened (Fig. 11c and e). Similar results were obtained when PTP oxidation model was compared with any other model.

Taken together, these results provided very strong support to two of the four regulatory mechanisms considered and we concluded that i) PTP oxidation is the most important mode of redox regulation in IL-4 signaling; and ii) nuclear-cytosolic translocation of STAT6 is phosphorylation dependent.

3.3.3 Inhibition of protein synthesis or protein degradation amplifies STAT6 phosphorylation

Jurkat cells pretreated with cycloheximide (CHX), an inhibitor of protein synthesis, were stimulated with IL-4 and time course of STAT6 phosphorylation was acquired. Phosphorylated STAT6 increased significantly within five minutes of IL-4 stimulation and then decreased steadily for 2 hours (Fig. 12a). Furthermore, the average phosphorylation of STAT6 was higher in CHX pretreated cells as compared to untreated cells. Pretreating the Jurkat cells with MG132, an inhibitor of 26S proteasome complex, prior to IL-4 stimulation also increased mean STAT6 phosphorylation compared to cells not pretreated with MG132 (Fig. 12a).

SOCS1 and SOCS3 have been shown to be downregulate IL-4 signaling [79]. We measured SOCS3 time course in response to IL-4 stimulation in order to elucidate the

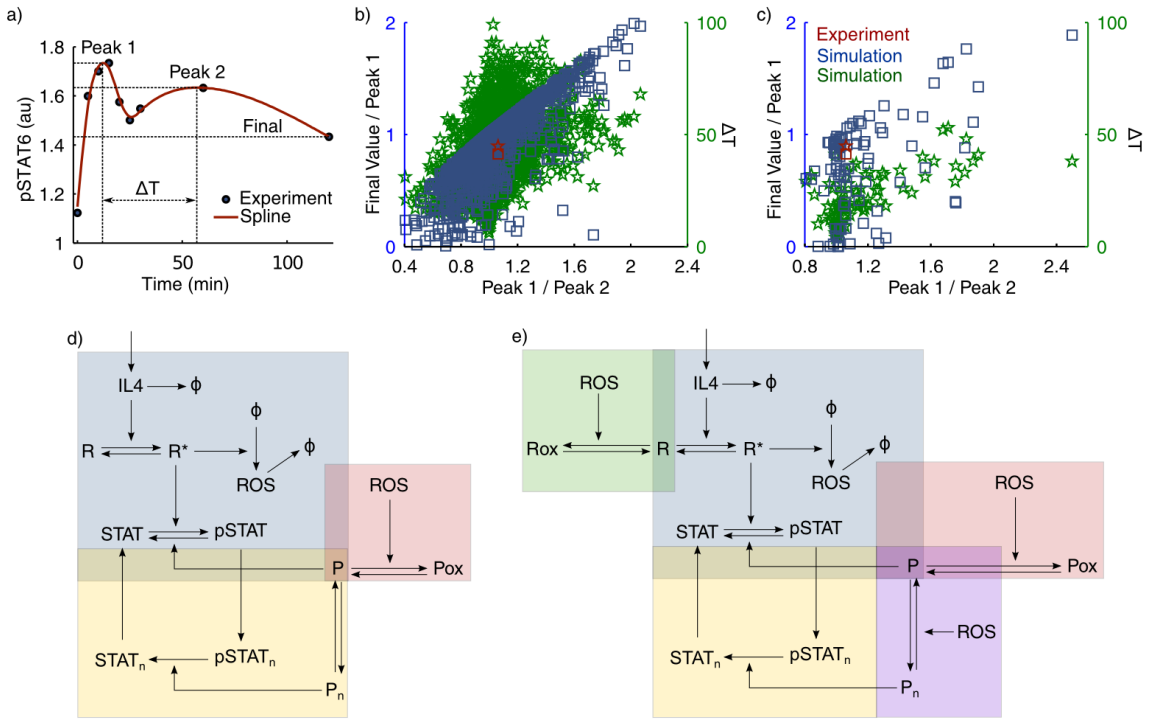

Figure 11: Inferring regulatory mechanisms using Monte Carlo simulations. (a) A smoothing spline (continuous line) was fitted to mean pSTAT6 time course, shown by dots, under IL-4 stimulation and distinguishing features of the curve were extracted. (b, c) Ratio of final value to height of peak 1 (left axis and squares) and time separation between peaks (right axis and stars) are plotted against the ratio of peak heights. Data points indicated by red markers show points corresponding to the fitted spline in a. (d, e) Models corresponding to simulation results in b and c, respectively. Simulation results overlap better with experimental results in b than in c; this was confirmed by numerical calculation of average distances between experiment and simulation generated data points.

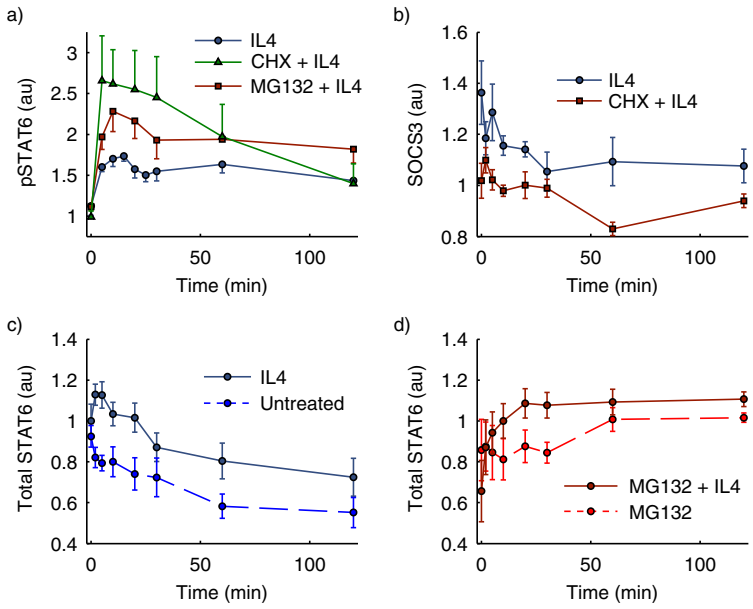

Figure 12: Mechanisms of downregulation in IL-4 signaling. (a) Jurkat cells were pretreated with 10 μM MG132, 20 μg/ml CHX or PBS (mock inhibitor) for 1 hour prior to stimulation with 100 ng/ml IL-4. pSTAT6 was measured. (b) SOCS3 was quantified in cells pretreated for 1 hour with cycloheximide (CHX) or PBS and stimulated with IL-4. (c) Total STAT6 was measured in Jurkat cells left untreated or treated with IL-4. (d) Jurkat cells were pretreated with MG132 and total STAT6 was measured with or without IL-4 stimulation. y-axis shows background subtracted normalized MFI values obtained using flow cytometry; all plots show mean ± standard error based on n = 3; au, arbitrary units.

pSTAT6 amplifying effect of CHX. SOCS3 expression in IL-4 treated Jurkat cells decreased from its baseline level over two hours (Fig. 12b). In cells pretreated with CHX, the basal expression of SOCS3 was reduced and did not change significantly over two hours. This suggests that inhibition of protein synthesis by CHX lowered the basal concentration of SOCS3, and the reduced SOCS3 expression weakened the downregulating signal present at time 0 to allow a larger response to IL-4 at a very early time point (Fig. 12a).

To assess the effect of MG132 on STAT6 levels in Jurkat cells, we quantified total STAT6 in cells stimulated with IL-4 with or without MG132 pretreatment. In the absence of any treatment, total STAT6 expression decreased over time. Stimulation with IL-4 slowed down the decrease in STAT6 (Fig. 12c). Pretreatment with MG132 lowered the average expression of STAT6 slightly and stopped the decay of STAT6 over time. Addition of IL-4 to MG132 pretreated cells resulted in further elevation of total STAT6 level over

time (Fig. 12d). These results suggest that proteasome mediated degradation of STAT6 acts as a mechanism to downregulate IL-4 signaling. Furthermore, IL-4 treatment elevates total STAT6 levels, whether or not the cells are exposed to MG132. This indicates that phosphorylation following IL-4 stimulation may be protecting STAT6 from proteasomal degradation.

3.3.4 A systems model of ROS mediated regulation of IL4 signaling

The experimental results presented above taken together with the results from the MC simulations suggest a complex picture of the IL-4 pathway with many regulatory mechanisms operating in tandem. We constructed an ordinary differential equation model of the IL-4 signaling pathway using mass action kinetics that incorporates these important regulatory mechanisms and explains the observed dynamics of various molecular species under a variety of experimental conditions. A graphical representation of the model is shown in Fig. 13. Mechanisms found to be most important from the MC analysis were built into the model. Experimental results on downregulation mechanisms were used to include SOCS and STAT6 degradation as important control mechanisms.

In the interest of parsimony several simplifying assumptions were made in the model. The IL-4 receptor alpha chain and the common gamma chain were not modeled separately. Instead, an abstraction of the receptor complex in the form of a single transmembrane molecule that binds IL-4 and gets activated was used. The JAK1 and JAK3 molecules that are constitutively bound to the receptor chains were also not modeled explicitly and were assumed to be implicit in the receptor molecule. SOCS family proteins have been shown to inhibit JAK/STAT signaling by binding directly to phosphorylated JAK molecules inhibiting their function, or by binding to the receptors and indirectly inhibiting JAK [9]. Since JAK and receptor molecules were abstracted into a single species, SOCS binding to activated receptor was taken to represent both possibilities. Dephosphorylation of the receptor complex was assumed to result in dissociation with SOCS. SOCS1 and SOCS3

are known to affect IL-4 signaling and were modeled together as a generic SOCS molecule. Multiple phosphatases including PTP1B and TCPTP have been shown to act on STAT6 [80, 81]. Similarly, multiple phosphatases, such as CD45 and SHP-1, can dephosphorylate the receptor and JAK molecules [57, 65]. We assumed that STAT6 and the receptor complex were dephosphorylated by distinct individual PTPs. All reaction were modeled using the law of mass action except active STAT6 mediated SOCS production ; the rate of production of SOCS was assumed to increase monotonically with the concentration of active STAT6 in a saturating fashion to model saturation of transcription factor binding sites.

Activation of the IL-4 receptor in Jurkat cells induced transient production of ROS (Fig. 7b). ROS dynamics estimated from experimental data were used as an input to the model, thus eliminating the need to explicitly model the sources and mechanisms of ROS production and elimination. Reduction of oxidized proteins was assumed to follow first order kinetics; in other words, the reducing capacity of the cell was assumed to be constant over time. The more reducing environment of the nucleus [67, 82] was modeled by eliminating any protein oxidation from the nuclear compartment.

Evolutionary strategies with hyper-mutation algorithm (described in Chapter 4) was used to estimate the parameters of the model. The objective function defined in the methods section was minimized to fit the model to experimentally measured time courses of multiple species across 3 different experimental conditions (Fig. 14). The fitted model explains well the dynamics of i) pSTAT6 in Jurkat cells following IL-4 stimulation with or without pretreatment by either MG132 or CHX (Fig. 14a, b); ii) total STAT6 following IL-4 stimulation with or without MG132 (Fig. 14c); and iii) SOCS3 under the conditions of IL-4 stimulation with or without inhibition by CHX(Fig. 14d).

3.3.5 Model successfully predicts behavior under extremes of intracellular redox state

To validate the model we tested its ability to predict the dynamics of IL-4 signaling under experimental conditions that were not used to train the model. DPI pretreatment followed

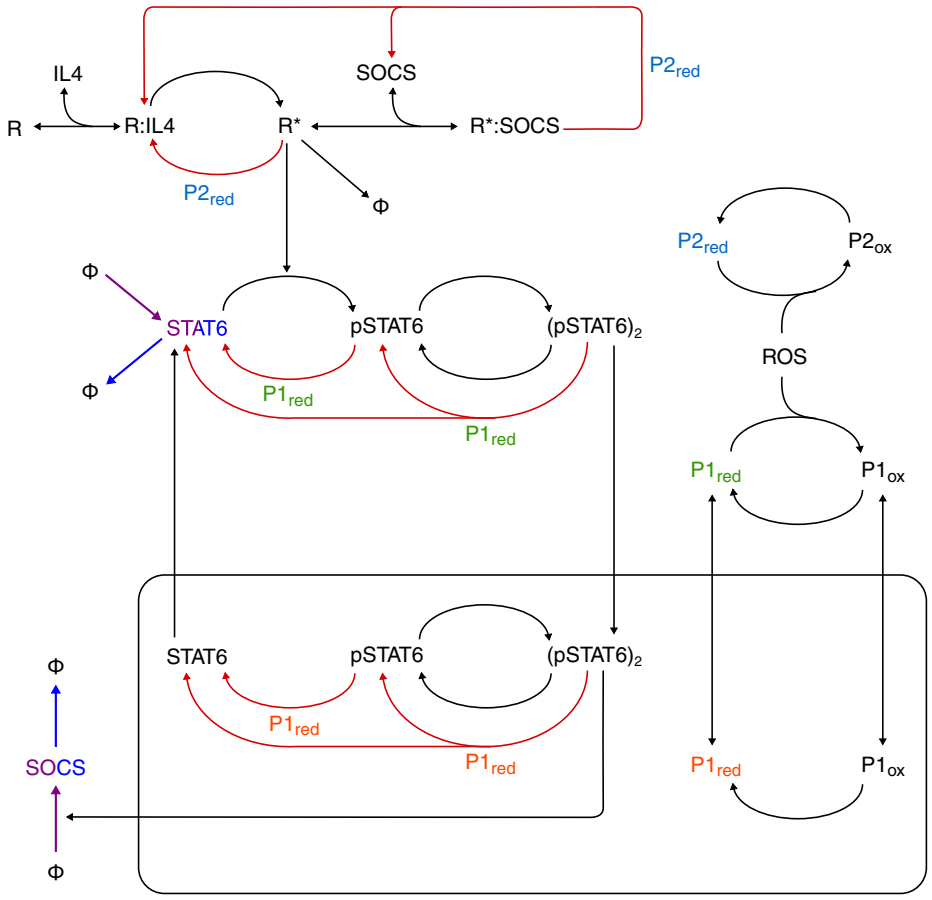

Figure 13: The IL-4 signaling network. Regulatory mechanisms including ROS mediated reversible phosphatase oxidation, proteasome mediated degradation of STAT6 and down-regulation by SOCS are incorporated into the model. P1 and P2 represent PTPs acting on STAT6 and the receptor complex, respectively; red edges, dephosphorylation reactions catalyzed by indicated phosphatases; arrows pointing into other edges, enzyme catalyzed reactions; Φ, infinite sources or sinks; purple edges and nodes, points affected by CHX in the model; blue edges and nodes, points affected by MG132. Intermediate complexes formed in enzyme catalyzed reactions are not explicitly shown.

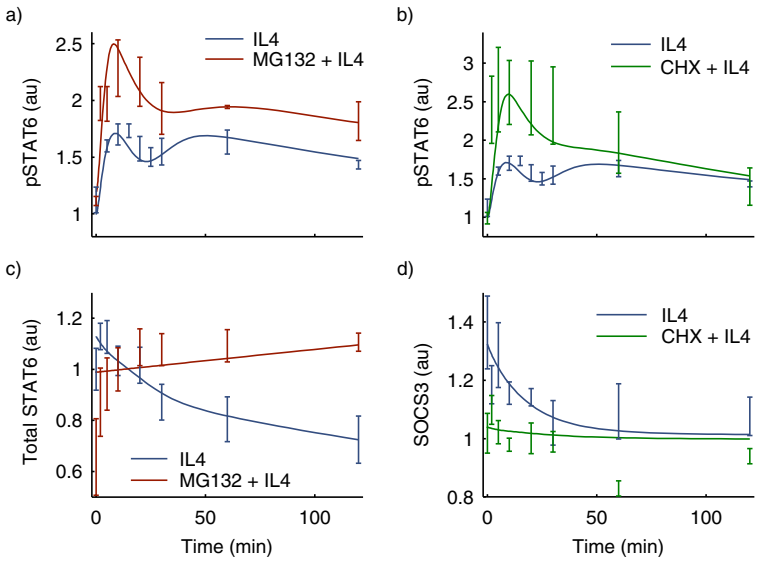

Figure 14: Model of IL-4 pathway fitted to experimental data. Parameters of the model were estimated to fit multiple species across 3 different experimental conditions. (a) Total phosphorylated STAT6 (cytosolic and nuclear) under IL-4 stimulation with or without MG132 pretreatment. (b) Total pSTAT6 under IL-4 stimulation with or without CHX pretreatment. (c) Total STAT6 (phosphorylated and unphosphorylated, cytosolic and nuclear) under IL-4 stimulation with or without MG132 pretreatment. (d) Generic SOCS molecule of the model fitted to experimental measurements of SOCS3 under IL-4 stimulation with or without CHX pretreatment. Simulation results were scaled as described in Section 3.2.3.

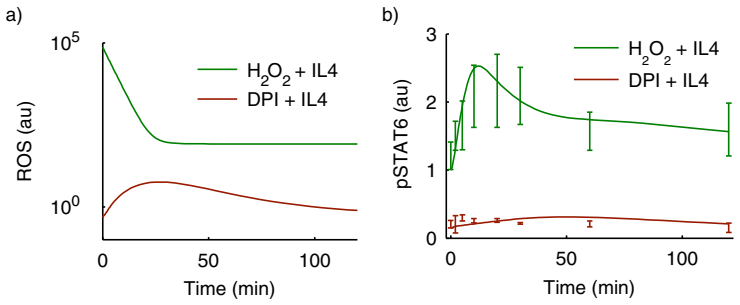

Figure 15: Model predicts behavior under extremes of redox state. (a) DPI pretreatment and addition of exogenous H_2O_2 with IL-4 stimulation were simulated using the fitted model. The predictions of the model overlayed with quantitative experimental data. (b) ROS profiles used to simulate DPI pretreatment and the effect of exogenous H_2O_2.

by IL-4 stimulation and addition of exogenous H_2O_2 along with IL-4 were simulated using the fitted model. The experimentally measured ROS profile under DPI pretreatment (Fig. 15a) was used as input to simulate the effect of DPI in the model. To mimic the effect of 10 μM exogenous H_2O_2 added along with IL-4, a large bolus of exponentially decaying ROS was added to the experimentally measured ROS profile under IL-4 treatment (Fig. 15a). The model predicted severely attenuated STAT6 phosphorylation under DPI pretreatment, whereas addition of exogenous H_2O_2 with IL-4 was predicted to amplify STAT6 phosphorylation in comparison to IL-4 treatment alone (Fig. 15b). Both these predictions matched quantitatively with experimental results, showing that the model is robust enough to predict the dynamics of IL-4 signaling over a wide range of redox conditions.

We attempted to further validate the model using the J45.01 cell line, a derivative of the Jurkat cell line. However, due to difficulty in characterizing the differential expression of multiple proteins in the J45.01 cells, we decided not to use these cells to test the model (details in Section B.5).

3.4 Discussion

With the recognition of reactive oxygen species as important regulators of cell signaling, new targets of thiol-based oxidative regulation are being discovered with consistent regularity. Even though most of these redox sensors seem to rely on the same principle of

cysteine thiol post-translational modification, their responses to oxidation can be very different [61]. For example, cysteine oxidation can result in loss of phosphatase activity in PTPs, loss of kinase activity in JAKs or altered subcellular localization of TCPTP. Since all of these processes are driven by the same underlying chemistry, it follows that given equal access to ROS, all these processes could take place simultaneously. Since the effects of multiple redox regulated changes in a given context may not always be consistent, inferring the underlying mechanism based on experimental data becomes challenging. For instance, in the context of IL-4 signaling, a heightened oxidative state can lead to PTP inactivation resulting in signal amplification, but can also cause JAK inactivation which would have the effect of attenuating the signal. While the individual outcomes of PTP or JAK oxidation are relatively easier to predict in a qualitative manner, the joint outcome of these changes is much harder to guess. Of course, ROS mediated regulation does not operate in a vacuum and overlaying it with other modes of regulation that are independent of ROS further complicates the picture. Recognizing this complexity, we have adopted a quantitative, systems level approach in our work to infer the mechanisms of redox regulation in the IL-4 pathway and found strong evidence to support reversible oxidative inactivation of PTPs as the dominant mode of ROS mediated regulation.

Jurkat cells were observed to quickly increase intracellular oxidation in response to IL-4, and DPI was able to suppress this ROS production. DPI is a flavoprotein inhibitor and known to inhibit the activity of NOX family enzymes. It has previously been shown that IL-4 signaling activates NOX1 and NOX5L in A549 cells to induce ROS production and DPI inhibits this [130]. Jurkat cells have been reported to express NOX1 [13] which could be involved in IL-4 induced transient ROS production in these cells. Suppression of ROS by DPI pretreatment significantly lowered baseline STAT6 phosphorylation and severely attenuated pSTAT6 response to IL-4 treatment, indicating that the ROS produced by activation of IL-4 receptor were playing an important role in the signaling pathway. The oxidation of CM-H_2DCFDA at the 0 min time point was also lower in the DPI pretreated

cells (Fig. 7a). We interpret this as maintenance of a positive concentration of ROS in the basal state keeping a fraction of STAT6 in the phosphorylated state. Failure of the DPI treated cells to respond to IL-4 suggests that baseline ROS also have a role in sustaining the system in a "primed" state so that it is ready to quickly respond to an activating stimulus. Supplementing IL-4 induced ROS with exogenous H_2O_2 amplified the pSTAT6 response; however, on its own, the same concentration of H_2O_2 did not elicit STAT6 phosphorylation. These observations taken together suggest that ROS may be playing two roles; first, to keep the system ready to respond to an input signal and second, to amplify the response once it is initiated by IL-4 input.

Having confirmed that IL-4 signaling in Jurkat cells is redox regulated, we used computational analysis relying on quantitative as well as qualitative information obtained experimentally to understand the control mechanisms by which ROS regulate IL-4 signaling. Experimentally acquired time course of IL-4 induced STAT6 phosphorylation in Jurkat cells had a distinctive shape presenting slowly oscillating dynamics over a two hour time period. This feature combined with simplified models of the pathway proved a remarkably useful tool for selecting models based simply on their ability to reproduce experiment-like pSTAT6 oscillations. When possible combinations of likely mechanisms were systematically examined, PTP oxidation stood out as the most likely mechanism by which ROS mediated regulation can take place. The other mechanisms considered, namely, JAK oxidation and ROS mediated PTP translocation, were not sufficient on their own to explain the observed dynamics. They did reproduce the oscillatory behavior when assumed to operate in tandem with PTP oxidation, but with a lower success rate and poorer quantitative matching with experimental data. Therefore, even though model complexity increased when additional redox regulatory mechanisms were added along with PTP oxidation, the quality of prediction of the model only worsened when tested within the selected parameter bounds. This double failure of the more complex models is compelling evidence in support of the PTP oxidation model which is not only parsimonious, but also matches the

data better, both qualitatively and quantitatively.

Examination of the PTP oxidation model suggests a motif similar to a coherent feed forward loop [84]. Addition of IL-4 results in rapid STAT6 phosphorylation resulting in the first pSTAT6 peak, and the activated receptor simultaneously upregulates intracellular ROS levels. As the effect of IL-4 starts to wane, the ROS oxidize enough PTPs to give a second boost to pSTAT6 levels and contribute to sustaining the second peak. This requires well tuned timings of the various events, which is why only a small number of the MC simulations produce the oscillatory behavior. Inactivation of JAK by oxidation and ROS mediated accumulation of PTP in the cytosol have a negative effect on STAT6 phosphorylation which is counter to the effect of PTP oxidation. These mechanisms, rather than help sustain the second peak, act to abolish it and are probably not relevant in the IL-4 pathway.

The tendency of pSTAT to decrease non-monotonically after reaching its first maximum has been previously found in erythropoietin mediated JAK2/STAT5 signaling [139]. However, in that case only cytosolic STAT was experimentally observed. The behavior was explained by phosphorylation dependent translocation of STAT5 into the nucleus and delayed translocation of dephosphorylated STAT5 out of the nucleus. Another computational study reported slow, damped oscillations of nuclear pSTAT1 caused by a combination of phosphorylation dependent nuclear-cytosolic movement of STAT1 and SOCS mediated negative feedback [161]. In contrast to these studies, we have measured total pSTAT6 present in the nuclear and cytosolic compartments. While these existing models do not attempt to explain the dynamics of total pSTAT and do not account for the role of ROS in JAK/STAT signaling, they provide important clues regarding the possible mechanisms that drive the observed oscillations. In agreement with these studies, we found in our analysis that phosphorylation dependent translocation of STAT6 was a very important control mechanism. Independent studies have concluded that cycling of STAT6 between cytosol and nucleus may or may not be be affected phosphorylation state depending on the cellular system [4, 16]. Nonetheless, even when STAT6 trafficking was found to be independent of

its phosphorylation state, greater residence time in the nucleus was reported for pSTAT6 due to DNA binding [16]. In agreement with these studies, our simulation results overwhelmingly favored configurations that supported preferential nuclear localization of the phosphorylated form. Future studies will be required to establish how nuclear shuttling of STAT6 relates to its phosphorylation state in Jurkat cells.

While the kinase-phosphatase balance is an important determinant of signaling dynamics, many other downregulation mechanisms are built into signaling networks to maintain a tight control over the response. Proteasomal degradation of STAT is known to play a role in downregulating cytokine signaling. Previous studies have found that inhibition of proteasome stabilizes the phosphorylated form of some members of the STAT family but not others [150]. In the case of STAT6, reported roles of proteasomal degradation have been suggested to range from not being significant to being very important by affecting STAT6 phosphorylation either directly, or through intermediaries [4, 138, 49]. In Jurkat cells we found that MG132 treatment increased IL-4 induced STAT6 phosphorylation and also stabilized total STAT6 levels irrespective of IL-4 treatment. IL-4 treatment had the effect of slightly increasing total STAT6 levels, whether or not the cells were treated with MG132. This suggests that phosphorylation had the effect of protecting STAT6 from degradation. Implementing a fixed rate of decay of unphosphorylated STAT6 and protecting pSTAT6 from degradation in the model helped explain the observed behavior under MG132 treatment.

Feedback regulation through SOCS family proteins is another mechanism for regulating JAK/STAT signaling. SOCS1 and SOCS3 expression has been variably reported to play a role in IL-4 signaling, in some cases being found to be important suppressors while not being significant in others [79, 49]. We measured SOCS3 protein in response to IL-4 and found that IL-4 treatment did not cause an increase in SOCS3 expression in 2 hours. Cycloheximide treatment lowered the basal expression of SOCS3 which again could not be increased by IL-4. In cycloheximide pretreated cells a much stronger response to IL-4 was

seen at very early time points. This can be attributed to the decrease in baseline level of SOCS3, and possibly other SOCS proteins such as SOCS1 which could be affecting IL-4 signaling in Jurkat cells. Not ruling out the involvement of other members of the SOCS family, we included a generic SOCS molecule in our model which could be upregulated by activated STAT6. Lowering the baseline level of this SOCS protein following CHX pretreatment was central in explaining the observed dynamics of SOCS3 and pSTAT6 in the model.

Based on inferences from analysis of reduced models of redox regulation and knowledge gained from the experimental data, we have developed the most comprehensive model to date of the IL-4 signaling pathway. The model incorporates redox regulation through reversible oxidation of PTPs and mechanisms for downregulation of the IL-4 signal through proteasomal degradation of STAT6 as well as feedback regulation through SOCS proteins. Interactions between these regulatory mechanisms allowed the model to successfully reproduce the dynamics of several molecular species over a variety of experimental conditions. We tested the model in highly oxidizing and reducing conditions and found that predictions of the model matched well with experimental data. The ability of the model to capture the dynamics of IL-4 signaling under normal as well as extreme redox conditions provides strong validation to our model. It also suggests that as a mechanism of redox regulation, PTP oxidation could be a relevant phenomenon over a wide range of cellular redox states. Collectively, the computational analysis indicates that while ROS mediated regulation is a very important arm of the control machinery in IL-4 signaling, systemic behavior of the pathway emerges from interactions of redox and non-redox regulatory mechanisms. For instance, none of the redox regulation mechanisms considered in our analysis were sufficient to explain pSTAT6 dynamics when working alone (Fig. 10), but combining them with other ROS-independent mechanisms changed the behavior of the system qualitatively. In other words, without considering the role of ROS-independent mechanisms we would have reached a faulty conclusion. This results is a strong argument in favor of adopting a

quantitative, systems based approach in trying to understand redox regulation of complex signaling networks.

An important concern regarding the ability of ROS to play a significant role in modulating cell signaling has to do with the relatively slow rates of H_2O_2 mediated cysteine oxidation in proteins. Since intracellular ROS concentration was modeled using direct scaling of fluorescence based measurements, it could not be assigned real units in the model. This means that protein oxidation rates are also to be understood in terms of these arbitrary units. However, the scaling factor was chosen such that the absolute value of ROS concentration was in the order of 10^2 units of ROS in simulations of IL-4 stimulated cell. Since intracellular ROS concentration is thought to be in the sub-micromolar range [135], a 1:1 scaling can be assumed between the model's arbitrary ROS units and nanomolarity. In other words, assuming 1 unit of ROS in the model corresponds to 1 nM ROS in the real cell would scale the simulated ROS level to the order of 100 nM, which is a reasonable estimate of intracellular H_2O_2 concentration. Assuming this scaling, the estimated rate of PTP oxidation turns out to be 2×10^6 $M^{-1}s^{-1}$. In a previously published systems model of H_2O_2 dispersion in Jurkat cells the second order rate of H_2O_2 mediated oxidation was estimated to range between 10×10^7 $M^{-1}s^{-1}$for the fastest reactions involving catalase and peroxiredoxin to 10×10^4 $M^{-1}s^{-1}$for the average intracellular protein [1]. The estimated rate of PTP oxidation in our model lies within this range. That it lies on the higher side is consistent with the fact that PTPs have a higher propensity towards oxidation than the average protein. These rates are still much higher than *in vitro* measurements of PTP oxidation rates, but *in vitro* estimates themselves have been found to be much slower than observed rates of PTP oxidation in insulin signaling [141]. Several hypotheses have been proposed to explain this high apparent rate of oxidation, including localization of ROS to create high concentration and transfer of oxidation state through relay proteins, and this continues to be an area of active investigation.

While computational models of ROS production and consumption have previously been

developed for cells [1, 5], the question of how competing ROS dependent mechanisms regulate cell signaling has not been addressed in computational studies. This is the first study to our knowledge that comprehensively explores the question of redox regulatory mechanisms in cell signaling using computational modeling. Aside from suggesting the most likely mode of redox regulation in the IL-4 pathway, our results also demonstrate the value of the integrative view in understanding redox regulation of cell signaling. Finally, the model suggests several interesting avenues for experimental and computational investigation in the future. For example, is nuclear-cytosolic cycling of STAT6 unidirectional or is it independent of phosphorylation state and the model is only reflecting increased residence time of pSTAT6 in the nucleus due to mechanisms like DNA binding? Considering that locally elevated concentrations of ROS may be important for their regulatory effects, and that cell membrane bound NOX1 may be an important source of ROS in IL-4 signaling, regions close to the cell membrane are likely to have the highest localized ROS concentrations in the cytosol. How is it then that JAK, which is constitutively bound to the receptor and always close to the membrane, contributes so little to regulating IL-4 signaling? The model was simplified by pooling multiple phosphatases into two groups and assuming that each pool has distinct targets in the form of STAT6 or the receptor/JAK complex. Furthermore, both these pools were assumed to have identical access to ROS and identical oxidation/reduction rates. However, in reality phosphatases may be shared between different targets, may have different rates of reduction and oxidation or may be more or less readily accessible by ROS. How can these factors be accounted for in the model and how do they influence signaling dynamics? The model presents these and other questions that require careful quantitative examination before the puzzle of redox regulation in cell signaling can be fully resolved.

CHAPTER IV

EVOLUTIONARY STRATEGY WITH HYPER-MUTATION: A RESTART STRATEGY TO IMPROVE OPTIMUM FINDING

4.1 Introduction

An essential step in the construction of biologically relevant models is estimation of parameters to fit model behavior to measured biological data. A variety of optimization algorithms are at a modeler's disposal to determine parameter sets of ODE systems that minimize the distance between model prediction and measured data [87], but because the objective function in ODE systems cannot be explicitly determined, often derivative-free approaches (the so called black-box methods), e.g., direct search methods [55, 96], simulated annealing [69], evolutionary computation methods [163] etc., are preferred. Such methods are computationally expensive as they require solving of the ODE system at all test points. Furthermore, ODE models with even a moderate amount of complexity often have highly multimodal objective functions, making it hard to find the true global optimum among the many local optima [6]. As a consequence of these factors, algorithms that can get close to the global optimum in multi-dimensional search spaces with relative efficiency are preferred.

Evolutionanary strategy (ES) is a population-based, stochastic, black box optimization algorithm inspired by the process of biological evolution [125]. A comparative study of several commonly used global optimization algorithms found that algorithms based on ES performed better than competing algorithms when tested on a specific systems biology model [91]. Starting with a random initial population of candidate solutions to the optimization problem, ES operates by repeated application of the operators of mutation,

recombination and selection to produce successive generations until defined stopping criteria are satisfied [125]. The mutation operator is important for introducing variation in the population and the strengths of mutations of all individuals are controlled by a set of internal parameters known as strategy parameters or step sizes. The step sizes need to be controlled, as very strong mutations can delay convergence and prevent directed evolution, while weak mutations can slow convergence and trap the solution in a local minimum [102]. Different types of strategy parameter control methods have been developed for use with ES, e.g., self-adaptation using mutative strategy parameter control and derandomization of self-adapdation using CMA [48]. Irrespective of their implementation details, all variants of ES utilize gradual damping of the step size to ensure convergence. As a result, in later stages of the evolution as the population begins to converge the step size becomes increasingly small, until the evolution slows down and the population tends to get trapped in a local minimum. Because of the stochastic nature of ES, each optimization run is likely to yield a different solution. This stochasticity is exploited to improve optimum finding by using restart strategies, i.e, repeated execution of the optimization algorithm, possibly with different settings each time, and selecting the best among several possible solutions [58]. The main drawback of restart strategies is the extra computational cost incurred by repeated runs of the optimization algorithm.

In this chapter a variant of ES is presented that uses a partial restart strategy [58] to improve the global optimum finding ability of the algorithm without dramatically increasing the computational cost. We have developed and empirically tested a simple method that dynamically monitors the evolution of the fitness score and when required, operates on the strategy parameters to create a subpopulation of hyper-mutants, hence the name ES-HM, to help the evolving population escape local minima at later stages of the algorithm and enable convergence to a better optimum. We tested the algorithm on a set of benchmarking functions under a variety of conditions and found that ES-HM performed better than other methods for several test functions under most conditions. An example of application to a

systems biology problem is also presented; ES-HM was used to estimate the parameters of a model of IL-4 signaling to fit the model to an experimentally derived data set. ES-HM was able to find better solutions even when the parameters of the model were poorly constrained.

4.2 Methods

The ES-HM algorithm described in Section 4.3.1 was implemented in Matlab. Source code of the Matlab implementation is provided in Listing 1. A suite of test functions was selected from a collection of benchmarking functions [140, 47] to assess the performance of the algorithm. The 1) sphere, 2) Schwefel's problem 2.21, 3) Rastrigin, 4) Ackley, 5) Rosenbrock, 6) Griewank, 7) Gallagher's Gaussian 21 peak, 8) rotated Weierstrass and 9) rotated Lunacek bi-Rastrigin functions were selected to represent a combination of separable, non-separable, unimodal and multimodal functions. The functions are defined in Appendix C.1.

The ODE model of the IL-4 pathway was coded and solved in Matlab. The ES-HM implementation was used to estimate the parameters and the objective function was defined as the root mean squared error between the model and average of normalized experimental data, summed over all time points and experimental conditions.

4.3 Results

To overcome the problem of stagnating search in ES due to very small step size in later stages of the search, we have developed a modification of the ES algorithm that scales up the step sizes of the evolving individuals along randomly selected dimensions if, i) the stopping criteria are satisfied; or ii) the evolution of the best score starts to stagnate over time. To prevent superfluous restarts, the evolution is stopped if three successive restarts result in no improvement of score or if a pre-set maximum number of restarts is achieved.

4.3.1 Evolutionary strategy with hyper-mutation

We present here the ES-HM algorithm in the context of a generic ES algorithm, but this strategy could easily be applied to other variants of the algorithm. To minimize the objective function $f : R^n \rightarrow R$ the algorithm consists of the following steps, with Steps 5-8 representing the hyper-mutation modifications we have introduced.

1. Initialize a population of μ individuals, the parents, where each individual is comprised of a pair of real-valued n-vectors $(\mathbf{x}_i, \boldsymbol{\sigma}_i)$, $\forall i \in \{1, \ldots, \mu\}$, where $\mathbf{x}_i$ and $\boldsymbol{\sigma}_i$ are object parameters and step-sizes, respectively. Generation number, $g = 1$; number of restarts, $R = 0$.

2. Recombine parents to generate λ new individuals, $(\mathbf{x}'_i, \boldsymbol{\sigma}'_i)$, $i \in \{1, \ldots, \lambda\}$.

3. Mutation: For all $i \in \{1, \ldots, \lambda\}$

   (a) mutate strategy parameters, $\boldsymbol{\sigma}'_i = \boldsymbol{\sigma}' \boldsymbol{\xi}_i$;

   (b) mutate object parameters, $\mathbf{x}'_i = \mathbf{x}'_i + \boldsymbol{\sigma}'_i \mathbf{z}_i$;

   where, $\boldsymbol{\xi}_i$ and $\mathbf{z}_i$ are real vectors whose values are determined by the specific flavor of ES algorithm.

4. Selection: Evaluate the fitness of $(\mathbf{x}'_i, \boldsymbol{\sigma}'_i)$, $\forall i \in \{1, \ldots, \lambda\}$. Select the fittest μ individuals to become the parents for the next generation. s^g = score of the fittest individual.

5. Check for stopping criteria and score stagnation. If

   (a) a stopping criterion is satisfied; or

   (b) if at least N_s generations have passed since last restart and the relative differences between scores of the fittest individuals over the last N_s generations are less than a threshold θ (i.e, for $g > N_s$, if

$$\frac{|s^i - s^{i+1}|}{s^i} < \theta, \forall i \in \{g - N_s, \ldots, g - 1\})$$

then go to step 6 to initiate hyper-mutation, otherwise, increment g by 1 and return to step 2.

6. Increment restart count R by 1. b^R = best score in generation g just before initiating hyper-mutation.

7. Introduce hyper-mutants by randomly scaling up on an average a fraction ϕ of all the step-sizes:
   For the j^{th} element σ_{ij} of the vector, $\boldsymbol{\sigma}_i$, $\forall i \in \{1, \ldots, \mu\}$, and $j \in \{1, \ldots, n\}$ generate a uniform random number r. If $r < \phi, \sigma_{ij} = \sigma_{ij} \times \rho, \rho > 1$. ρ determines the strength of hyper-mutation.

8. If $R > R_{max}$, stop.

9. If b^R, the best score just before a new round of hyper-mutation is initiated, does not improve for 3 successive value of R, stop.

ES-HM introduces 4 new internal parameters into the algorithm, namely, N_s and θ, which determine the stagnation criteria and ϕ and ρ, which define hyper-mutant frequency and hyper-mutation strength. For all subsequent analyses we have chosen, $N_s = n$, the problem dimension, and $\theta = 1\%$. We have implemented the (μ, λ) ES-HM algorithm in Matlab (Listing 1) with mutative strategy parameter control and multi-parent-recombination as described in Appendix C.2 [125]. Fig. 16 shows a comparison of the search characteristics of (μ, λ)-ES compared with (μ, λ)-ES-HM for the Ackley function. Search trajectories of ES and ES-HM are superimposed on the contour plot of the 2-dimensional Ackley function. The search was initialized identically for both algorithms to enable comparison. While ES quickly stopped in a local minimum (Fig. 16a), ES-HM was able to escape this minimum and reached close to the global optimum (Fig. 16b). A similar comparison of the two methods for the 30-dimensional Ackley function was performed (Fig. 16c). Starting under identical settings, the two methods proceeded identically for some time until ES stopped.

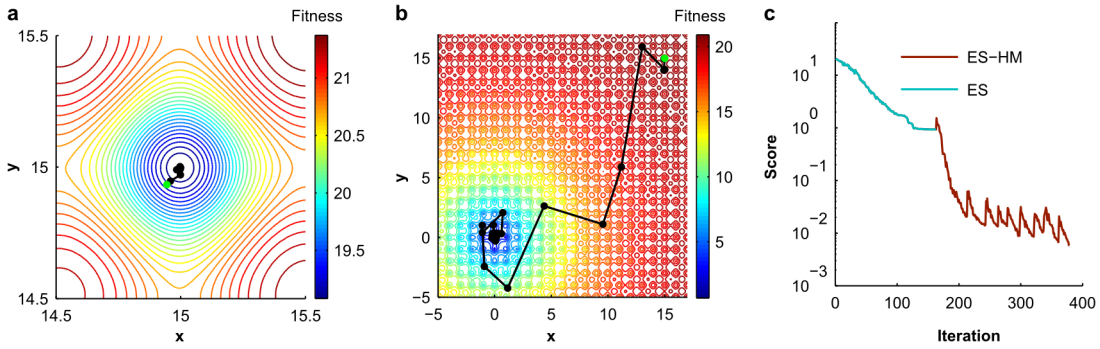

Figure 16: Comparison of search characteristics of ES-HM with ES. (μ, λ)-ES and ES-HM were used to find the global optimum of the 2-dimensional Ackley function in $[-30, 30]^2$ (contour plots in a and b). The search was started far from the optimum (0, 0) by forcing the initial population in $[14.5, 15]^2$. The random number generator was seeded identically for ES and ES-HM to enable comparison. Black lines, trajectory of best score; black dots, coordinates of the best individual; green dot, starting position. (a) ES stopped quickly in a local minimum. (b) ES-HM took a longer time but ended close to the global optimum. (c) Similar comparison on 30-dimensional Ackley function by starting (μ, λ)-ES and ES-HM with identically seeded random number generator. Best score for each generation is plotted. Search is identical in the beginning and scores coincide. ES stops in less than 200 iterations; ES-HM introduces hyper-mutants several times (spikes) ultimately improving the score by nearly 2 orders of magnitude.

ES-HM continued the search with increased step sizes and although the new step sizes often resulted in temporary worsening of the score (spikes in red line Fig. 16c), ultimately a better score was found. In the example shown in Fig. 16c, the score was improved by nearly two orders of magnitude by ES-HM.

4.4 ES-HM shows improved performance compared to other ES-based restart algorithms

As is clear from the description of the algorithm and Fig. 16c, ES-HM is a type of restart strategy. However, instead of forcing a complete restart, it only changes some randomly selected strategy parameters and can therefore be thought of as a soft or partial restart method [58]. To further assess the performance of the ES-HM algorithm, we implemented a (μ, λ) version of ES-HM as described above and compared it with 3 variants of ES, two of which are restart methods. First, (μ, λ)-ES-HM was compared with (μ, λ)-ES with mutative strategy parameter control and multi-parent recombination (hereafter, pure ES). Next,

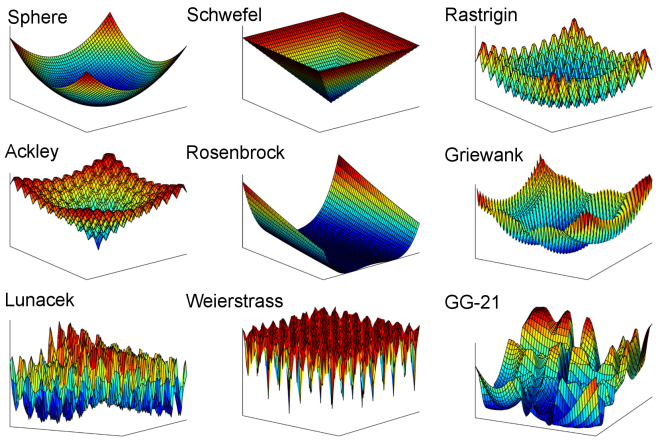

Figure 17: Two-dimensional representation of test function used.

we compared ES-HM with a naive restart algorithm, where the pure ES algorithm was independently run 10 times and the best solution was accepted (hereafter, naive restart). Finally, we compared it with an algorithm similar to the ES-IPOP restart strategy [8], where the population size is doubled with each restart and evolution stops when an upper limit on number of restarts or objective function evaluations is reached.

Since the optimization algorithm needs to strike a balance between the goodness of fit and the computational cost, we devised a performance score that takes into account both the quality of score and the cost of computation to generate a comparative score $S_{A2/A1}$ of algorithm $A2$ against algorithm $A1$ as follows:

$$S_{A2/A1} = -\log_a \left(\frac{\tilde{s}_{A2}}{\tilde{s}_{A1}} \frac{\tilde{e}_{A2}}{\tilde{e}_{A1}} \right) \tag{1}$$

where, $\tilde{s}_A$ represents the median score obtained from independent runs of algorithm A and $\tilde{e}_A$ is the median number of objective function evaluations required by the algorithm. This metric implies that an x-fold improvement (or worsening) of the optimized score is exactly offset by an x-fold worsening (or improvement) of the computational cost. In other words, a score of 0 implies identical performance, whereas a positive (negative) score means the performance of $A2$ is better (worse) than $A1$. A more generalized performance score that assigns different weights to fitness of the solution and computational cost could be obtained by using different log bases for the two ratios, but we have used a log

Table 1: Frequency with which each (ϕ, ρ) pair produced the best performance score for ES-HM against pure ES according to Eq. (1). A total of 54 conditions were run by varying test functions (all 9 types), problem dimension (10, 30 and 50) and population size ($\lfloor n/3 \rfloor$ and n) as described in Fig. 18.

ρ	$\phi = 0.2$	$\phi = 0.6$	$\phi = 0.8$
2	17	3	4
20	13	5	3
100	3	0	6

base of 2 for both terms in our analysis.

Performance of the algorithms was compared using 9 different test functions (2 dimensional versions in Fig. 17, equations in Appendix C.1). The parameters ϕ and ρ were varied to study their influence on performance. For each test function, 30 independent runs were executed for each (ϕ, ρ) pair to calculate the performance scores as defined in Eq. (1). Problem dimensions (i.e., n) of 10, 30 and 50 were chosen and the number of parents, μ, was chosen to be $\lfloor n/3 \rfloor$ or n. As recommended in [125], λ was fixed at 6μ. Fig. 18a shows the performance of ES-HM against pure ES for all the test functions over different problem dimensions and population sizes. For a given test function and (μ, λ) value (i.e., a given cell in the heat maps in Fig. 18), 9 pairs of (ϕ, ρ) values were used in independent runs. The (ϕ, ρ) pair for which the performance score of ES-HM was best was used for each cell in the heat maps in Fig. 18. ES-HM performed better than ES for most test functions under various conditions producing positive performance scores. However, the performance was worse than ES under most conditions for the Rastrigin and Lunacek functions. ES-HM was next compared against naive restart ES and the scores were found to favor ES-HM for almost all test conditions (Fig. 18b). ES-HM also compared favorably against ES-IPOP (Fig. 18c).

The frequency with which each hyper-mutation frequency and strength pair, (ϕ, ρ), produced the best performance score for ES-HM against ES when run over the 54 different conditions in Fig. 18a (9 test functions times 6 (μ, λ) pairs), is shown in Table 1. The best performance scores were most frequently obtained for the lowest values of ϕ and ρ.

Table 2: Comparison of the fittest solutions found by ES-HM to those found by ES from 30 independent runs. The internal parameters of the algorithms were varied as described in Fig. 18. For each cell in the table, the (ϕ, ρ) pair which produced the fittest solution was chosen for ES-HM. FR (fitness ratio) is the ratio of fittest solution found by ES to that found by ES-HM. CR (cost ratio) is the ratio of number of function evaluation required by ES to find the fittest solution to that required by ES-HM. * indicates fitness scores found by ES-HM were significantly lower than those found by ES at a significance of 0.05 in one-sided 2-sample Kolmogorov-Smirnov test

	n = 10				n = 30				n = 50			
	$\mu = n/3$		$\mu = n$		$\mu = n/3$		$\mu = n$		$\mu = n/3$		$\mu = n$	
Fun	FR	CR	FR	CR	FR	CR	FR	CR	FR	CR	FR	CR
Sp	5.9*	0.7	3.6*	0.8	2.4*	0.9	2.4*	0.8	2.2*	0.9	1.8*	0.8
Sc	7.0*	0.3	2.0*	0.8	31.8*	0.4*	2.1*	0.8	9.5*	0.4	3.4*	0.7
Ra	3.4*	0.3	3.0	0.4	1.3	0.5	1.2	0.4	1.2	0.8	1.5	0.6
Ac	6.6	0.7	1.3*	0.8	2.8*	0.7	1.6*	0.8	1.7*	0.8	1.5*	0.8
Ro	72.7	1.0	0.1	2.3	21.5	1.0	0.1	1.9	5.6	0.8	0.7	1.8
Gr	3.7*	0.6	6.3*	0.9	2.1*	0.9	2.0*	0.8	1.7*	0.8	1.8*	0.8
Lu	10.7*	0.6	3.7*	0.9	3.7*	0.6	3.7*	0.8	2.7*	0.7	2.7*	0.7
We	2.6	5.7	2.1	29.2	2.0	15.1	1.0	5.0	1.6	9.5	1.0	4.1
GG	1.0	0.4	4.0	0.3	1.3*	.7	1.8*	0.8	1.0*	0.3	2.1	0.2

As pure-ES performed closest to ES-HM (compare Fig. 18a against b and c), we compared the fittest solutions found using ES and ES-HM and their relative computational costs (Table 2). ES-HM usually found better fitness values than ES for lower problem dimensions and for the smaller population size for a given problem dimension. The table also shows that ES-HM usually found a better score than ES but at a greater computational cost, which is to be expected since ES-HM uses restarts. The Weierstrass function was a notable exception to this trend where the computational cost was much lower for ES-HM.

4.5 ES-HM improves data fitting in an ODE model of IL-4 signaling

As ES-HM showed better optimum finding ability than the other algorithms for several test functions, we next tested it on a problem that is more representative of parameter optimization in systems biology modeling. We developed a simplified ODE model of redox regulation in IL-4 signaling and used the algorithm to optimize its parameters to fit the model to experimentally measured time-course data.

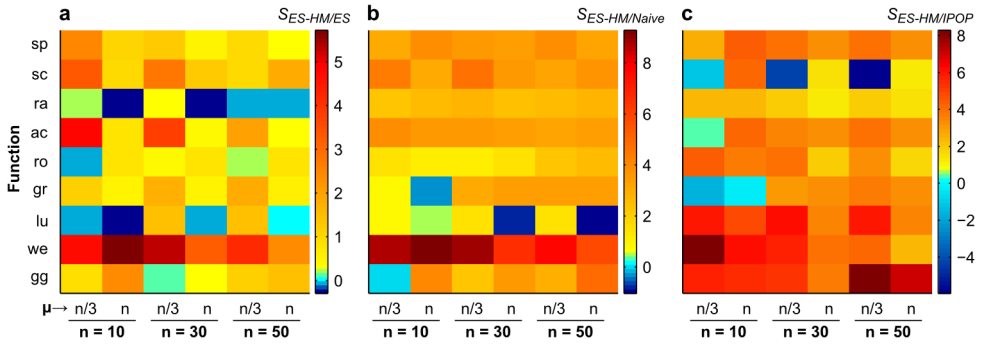

Figure 18: Performance of ES-HM compared with other ES-based algorithms. Performance score Eq. (1), (a) $S_{ES-HM/ES}$, of ES-HM against pure ES, (b) naive restart and (c) ES-IPOP. Function names are abbreviated to first 2 letters. n denotes problem dimension; μ, the number of parents was varied over $\{\lfloor n/3 \rfloor, n\}$ and λ was fixed at 6μ. ϕ and ρ were varied over 0.2, 0.6, 0.8 and 2, 20, 100, respectively; for each of the 9 (ϕ, ρ) pairs ES-HM was run 30 times; ES was run 30 times for each test function; naive restart was executed 3 times; IPOP was executed once. Fewer runs were performed for the restart methods because they inherently include multiple runs of ES algorithm. Of the 9 (ϕ, ρ) pairs for each cell on the heat maps, the pair which produced the best performance score for ES-HM was selected.

4.5.1 Experimental data and ODE model

Experimentally measured pSTAT6 time courses with and without DPI pretreatment (as shown in Chapter 3) were used. A model of IL-4 signaling with phosphatase oxidation as a mechanism of redox regulation was created (Fig. 19; this is a simplified model of the fully detailed IL-4 model and was used only for testing the optimization algorithms). Equations comprising the ODE system are described in Appendix C.3.

4.5.2 Parameter estimation and comparison of algorithms

We used ES-HM to optimize 18 parameters of the model, which include initial values and rate constants of the ODE system (Appendix C.3), and compared its performance with ES. When assigned very broad ranges (lower limit 10^{-6} and upper limit 10^{6}) to the values of all parameters, both ES and ES-HM could not produce satisfactory fits after several independent runs. Therefore, we adjusted the parameter values by hand to obtain a better first guess that produced a reasonable fit as assessed by visual inspection (Appendix C.3). The parameter optimization algorithms were then applied to search in parameter space

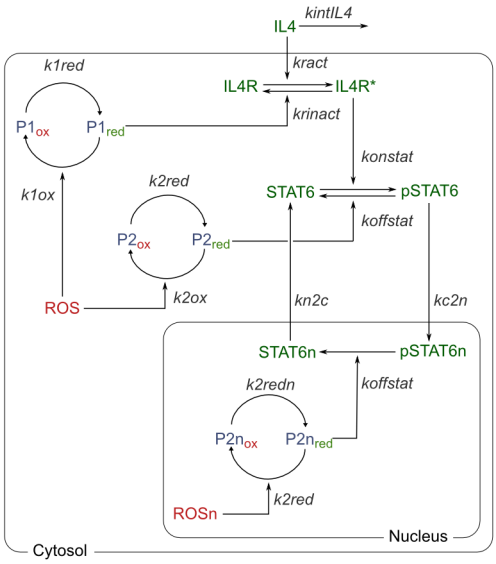

Figure 19: Schematic of the IL-4 signaling pathway representing the components modeled in the ODE system. Symbols used for the rate constants in the ODE model are shown in italicized text. This simplified model was created only to test the optimization algorithms and does not represent the actual model of IL-4 signaling developed in Chapter 3

bounded by values 1000 fold lower and 1000 fold higher than the first guess for each parameter.

9 different (ϕ, ρ) pairs were used in the ES-HM algorithm and 10 independent runs were executed for each pair resulting in 90 independent runs. Distributions of the parameters and scores for all 9 conditions are shown in Appendix C.4. Results from all 90 runs combined together are presented in Fig. 20b showing that the optimized values had a wide spread over the search range for most parameters. To compare ES-HM with ES, we executed 90 independent runs of ES over the same search range; the resulting distribution of optimized parameters is shown in Fig. 20a. Comparison of Fig. 20a against Fig. 20b shows that most parameters have a smaller spread for ES as compared to ES-HM. The distributions of the fitness scores obtained from the 90 independent runs of both methods are shown in Fig. 20c. The median score found by ES-HM was only marginally better than that obtained by using ES but the fittest solution found by ES-HM improved upon that found by ES by about 27%. Visual inspection of the fits generated by the best parameter vectors from both the algorithms confirms that ES-HM produces the better fit (Fig. 21). The parameter vectors

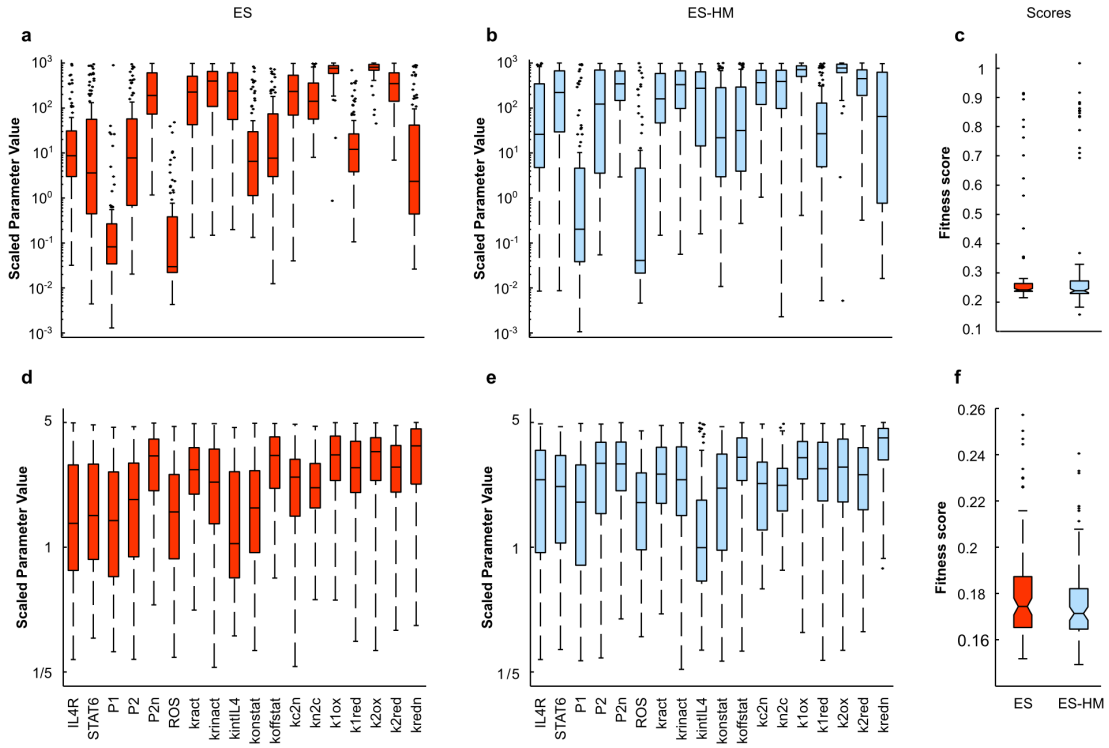

Figure 20: Box-whisker plots of parameter values and score distributions. Search space was limited to 1000 fold on either side of the first guess for each parameter value for a, b and c, and 5 fold for d, e and f. 90 independent optimizations were performed for ES. Distribution of optimized value for each parameter is shown as ratio of the initial guess (a, d). For ES-HM ϕ and ρ were varied over 0.2, 0.6, 0.8 and 2, 100, 1000, respectively, resulting in 9 (ϕ, ρ) pairs; for each pair 10 independent optimizations were executed. Results from all 90 runs were combined to generate the distributions for ES-HM (b, e). Distribution of scores corresponding to the distribution of parameter values for 1000 fold (c) and 5 fold (f) search ranges. $\mu = n/3, \lambda = 6\mu$

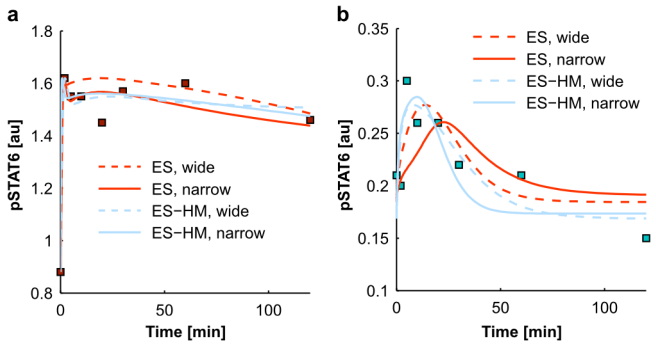

Figure 21: Fits generated by ES and ES-HM algorithms. Fitted pSTAT6 under IL-4 treatment (a) without and (b) with DPI pre-treatment. Fits corresponding to the best fitness score generated by ES and ES-HM when the search range is 1000 fold around initial guess (ES, wide and ES-HM, wide); fits corresponding to median fitness score generated when the search range is 5 fold around initial guess (ES, narrow and ES-HM narrow).

corresponding to the median scores for both algorithms produced poor fits.

To further study the performance of ES-HM against ES, we constrained the size of the search space assigning upper and lower bounds to 5 times higher or lower than the first guess for each parameter and repeated our analysis. The parameter distributions are shown in Fig. 20d and e. Comparison of the fitness distributions resulting from ES and ES-HM shows that ES-HM found a lower median score and the best score found by ES-HM was also lower than that determined using ES (Fig. 20f). Moreover, with the more tightly constrained search range the distribution of scores found by ES-HM was narrower than that for ES. With the narrowed down search range, the parameter vectors returned by both the algorithms produced good fits. Fits corresponding to the median scores returned by both the algorithms are shown in Fig. 21. It is clear from visual inspection that the parameter vector corresponding to ES-HM produced the better fit, especially with respect to the DPI treated condition.

4.6 Discussion

In this work we have presented a modification of the evolutionary strategy algorithm that improves its performance by introducing hyper-mutants into the evolving population when the evolution approaches stagnation. The hyper-mutants increase the step-size of the search

which may enable a jump out of local minima or accelerate the rate at which the minimum is approached. This method is essentially a partial restart strategy where instead of resetting all the parameters with each restart, only the step sizes are perturbed. The introduction of hyper-mutants to increase step sizes of the ES algorithm is conceptually very similar to the idea or reheating in simulated annealing, where the temperature of the annealing system is raised as the annealing converges [101, 3]. An advantage of the ES-HM algorithm is that unlike a complete restart, successive rounds of hyper-mutation lead to quicker convergence, therefore increasing the probability of improving the search without incurring as much computational cost as a complete restart might. A second benefit of the ES-HM algorithm is that it is independent of the other operators used in evolutionary strategy-based algorithms; therefore, hyper-mutation can be easily combined with different types of ES algorithms. The major limitation of the algorithm is that because the object parameters are not perturbed during each restart, it is possible that despite the increased step-sizes, searches following partial restarts will not be able to find better optima that are further away from the current value of the object parameters.

We empirically tested the performance of a (μ, λ) implementation of ES-HM to optimize real valued parameters of a suite of 9 test functions under a variety of conditions. To compare the performance of algorithms we devised a new performance metric that takes into account both the extent of improvement of the score as well as the cost of computation. Unlike some performance metrics that ignore the actual value of the optimized score by discretizing each run as a success or failure [7], the performance measure we have proposed can provide a better view of compromise that the algorithm has to make in terms of cost and benefit. We found that ES-HM outperformed naive restart and ES-IPOP type restart for a majority of the conditions tested. This can be largely attributed to the huge computational effort required by complete restart strategies. While the optimum finding abilities of the complete restart methods may be similar to ES-HM, the much higher cost offsets their

advantage. Because ES-HM is also a restart strategy, it typically runs over a greater number of generations than pure ES, implying that ES-HM is usually the more expensive of the two methods. Despite this limitation, a comparison of ES and ES-HM using the performance score in Eq. (1) showed that ES-HM performed better than ES for a large number of test conditions and objective functions. Surprisingly, for the Weierstrass function ES-HM not only improved the fitness score over ES for many test conditions, it managed to do so in fewer iterations. This happens because the Weierstrass function has a large number of very closely spaced minima; this leads to very quick stagnation of the search and ES-HM forces a restart. Again, because of the construction of the function, restarted searches hit stagnation quickly and after a quick succession of restarts, ES-HM reaches its threshold on the total number of restarts and stops. ES on the other hand, typically gets stuck in a local minimum and continues to refine its search in a confined parameter space without any significant improvement to the fitness score. This shows that on some difficult objective function surfaces ES-HM may also improve the cost of optimization despite being a restart strategy.

Our empirical tests with the algorithm enabled us to find the internal parameters of ES-HM that produced the best results for these test functions. We found that keeping hyper-mutant frequency and hyper-mutation strength parameters low usually produced better output in terms of the performance score of ES-HM compared to other algorithms. Introducing large perturbations or perturbing too many strategy parameters can introduce randomness in the search and even though it has the possibility of enabling the search to find far removed optima, it can lead to undirected evolution resulting in poorer search results or much higher computational costs.

To demonstrate a more practical application of the algorithm to a problem relevant for modeling in systems biology, we used ES-HM to optimize the parameters of an ODE model of IL-4 signaling. The structure of the model was based on knowledge from the literature

and the parameters were optimized to fit the behavior of the model to experimentally acquired data on redox regulation of IL-4 signaling. For this problem we focused on the goodness of fit alone, but we note that the typical ratio of computational cost of ES-HM against ES was similar to that seen for the test functions (Table 2). During the fitting exercise we found that most parameters of our model could vary over very large ranges of values without affecting the fitness score too much. When searched over a loosely constrained parameter space, ES-HM showed a broader distribution of fitted parameter values as well as scores as compared to ES (Fig. 20a, b and c). Thus the hyper-mutation strategy enabled exploration of a larger portion of the search space and the best scores found by ES-HM surpassed the best scores found by ES. However, the broader distribution of scores also meant that worst scores found by ES-HM were poorer than the worst scores found by ES. Restricting the search space to a narrower range gave a double advantage to ES-HM so that scores found by ES-HM were better than those found by ES at both ends of the spectrum, even though the parameter values were still broadly distributed over the search space.

Our results show that hyper-mutation strategy can improve the search characteristics of ES for a wide variety of objective functions including complex parameter optimization problems encountered in ODE models commonly used in systems biology. Advantages could be seen in terms of improved optimum finding as well as cost reduction, depending on the objective function. Furthermore, when the computational cost was increased, the gain in fitness was usually sufficient to offset the increased cost. Finally, better results can be expected in situations with both poorly and well constrained parameter spaces when applied to ODE models.

CHAPTER V

FUNCTIONAL CONSEQUENCES OF ROS-MEDIATED CROSSTALK [1]

5.1 Introduction

In 1999, Hartwell et al. introduced the concept of modular biology, where a functional module is created by interacting molecules collectively performing a discrete function. The functional modules could in turn be connected in different patterns resulting in higher level properties of the system. Such a modular construction is advantageous in terms of making the system both robust and evolvable at the same time – the individual modules could be robust to perturbations but connections between them could be changed to allow for changes in phenotype [51]. Intuitively, the requirements of evolvability and robustness seem contradictory, since a robust system should be insensitive to external perturbation whereas an evolvable system must be sensitive to environmental change. Reconciling the divergent requirements of evolvability and robustness requires knowledge of the connections between the functional units constituting the system and an appreciation of how each module integrates information arriving from multiple inputs.

Signaling pathways fit the modular description quite well by virtue of enzyme-substrate specificity in biochemical reactions; that is to say that activation of a particular receptor activates specific enzymes that act on well-defined targets. Therefore, even though there may not be spatial segregation between components of distinct signaling pathways, enzyme-substrate specificity ensures isolation of active reactions [51]. Introducing a non-specific actor in the context of modular signaling pathways allows for a mechanism to integrate the modules. As introduced in Chapter 1, ROS can play this role because of their relative

[1] Modified from [78]

promiscuity when compared to enzyme catalyzed reactions. In other words, the effects of ROS, instead of being directed towards specific proteins, are directed towards specific amino acid residues (Section 1.3). This could allow ROS produced by activation of one signaling pathway to influence another redox sensitive pathway. Recognizing this possibility, quantitative analysis of the potential of ROS to act as integrators of signaling modules was carried out and the functional consequences of ROS mediated crosstalk were examined.

Mathematical tools are required to quantitatively study how function can be segregated in signaling modules while still allowing for integration through agents like ROS. The concept of degeneracy has previously been developed to study these properties in complex biological systems. As first introduced in [144], structural complexity can be understood in terms of the interplay between specialization of functions in individual modules (functional segregation) and the ability of the modules to interact and perform functions coherently (functional integration). A highly complex system maintains segregation of function in modules while still allowing for functional integration through connections between modules [145]. Degeneracy is defined as a measure of how well functionally independent modules can interact to produce the same output. Modules that are structural duplicates form a completely redundant system and always produce the same output; degenerate systems arise from structurally distinct modules with different outputs interacting to produce the same output under certain conditions [31]. In the context of interacting signaling pathways, existence of degeneracy can be interpreted to mean that while the interacting signaling pathways perform separate functions, the possibility exists that the pathways could cooperate with, or compensate for each other to produce the same output. This intuitive understanding of the concept of degeneracy can be applied more meaningfully to biological networks if degeneracy is defined mathematically.

A mathematical definition of degeneracy was first introduced in the context of neural networks [144]. However, since regulatory features of cell signaling networks are often

described using differential systems, theory compatible with kinetic description of biochemical reactions rather than neural network [145] or logic-based descriptions [118] is required. Although some features like regulation and robustness of biochemical networks have been studied quantitatively [70, 118], degeneracy and complexity were not formalized mathematically in terms of ordinary differential equation until very recently [78].

In this chapter an explanation of the definition developed by Li et al. is first provided. This definition is then used to study ROS mediated crosstalk between the IL-4 and erythropoietin (Epo) pathways. Finally, implications of ROS mediated crosstalk are discussed.

5.2 Results

5.2.1 Definition of degeneracy for a differential system

The strategy used in [78] to determine the degeneracy of a differential system is described here. A stochastic perturbation is first injected into the differential system making the modules of the network stochastic processes. Two modules with strong functional connectivity are expected to have high statistical correlation; conversely, functionally independent components must be statistically independent. The statistical connectivity between two components I_1 and I_2 is measured using the mutual information, $MI(I_1; I_2)$, of the components. Network degeneracy is then quantified using a linear combination of the calculated MI between components as shown by the following illustrative example.

Consider a simple network consisting of three modules A, B and C as shown in Fig. 22. A and B serve as inputs while C is the output. If module A has a functional relationship with the output module C, the mutual information between the two is high. Similarly, if modules B and C share high mutual information, they are functionally related as well. However, both modules A and B being functionally related to the output is not enough for degeneracy. We also require A and B to be structurally different. This can be checked by treating A and B as a single unit, measuring its mutual information with the output and

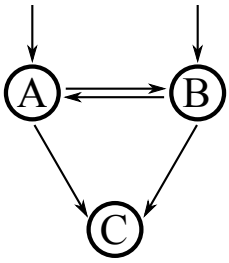

Figure 22: A simplified example of a modular biological network

comparing it with the mutual information A and B share individually with C. The value

$$D = MI(A;C) + MI(B;C) - MI(\{A,B\};C) \tag{2}$$

thus measures the degeneracy, or how much more correlation the inputs A and B share with the output C than expected. This definition enables exploration of degeneracy in signaling networks in a quantitative manner.

5.2.2 ROS mediated crosstalk increases the degeneracy of IL-4 and Epo signaling pathways

ROS mediated crosstalk between the IL-4 and Epo pathways was examined in terms of the effects of crosstalk on degeneracy. Epo is a cytokine that plays an important role in erythrocyte development and signals through the JAK2/STAT5 pathway [116]. A previous study has shown that both IL-4 and Epo signaling can increase intracellular ROS production, and ROS generated by Epo signaling could affect the IL-4 pathway by amplifying IL-4 mediated JAK3/STAT6 signaling [130].

As illustrated in Chapter 2 and Chapter 3, phosphatase oxidation is a crucial mechanism for redox regulation of signaling pathways. Based on this knowledge, we hypothesized that a redox sensitive phosphatase could be the common link between the two pathways that is affected by ROS, thus enabling crosstalk between the pathways. Previous studies have shown that PTP1B is an important phosphatase in both IL-4 and Epo signaling pathways. In the IL-4 pathway it directly dephosphorylates STAT6 whereas the substrate of

PTP1B in the Epo pathway is JAK2 [81, 93]. PTP1B is also susceptible to physiological ROS-mediated oxidative inactivation [130]. This information was compiled to create a simplified, hypothetical model of IL-4/Epo crosstalk as shown in Fig. 23a. The details of model implementation are provided in Appendix D.

The model in Fig. 23a was used to empirically study the degeneracy of the pathway under different scenarios. The receptors IL-4R and EpoR were chosen as a pair of inputs to the system and activated STAT molecules (STAT5* and STAT6* in Fig. 23a) as the output. Using the "Lyapunov algorithm" described in [78], the model in Fig. 23a was found to be degenerate with the calculated value of degeneracy equal to 0.4267. To check if ROS mediated crosstalk contributed to this value of degeneracy, we abrogated all cross-talk by switching off ROS production and regulation by the common phosphatase PTP1B to get independent signaling systems shown in Fig. 23b. The calculated value of degeneracy decreased by more than 99% for this system as compared to the pathway in Fig. 23a and the value was calculated to be 0.0016. This demonstrates that ROS mediated cross-talk between the signaling pathways is an important contributor to the degeneracy of the system.

Complexity in biological networks is thought to be related to degeneracy and systems with greater complexity are likely to be more degenerate [31]. Fully redundant systems, that is systems with exactly identical modules, can also have high structural complexity by means of crosstalking connections between modules. However, a redundant system is by definition not degenerate because the redundant modules can only perform identical functions, irrespective of the conditions. To test how a redundant system compares with a degenerate system, we modified the pathway in Fig. 23a to that shown in Fig. 23c by inserting some hypothetical connections. This was done to ensure that the two modules were structurally identical and affected the output (STAT5* and STAT6*) identically. The rate parameters were also identical for the two modules resulting in a completely redundant system where EpoR and IL-4R affect STAT5 and STAT6 identically. The redundant system was found to still have positive degeneracy but the magnitude was reduced by more

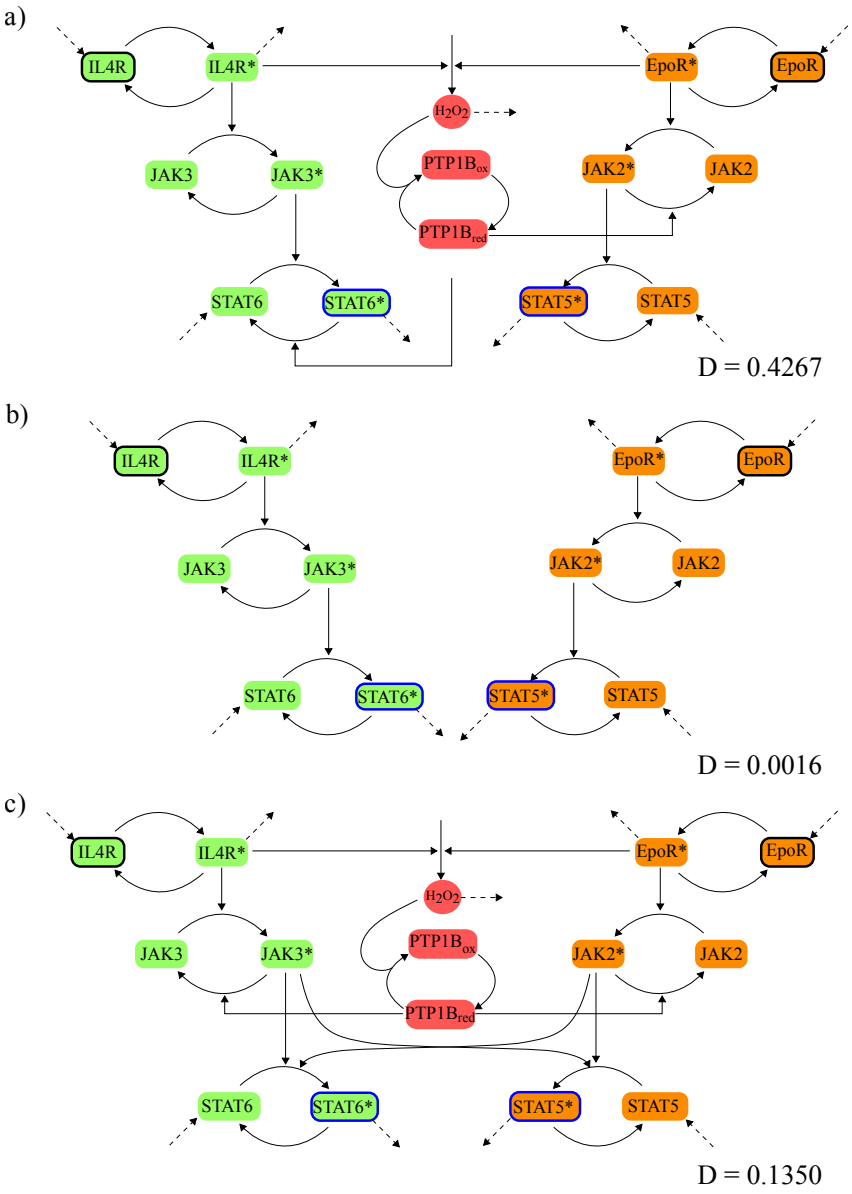

Figure 23: Hypothetical model of crosstalk between IL-4 and Epo pathways. a) The core JAK-STAT modules of IL-4R and EpoR pathways with crosstalk. Both modules are regulated by PTP1B, both generate ROS which oxidatively inactivates PTP1B. b) The links connecting the two modules were abolished resulting in independent IL-4R and EpoR signaling modules. The absence of crosstalk resulted in reduced degeneracy. c) The edges in panel A were modified to construct a hypothetical signaling system with completely redundant modules with crosstalk. Redundant networks were found to have reduced degeneracy. * indicates phosphorylated protein; ox, oxidized; red, reduced; arrows pointing at other edges, catalyzed reactions; dashed arrows entering into species, constant production; dashed arrows exiting species, first order decay; species highlighted in black, inputs; species highlighted in blue, outputs ; D, degeneracy.

than 68% as compared to the value calculated for the system in Fig. 23a. Therefore, the calculated value of degeneracy agreed with the notion that redundancy does not lead to degeneracy even if the system is richly connected and complex.

5.3 Discussion

Theoretical considerations, i.e, the potential of ROS to non-specifically affect protein function, as well as experimental results [94, 130] suggest that ROS could be important mediators of crosstalk between signaling pathways. Given the relatively non-specific nature of ROS mediated regulation, is there any advantage in biological terms in using ROS as mediators of crosstalk between signaling pathways? The notion of degeneracy in biological networks was applied in an attempt to answer this question. Degeneracy can be generally understood as the ability of structurally distinct components of a system to behave similarly under certain conditions, while the behavior may be different under other conditions. This definition of degeneracy appears to focus on how structural modules are organized and how they interact, but has greater significance because of profound connections of degeneracy with complexity, robustness and evolvability [156]. Mathematical formalisms developed to study degeneracy in neural networks as well as in differential systems indicate that degeneracy and complexity have strong positive correlation [145, 78]. Similarly, robustness and high degeneracy have been suggested to increase together [78]. Finally, highly degenerate systems are also likely to be more evolvable [155]. Because of these extremely important implications of degeneracy, it is a very useful concept for studying functional consequences of crosstalk between signaling pathways.

Mathematical theory to study degeneracy in differential systems has recently been developed [78]. Using those results we have studied the implications of ROS mediated crosstalk between distinct signaling pathways. It was found that in the presence of ROS mediated crosstalk between the IL-4 and Epo pathways, the system exhibited positive degeneracy. Abolishing this crosstalk reduced degeneracy drastically. At the same time, a

complex but redundant network was found to have lower degeneracy than a non-redundant one. The most direct interpretation of these results is that ROS mediated crosstalk can increase the degeneracy of a biological network by interfacing otherwise separate signaling modules. If the implications of degeneracy highlighted above are also taken into consideration, by association, ROS mediated crosstalk could be functionally important in conferring very important properties like robustness and evolvability to the network. As suggested in [51], the requirements of robustness and evolvability could be reconciled by having functionally robust modules, but allowing easily adjustable interactions between the modules to allow for evolvability. ROS mediated crosstalk can very effectively satisfy these criteria — enzymatic regulation of distinct signaling pathways can keep them modular and the promiscuous reactivity of ROS could be the flexible link connecting these pathways. In their explanation of how ROS signaling could have evolved to become an important regulatory mechanism, Mittler et al. propose that ROS production mechanisms could have evolved to act as a flexible link between functional modules, for example to facilitate communication between cells (cells being the modules here) [90].

From a more practical standpoint, quantitative measures of degeneracy conferred on a network by ROS mediated crosstalk could be important in the search for the right way to utilize antioxidant therapy. By definition, degeneracy is a measure of how well distinct modules can perform the same function, or in other words, compensate for each other. Therapeutic strategies that target specific nodes in a network without effectively lowering system degeneracy could fail because of the compensatory behavior of modules. Therefore, degeneracy also gives a useful way to think about and optimize targeted therapeutic approaches.

Results from simplified models of crosstalk between IL-4 and Epo signaling pathways suggest that ROS could be an important vehicle for integrating these pathways. The notion of degeneracy was used as a way to quantify ROS mediated functional integration between the distinct signaling modules. Biologically meaningful implications of degeneracy suggest

that ROS mediated crosstalk may have very important functional consequences for the crosstalking pathways.

CHAPTER VI

CONCLUSIONS AND FUTURE DIRECTIONS

6.1 Modeling complements experimentation generating new insights into redox regulation

An array of complex regulatory mechanisms is responsible for controlling the dynamics of cell signaling in mammalian cells, and ROS-mediated regulation has emerged as another layer of control in signaling pathways. Since ROS are thought to cause or aggravate a number of pathologies, a mechanistic understanding of how redox signaling operates is very important. Acknowledging the fact that redox regulatory mechanisms do not operate in isolation, but richly interact with redox independent mechanisms, it is crucial that a systems perspective be employed to study these interactions. While ROS affect the dynamics of phosphorylation and dephosphorylation in signaling pathways, their mode of action is quite distinct from kinases and phosphatases, which are the primary determinants of phosphorylation dynamics. In particular, unlike the kinase and phosphatase enzymes, the targets of ROS are a lot less precisely defined. To further complicate matters, experimental methods to detect redox modifications of proteins are still evolving and remain qualitative in nature. Therefore the challenge of understanding redox regulation in cell signaling is three-fold – i) the need for integrative analysis of redox regulation; ii) the difficulty of confidently knowing *a priori* the targets of redox regulation in a given signaling pathway; and iii) the inability to experimentally interrogate, with quantitative accuracy, oxidative modifications of proteins.

In the face of these daunting challenges, this dissertation set out to enhance the understanding of redox regulation of cell signaling using the IL-4 pathway as a model system. It was hypothesized that mathematical and computational tools could be leveraged to

draw inferences about the hidden modes of redox regulation in IL-4 signaling using experimental data that is not directly indicative of protein oxidation dynamics. Collectively, the results provide strong support to this hypothesis as a detailed model of regulation in the IL-4 pathway was developed using only total and phosphorylated protein time courses, and predictions of the model under extreme redox conditions were experimentally validated.

6.2 Phosphatase oxidation is an important motif in redox regulation

Computational models trained using experimental data were used to study redox regulation in two different signaling systems. While the primary focus of this work was the IL-4 pathway, redox regulation in the MAP kinase cascade was also briefly examined. When modeling the MAP kinase cascade, attention was focused on assessing the importance of differential rates of oxidative phosphatase inactivation across the three tiers of the MAP kinase cascade. Analysis of this model indicated that different, but finely-tuned rates of phosphatase oxidation at each level of the cascade could explain the experimental observations.

In the case of the IL-4 pathway, the possibilities of redox regulation were examined more exhaustively. Three different mechanisms of redox regulation, namely, i) PTP oxidation; ii) JAK oxidation; and iii) ROS dependent redistribution of phosphatase between subcellular compartments, were examined. Reduced representations of the IL-4 signaling system were used to extensively test 16 alternate model topologies. The characteristic, slow oscillation of pSTAT6 observed in experiments proved to be a very powerful discriminator of candidate models. One of the simplest models, one that used PTP oxidation as the only mode of redox regulation, outcompeted all alternative models in qualitative as well as quantitative interpretation of results. Importantly, accounting for interactions between ROS dependent and independent mechanisms was also found to be essential in correctly inferring the effects of redox regulation. In contrast with the MAP kinase model, differential redox sensitivity across the phosphatases (there were two different phosphatases in the

model) was not found to be essential.

Both models demonstrate the power of mathematical modeling for testing alternative hypotheses and understanding the underlying architecture of biological networks, therein providing support to the central hypothesis of this work. Results from the analysis of the IL-4 pathway additionally highlight the value of modeling small sub-networks to gain meaningful biological insights.

The two models are also similar in suggesting that phosphatase oxidation is an important mechanism of redox regulation. This is an important result because the same regulatory motif, i.e., reversible oxidative inactivation of phosphatases, was instrumental in explaining and predicting the behavior of two signaling systems with very different topologies. Taken together with the fact that both the signaling pathways studied are representatives of larger "families" of signaling pathways, it is very likely that phosphatase oxidation is used as a common design principle across a number of signaling pathways.

6.3 ROS as mediators of pathway crosstalk

As highlighted above, the action of ROS on proteins is distinct from that of enzymes because freely diffusing ROS can react relatively non-specifically with any accessible protein susceptible enough to oxidation. Moreover, the components of separate signaling modules may not always be spatially segregated in a cell, for example two phosphatases regulating two separate pathways may both be distributed similarly in the cytosol. If these two phosphatases were to be equally sensitive to oxidation, it follows that ROS coming from any source would equally affect both the phosphatases, and hence the signaling pathways they regulate. The ability of ROS to mediate crosstalk was examined using the framework of degeneracy — the ability of structurally distinct modules to perform identical function.

Using previously established mathematical definition of degeneracy for differential systems [78], it was found that ROS mediated crosstalk indeed resulted in increased degeneracy in the crosstalking IL-4 and Epo pathways. Degeneracy has been argued to be related

to other properties of biological systems like robustness and evolvability. The divergent requirements of robustness and evolvability could be satisfied by having functionally robust modules with easily evolvable links between them. In this way the modules are resistant to perturbation but at a higher level, the system can evolve by changing connections between modules. It is possible that non-specific ROS mediated cross talk acts as this flexible link between robust signaling modules. Altering the mechanism of activation or subcellular localization of one ROS producing enzyme to alter the connections between ROS-sensitive modules is easier than successfully re-tuning all components of complex signaling modules. Multiple NOX enzymes localized in different subcellular compartments and regulated by different mechanisms could have evolved in this manner.

As argued in Chapter 5, degeneracy introduced by ROS could also lead to compensatory behaviors between signaling pathways and this could have important implications for the outcome of targeted therapeutic strategies.

6.4 Development of new computational tools

New computational tools have been developed to study the biological questions that were the focus of this dissertation. A novel restart strategy for use with the evolutionary strategy algorithm, named ES with hyper-mutation (Chapter 4), was developed to support the need for parameter estimation in the models. An innovative model selection strategy based on qualitative matching of simulation output with experimental data was successfully employed. Of course, the success of this method was contingent on the characteristic dynamics of STAT6 phosphorylation (Chapter 3). This result suggests that when distinctive features are presented by experimental data, the qualitative ability of a model to reproduce those features can be an effective discrimination tool. Finally, a detailed model of the IL-4 pathway was developed by building in known mechanisms of regulation in the pathway together with ROS dependent mechanisms. Two predictions of this model were successfully validated by experimental results. Other falsifiable predictions can be generated and used

to refine the model to build a more comprehensive understanding of the IL-4 pathway.

6.5 Future directions

6.5.1 Alternative patterns of distribution of redox control

Although the models of redox regulation developed in this work provide satisfactory explanation of the data currently available, several simplifying assumptions have been made whose validity needs to be checked. In the MAPK model as well as the IL-4 model, a one-to-one correspondence was assumed between phosphatases and their substrates. Based on experimental evidence, one substrate could have multiple phosphatases, and the total activity of one phosphatase could be distributed over multiple substrates. Moreover, subcellular localizations of these phosphatases may be distinct and their reactivities to ROS may vary. Different patterns of distribution of phosphatase activity between substrates and varying reactivities to ROS are likely to affect the dynamics of signaling.

While these points are challenging to explore through experimental methods, hypothetical models derived from the one already constructed could be a good starting point to explore these alternatives. Interesting scenarios suggested by these simulations could be specifically selected for experimental investigation.

In the context of the MAPK cascade, only phosphatase oxidation was explored as the possible mechanism of redox regulation. Recently, oxidative activation of receptor tyrosine kinase has been reported [104] and would be an interesting point to explore through model-based simulations.

6.5.2 Mechanisms of protein oxidation and reduction

How sufficient ROS can be generated to substantially oxidize proteins is an open question. Locally elevated ROS concentrations [158] and the use of relay proteins [44] to efficiently transfer oxidative state have been suggested as possible mechanisms. These mechanisms could be explored using the IL-4 model. While partial differential equation based descriptions may be appropriate to explore the spatio-temporal effects of ROS distribution on cell

signaling, simplified spatio-temporal representations can be generated using ODEs. For example, the cytosol could be divided into two sub-compartments – one cell membrane-proximal with higher ROS due to proximity with, say NOX1; the other membrane-distal with lower ROS concentration. Signaling proteins, which could have different distributions between these compartments, would be differently affected by ROS. Implementing oxidation state relays is a relatively simple process and could be explored more easily.

The model also assumes steady availability of enzymes to reduce the oxidized phosphatases. Because receptor activation causes transient change in intracellular redox state, the buffering capacity of the cell can be expected to change dynamically. A more faithful implementation of this phenomenon in the model may be desirable.

6.5.3 Role of nuclear-cytosolic shuttling of STAT6

The model predicts that phosphorylation dependent nuclear-cytosolic shuttling of STAT6 is an important mechanism of redox regulation in the pathway. Pharmacological inhibitors of nuclear import or export could be used to test this prediction of the model. However, pharmacological inhibition will also simultaneously affect the nuclear-cytosolic distribution of the phosphatases of STAT6. An alternative approach could be to separate out nuclear and cytosolic fractions of pSTAT6 experimentally in order to falsify and improve the model.

6.5.4 Testing mechanisms of ROS mediated crosstalk

ROS mediated crosstalk was found to enhance system degeneracy, which could have many important biological implications as discussed in Chapter 5. However, the question that remains unanswered is that how is specificity of response maintained in the face of a non-specific second messenger, like H_2O_2. The findings of this dissertation do not address this question and concerted modeling and experimental efforts will be required in the future to find a satisfactory answer.

APPENDIX A

DETAILS OF THE MAP KINASE MODELS

Details of implementation of all models used in Chapter 2 are given here.

A.1 The base model

The equations and parameter values for the model used in Fig. 2b (referred to as the base model) are presented below. The model was adopted from the Raf/MEK/ERK module of the model in [124].

Table 3: Equations of the base MAPK model

Reaction	**Rate equation**
Raf + RasGTP ↔ [Raf:RasGTP]	k1×Raf×RasGTP − k_1×[Raf:RasGTP]
[Raf:RasGTP] → [Raf*] + RasGTP	k2×[Raf:RasGTP]
MEK + [Raf*] ↔ [MEK:Raf*]	k3×MEK×[Raf*] − k_3×[MEK:Raf*]
[MEK:Raf*] → MEKp + [Raf*]	k4×[MEK:Raf*]
MEKp + [Raf*] ↔ [MEKp:Raf*]	k5×MEKp×[Raf*] − k_5×[MEKp:Raf*]
[MEKp:Raf*] → [MEK*] + [Raf*]	k6×[MEKp:Raf*]
ERK + [MEK*] ↔ [ERK:MEK*]	k7×ERK×[MEK*] − k_7×[ERK:MEK*]
[ERK:MEK*] → ERKp + [MEK*]	k8×[ERK:MEK*]
ERKp + [MEK*] ↔ [ERKp:MEK*]	k9×ERKp×[MEK*] − k_9×[ERKp:MEK*]
[ERKp:MEK*] → [ERK*] + [MEK*]	k10×[ERKp:MEK*]
[Raf*] + P1 ↔ [Raf*:P1]	k11×[Raf*]×P1 − k_11×[Raf*:P1]
[Raf*:P1] → Raf + P1	k12×[Raf*:P1]

Continued on next page

Table3 – continued from previous page

Reaction	Rate equation
[MEK*] + P2 ↔ [MEK*:P2]	k13×[MEK*]×P2 − k_13×[MEK*:P2]
[MEK*:P2] → MEKp + P2	k14×[MEK*:P2]
MEKp + P2 ↔ [MEKp:P2]	k15×MEKp×P2 − k_15×[MEKp:P2]
[MEKp:P2] → MEK + P2	k16×[MEKp:P2]
[ERK*] + P3 ↔ [ERK*:P3]	k17×[ERK*]×P3 − k_17×[ERK*:P3]
[ERK*:P3] → ERKp + P3	k18×[ERK*:P3]
ERKp + P3 ↔ [ERKp:P3]	k19×ERKp×P3 − k_19×[ERKp:P3]
[ERKp:P3] → ERK + P3	k20×[ERKp:P3]
P1 + H_2O_2→ $P1_{ox}$	k21×P1×H2O2
P2 + H_2O_2→ $P2_{ox}$	k22×P2×H_2O_2
P3 + H_2O_2→ $P3_{ox}$	k23×P3×H_2O_2
$P1_{ox}$ → P1	k24×$P1_{ox}$
$P2_{ox}$ → P2	k25×$P2_{ox}$
$P3_{ox}$ → P3	k26×$P3_{ox}$

A.1.1 Input functions

$$\text{RasGTP} = \text{peakRas}*\exp\left(\frac{-(\text{time}-\text{peakTime})^2}{\text{stdDev}^2}\right)*(1+\text{erf}(\text{skewRas}*\text{time})) + \text{basalRas}$$

$$H_2O_2 = a*\exp(-((\text{time}-b)/c)^2) * (1 + \text{erf}(d*\text{time}))$$

A.1.2 Outputs

Total ERKpp = [ERK*] + [ERK*:P3]

Total phospho MEK = [MEK*] + [MEK*:P2] + [ERK:MEK*] + [ERKp:MEK*] + MEKp + [MEKp:P2] + [MEKp:Raf*]

A.1.3 Parameter values

Table 4: Parameter values of the base model

Parameter	Value	Units
k1	6.00×10^{1}	1/(μM.min)
k_1	$3.18\times10^{-1}1$	1/min
k2	6.00×10^{1}	1/min
k3	6.66×10^{2}	1/(μM.min)
k_3	1.08+000	1/min
k4	2.10×10^{2}	1/min
k5	6.66×10^{2}	1/(μM.min)
k_5	1.08	1/min
k6	1.74×10^{2}	1/min
k7	6.60	1/(μM.min)
k_7	1.80	1/min
k8	9.60×10^{2}	1/min
k9	6.60	1/(μM.min)
k_9	1.80	1/min
k10	3.42×10^{2}	1/min
k11	4.30×10^{3}	1/(μM.min)
k_11	1.20×10^{1}	1/min
k12	6.00×10^{1}	1/min
k13	8.58×10^{2}	1/(μM.min)
k_13	4.80×10^{1}	1/min
k14	3.48	1/min
k15	1.50×10^{1}	1/(μM.min)
k_15	3.00×10^{1}	1/min

Continued on next page

Table4 – continued from previous page

Parameter	Value	Units
k16	3.48	1/min
k17	8.70×10^{2}	1/(μM.min)
k_17	3.60×10^{1}	1/min
k18	1.62×10^{1}	1/min
k19	3.00×10^{2}	1/(μM.min)
k_19	3.00×10^{1}	1/min
k20	1.80×10^{1}	1/min
k21	1.00×10^{-4}	1/(μM.min)
k22	1.00×10^{-6}	1/(μM.min)
k23	3.00×10^{1}	1/(μM.min)
k24	1.00×10^{-1}	1/min
k25	1.00×10^{-1}	1/min
k26	1.00×10^{-1}	1/min
peakRas	1.70×10^{-2}	μM
peakTime	9.00	min
stdDev	3.00	min
skewRas	6.60×10^{-2}	1/min
basalRas	1.00×10^{-3}	μM
a	1.06×10^{2}	undefined
b	1.20	undefined
c	8.20×10^{1}	undefined
d	5.00×10^{-1}	undefined

Table 5: Non-zero initial values in the base model

Name	Initial concentration	Units
ERK	35	μM
MEK	36.52	μM
P1	0.066	μM
P2	0.7	μM
P3	16.67	μM
Raf	0.066	μM
RasGTP	1.001	μM

A.2 Simulation of other experimental conditions in Fig. 2

A.2.1 Catalase pretreatment

This was simulated by setting a = 0 in the base model resulting in 0 H_2O_2 over time.

A.2.2 H_2O_2 bolus addition

The H_2O_2 input function was disabled in the base model and the following reaction was added to the system.

$H_2O_2 \rightarrow$ null, rate = k27× H_2O_2

k27 = 0.09 min^{-1} and initial value of H_2O_2 was 4.5×10^4.

A.3 Nuclear shuttling model

The following reactions were added to the base model to obtain the nuclear shuttling model in Fig. 4.

Table 6: Equations of the nuclear shuttling model

Reaction	Rate
$ERK \leftrightarrow ERK_n$	$kcyt2nuc \times ERK - knuc2cyt \times ERK_n$
$ERKp \leftrightarrow ERKp_n$	$kcyt2nuc \times ERKp - knuc2cyt \times ERKp_n$
$[ERK^*] \leftrightarrow [ERK^*_n]$	$kcyt2nuc \times [ERK^*] - knuc2cyt \times [ERK^*_n]$
$P3 \leftrightarrow P3_n$	$kcyt2nuc \times P3 - knuc2cyt \times P3_n$
$P3_{ox} \leftrightarrow P3_{ox,n}$	$kcyt2nuc \times P3_{ox} - knuc2cyt \times P3_{ox,n}$
$P3_{ox,n} \rightarrow P3_n$	$k26 \times P3_{ox,n}$
$[ERK^*_n] + P3_n \leftrightarrow [ERK^*_n{:}P3_n]$	$k17 \times [ERK^*_n] \times P3_n - k\_17 \times [ERK^*_n{:}P3_n]$
$[ERK^*_n{:}P3_n] \rightarrow ERKp_n + P3_n$	$k18 \times [ERK^*_n{:}P3_n]$
$ERKp_n + P3_n \leftrightarrow [ERKp_n{:}P3_n]$	$k19 \times ERKp_n \times P3_n - k\_19 \times [ERKp_n{:}P3_n]$
$[ERKp_n{:}P3_n] \rightarrow ERK_n + P3_n$	$k20 \times [ERKp_n{:}P3_n]$

The subscript 'n' denotes nuclear concenration and the subscript 'ox' indicates oxidized protein. The new parameters introduced were taken to be kcyt2nuc = knuc2cyt = 1/min.

A.4 Kinase oxidation model

The following additional reactions were added to the base model.

Table 7: Additional reaction of the kinase oxidation model

Reaction	Rate
$[ERK^*] + H_2O_2 \rightarrow [ERK^*_{ox}]$	$k27 \times [ERK^*] \times H_2O_2$
$[ERK^*_{ox}] \rightarrow [ERK^*]$	$k28 \times [ERK^*_{ox}]$

The subscript 'ox' denotes oxidized protein. The new parameters introduced are k27 = 5×10^{-3}/(μM.min) and k28 = 5×10^{-2}/min.

A.5 Akt-ERK crosstalk model

Equations for the Akt-ERK crosstalk model are presented below. The model, along with the symbols for molecules and complexes, was adopted from [52].

A.5.1 Reactions

Table 8: Equations of the Akt-ERK crosstalk model

Reaction	**Rate**
R + HRG ↔ [R:HRG]	$k1 \times R \times HRG - k\_1 \times [R:HRG]$
2 [R:HRG] ↔ $[(R:HRG)_2]$	$k2 \times [R:HRG]^2 - k\_2 \times [(R:HRG)_2]$
$[(R:HRG)_2]$ ↔ RP	$k3 \times [(R:HRG)_2] - k\_3 \times RP$
RP → $[(R:HRG)_2]$	$\frac{V4 \times RP}{K4 + RP}$
RP + Shc ↔ [R-Shc]	$k5 \times RP \times Shc - k\_5 \times [R\text{-}Shc]$
[R-Shc] ↔ [R-ShP]	$k6 \times [R\text{-}Shc] - k\_6 \times [R\text{-}ShP]$
[R-ShP] + GS ↔ [R-ShGS]	$k7 \times [R\text{-}ShP] \times GS - k\_7 \times [R\text{-}ShGS]$
[R-ShGS] ↔ RP + ShGS	$k8 \times [R\text{-}ShGS] - k\_8 \times RP \times ShGS$
ShGS ↔ GS + ShP	$k9 \times ShGS - k\_9 \times GS \times ShP$
ShP → Shc	$\frac{V10 \times ShP}{K10 + ShP}$
RasGDP → RasGTP	$\frac{k11 \times ShGS \times RasGDP}{K11 + RasGDP}$
RasGTP → RasGDP	$\frac{V12 \times RasGTP}{K12 + RasGTP}$
Raf → [Raf*]	$\frac{k13 \times RasGTP \times Raf}{K13 + Raf}$
[Raf*] → Raf	$\frac{k14 \times E \times [Raf^*]}{K14 + [Raf^*]}$
[Raf*] → Raf	$\frac{k14b \times [Akt:PIPP] \times [Raf^*]}{K14b + [Raf^*]}$
MEK → MEKp	$\frac{k15 \times [Raf^*] \times MEK}{K15 \times (1 + MEKp/K17) + MEK}$
MEKp → MEK	$\frac{k16 \times PP2A \times MEKp}{K16 \times (1 + MEKpp/K18 + [Akt:PIP]/K31 + [Akt:PIPP]/K33) + MEKp}$
MEKp → MEKpp	$\frac{k17 \times [Raf^*] \times MEKp}{K17 \times (1 + MEK/K15) + MEKp}$

Continued on next page

Table8 – continued from previous page

Reaction	**Rate**
MEKpp → MEKp	$\frac{k18\times PP2A\times MEKpp}{K18\times(1+MEKp/K16+[Akt:PIP]/K31+[Akt:PIPP]/K33)+MEKpp}$
ERK → ERKp	$\frac{k19\times MEKpp\times ERK}{K19\times(1+ERKp/K21)+ERK}$
ERKp → ERK	$\frac{k20\times MKP3\times ERKp}{K20\times(1+ERKpp/K22)+ERKp}$
ERKp → ERKpp	$\frac{k21\times MEKpp\times ERKp}{K21\times(1+ERK/K19)+ERKp}$
ERKpp → ERKp	$\frac{k22\times MKP3\times ERKpp}{K22\times(1+ERKp/K20)+ERKpp}$
RP + PI3K ↔ [R-PI3K]	$k23 \times RP \times PI3K - k\_23 \times [R\text{-}PI3K]$
[R-PI3K] ↔ [R-PI3K*]	$k24 \times [R\text{-}PI3K] - k\_24 \times [R\text{-}PI3K^*]$
[R-PI3K*] ↔ RP + [PI3K*]	$k25 \times [R\text{-}PI3K^*] - k\_25 \times RP \times [PI3K^*]$
[PI3K*] → PI3K	$\frac{V26\times[PI3K^*]}{K26+[PI3K^*]}$
PI → PIP3	$\frac{k27\times[PI3K^*]\times PI}{K27+PI}$
PIP3 → PI	$\frac{V28\times PIP3}{K28+PIP3}$
Akt + PIP3 ↔ [Akt:PIP3]	$k29 \times Akt \times PIP3 - k\_29 \times [Akt:PIP3]$
[Akt:PIP3] → [Akt:PIP]	$\frac{k30\times PDK\times[Akt:PIP3]}{K30\times(1+[Akt:PIP]/K32)+[Akt:PIP3]}$
[Akt:PIP] → [Akt:PIP3]	$\frac{k31\times PP2A\times[Akt:PIP]}{K31\times(1+MEKp/K16+MEKpp/K18+[Akt:PIPP]/K33)+[Akt:PIP]}$
[Akt:PIP] → [Akt:PIPP]	$\frac{k32\times PDK\times[Akt:PIP]}{K32\times(1+[Akt:PIP3]/K30)+[Akt:PIP]}$
[Akt:PIPP] → [Akt:PIP]	$\frac{k33\times PP2A\times[Akt:PIPP]}{K33\times(1+MEKp/K16+MEKpp/K18+[Akt:PIP]/K31)+[Akt:PIPP]}$
RP → null	$k34 \times RP$
PP2A + H_2O_2→ $PP2A_{ox}$	$k35 \times PP2A \times H_2O_2$
$PP2A_{ox}$ → PP2A	$k36 \times PP2A_{ox}$
Raf → [Raf*]	$\frac{k37\times PP2A\times Raf}{K37+Raf}$
MKP3 + H_2O_2→ $MKP3_{ox}$	$k38 \times MKP3 \times H_2O_2$
$MKP3_{ox}$ → MKP3	$k39 \times MKP3_{ox}$

The subscript ‘ox’ represents oxidized protein.

A.5.2 Parameters

Table 9: Parameters of the Akt-ERK crosstalk model

Parameter	Value	Units
k_1	4.56×10^{-2}	1/min
k1	7.20×10^{-2}	1/(nM.min)
k2	6.00×10^{-1}	1/(nM.min)
k_2	6.00	1/min
k3	6.00×10^{1}	1/min
k_3	6.00×10^{-1}	1/min
V4	3.75×10^{3}	nM/min
K4	5.00×10^{1}	nM
k5	6.00	1/(nM.min)
k_5	6.00×10^{1}	1/min
k6	1.20×10^{3}	1/min
k_6	3.00×10^{2}	1/min
k7	3.60×10^{3}	1/(nM.min)
k_7	3.28×10^{4}	1/min
k_8	9.42×10^{5}	1/(nM.min)
k8	1.22×10^{5}	1/min
k9	1.17×10^{1}	nM
k_9	0.00	1/(nM.min)
V10	9.24×10^{-1}	nM/min
K10	3.40×10^{2}	nM
k11	1.33×10^{1}	1/min
K11	1.81×10^{-1}	nM

Continued on next page

Table9 – continued from previous page

Parameter	Value	Units
V12	1.73×10^{1}	nM/min
K12	5.71×10^{-2}	nM
k13	6.00	1/(nM.min)
K13	$1.20\times10^{+2}$	1/min
K14b	$5.91\times10^{+2}$	1/min
k14b	5.91	1/min
K14	$2.75\times10^{+3}$	1/min
k14	2.82	1/(nM.min)
k15	1.57×10^{5}	nM/min
K15	3.68×10^{3}	nM
k16	6.00×10^{-2}	1/min
K16	2.10×10^{2}	1/min
k17	3.17×10^{2}	nM
K17	3.48	1/min
k18	2.20×10^{3}	nM
K18	1.74×10^{2}	1/min
k19	3.17×10^{2}	nM
K19	3.48	1/min
k20	4.35	nM
K20	1.20×10^{1}	nM
K21	6.00×10^{1}	nM
k21	1.46×10^{5}	nM
K22	5.70×10^{2}	1/min
k22	1.46×10^{5}	nM

Continued on next page

Table9 – continued from previous page

Parameter	Value	Units
k23	1.80×10^{1}	1/min
k_23	1.60×10^{2}	nM
k24	6.00×10^{1}	nM
k_24	9.60×10^{2}	1/min
k25	1.62×10^{1}	1/min
k_25	1.01×10^{3}	1/min
V26	3.91×10^{1}	nM
K26	1.02×10^{6}	nM/min
k27	1.20×10^{6}	1/min
K27	8.00×10^{4}	nM
V28	8.00×10^{4}	nM
K28	6.42	1/min
k29	1.20×10^{6}	1/min
k_29	1.27×10^{1}	1/min
k30	2.45×10^{3}	1/min
K30	1.00×10^{4}	1/(nM.min)
k31	8.07	nM
K31	3.04×10^{4}	1/(nM.min)
k32	4.04×10^{-1}	1/min
K32	2.00×10^{-1}	1/min
k33	9.18×10^{1}	1/min
K33	1.40×10^{4}	1/min
k34	9.02	nM
k35	5.00×10^{-3}	1/(nM.min)

Continued on next page

Table9 – continued from previous page

Parameter	Value	Units
k36	1.00	1/min
k37	9.18×10^{-2}	1/min
K37	1.17×10^{-1}	nM
k38	5.00×10^{-3}	1/(nM.min)
k39	1.00	1/min
synthH_2O_2	8.07	nM
decayH_2O_2	4.04×10^{-1}	1/min

A.5.3 Initial values

Species with non-zero initial values are listed below.

Table 10: Non-zeros initial values of the Akt-ERK crosstalk model

Name	Initial concentration	Units
Akt	10	nM
E	7	nM
ERK	1000	nM
GS	10	nM
HRG	330	nM
MEK	120	nM
MKP3	2.4	nM
PDK(constant)	1	nM
PI	800	nM
PI3K	10	nM

Continued on next page

Table10 – continued from previous page

Name	Initial concentration	Units
PP2A	11.4	nM
R	80	nM
Raf	100	nM
RasGDP	120	nM
Shc	1000	nM

Fig. 6c was obtained by making the following modifications to the above model K14b = 0.1, k14b = 4.038, K18 = 500.

APPENDIX B

DETAILS OF ANALYSIS OF THE IL-4 PATHWAY

Implementation details of models used in Chapter 3 are provided in this Appendix.

B.1 Model used for Monte Carlo simulations

ODE system representing the reduced model used for MC Simulations is given below. The quantities represented by the variables are shown in Table 11 and Table 13.

$$\dot{x}(1) = -k(1) \times x(1) \times x(3) + k(2) \times x(2) - k(11) \times x(1) \times x(10) + k(12) \times x(12)$$

$$\dot{x}(2) = +k(1) \times x(1) \times x(3) - k(2) \times x(2)$$

$$\dot{x}(3) = -k(3) \times x(3)$$

$$\dot{x}(4) = -k(4) \times x(4) \times x(2) + k(5) \times x(5) \times x(8) + k(7) \times x(7) - k(6) \times x(4)$$

$$\dot{x}(5) = +k(4) \times x(4) \times x(2) - k(5) \times x(5) \times x(8) - k(6) \times x(5) + k(7) \times x(6)$$

$$\dot{x}(6) = +k(6) \times x(5) - k(5) \times x(6) \times x(9) - k(7) \times x(6)$$

$$\dot{x}(7) = +k(5) \times x(6) \times x(9) - k(7) \times x(7) + k(6) \times x(4)$$

$$\dot{x}(8) = -k(6) \times x(8) + k(8) \times x(9) \times x(10) - k(11) \times x(8) \times x(10) + k(12) \times x(11)$$

$$\dot{x}(9) = +k(6) \times x(8) - k(8) \times x(9) \times x(10)$$

$$\dot{x}(10) = +k(9) \times x(2) - k(10) \times x(10)$$

$$\dot{x}(11) = +k(11) \times x(8) \times x(10) - k(12) \times x(11)$$

$$\dot{x}(12) = +k(11) \times x(1) \times x(10) - k(12) \times x(12)$$

This ODE system represents the largest possible model with all regulatory mechanism shown in Fig. 9 operating in parallel. To simulate the other models, terms were removed

from this model accordingly. The meanings of the symbols are as follows.

B.1.1 Species

Table 11: List of species used in MC simulations with reduced models

Symbol	Molecule
x(1)	R
x(2)	R*
x(3)	IL4
x(4)	SAT6
x(5)	pSTAT6
x(6)	$pSTAT6_n$
x(7)	$STAT6_n$
x(8)	P
x(9)	P_n
x(10)	ROS
x(11)	P_{ox}
x(12)	R_{ox}

The names of molecules in the right hand column correspond to the names used in Fig. 9

After setting up the ODE system, parameters were sampled uniformly in the log space in the ranges given Table 12 and Table 13. The system was allowed to equilibrate before IL-4 was added (0.05 unit). These ranges were estimated by roughly fitting the model to experimental data.

B.1.2 Initial value

Initial values of the following species were non-zero at the beginning. The ranges in which values were sampled are shown.

Table 12: Sampling ranges of initial values for MC simulations

Molecule	Lower Bound	Upper Bound
P	1	20
R	.1	1
STAT6	1	10

B.1.3 Rate constants

Rate constants were sampled from the ranges specified below.

Table 13: Sampling ranges of rate constants for MC simulations

Symbol	**Lower bound**	**Upper bound**	**Description**
k(1)	0.8	8	Receptor activation
k(2)	0.1	1	Receptor inactivatin
k(3)	0.08	0.8	IL-4 removal
k(4)	1	10	STAT activation
k(5)	0.01	0.1	STAT inactivation
k(6)	0.08	0.8	Nuclear translocation rate
k(7)	0.08	0.8	Cytosolic translocation rate
k(8)	0.3	3	ROS production rate
k(9)	0.01	0.1	ROS removal rate

Continued on next page

Table13 – continued from previous page

Symbol	Lower bound	Upper bound	Description
k(10)	0.8	8	Protein oxidation rate
k(11)	0.0001	0.001	Protein reduction rate
k(12)	5	50	ROS mediated PTP translocation

B.2 Systems level model of the IL-4 pathway

The biochemical reactions modeled in the network shown in Fig. 13 are presented here. Descriptive names have been used for rate constants and molecular species to clarify their meaning.

Table 14: Equations of the IL-4 system model

Reaction	Rate
R + L ↔ RL	kRLBind×R×L − kRLUnbind×RL
RL → Ract	kRact×RL
Ract + Stat ↔ StatRact	kStatRBind×Ract×Stat − kStatRUnbind×StatRact
StatRact → Statp + Ract	kStatPhos×StatRact
2Statp ↔ StatAct	kStatDimerize×Statp×Statp − kStatDissoc×StatAct
StatAct → StatActNuc	kcyt2nuc×StatAct
StatActNuc + P1n ↔ P1nStatActNuc	kPTPBind×StatActNuc×P1n − kPTPUnbind×P1nStatActNuc
P1nStatActNuc → P1n + StatpNuc + StatNuc	kcatPTP×P1nStatActNuc
StatNuc → Stat	knuc2cyt×StatNuc
Ract + P2 ↔ RactP2	kPTPBind×Ract×P2 − kPTPUnbind×RactP2
RactP2 → RL + P2	kcatPTP×RactP2
P1 + StatAct ↔ StatActP1	kPTPBind×P1×StatAct − kPTPUnbind×StatActP1
StatActP1 → Stat + Statp + P1	kcatPTP×StatActP1
P1 + Statp ↔ StatpP1	kPTPBind×P1×Statp − kPTPUnbind×StatpP1

Continued on next page

Table14 – continued from previous page

Reaction	Rate
StatpP1 → Stat + P1	kcatPTP×StatpP1
StatActNuc → StatActNuc + Socs	$\frac{\text{vmTrans}\times\text{StatActNuc}}{\text{KmTrans}+\text{StatActNuc}}$
Ract + Socs ↔ RactSocs	RSocsBind×Ract×Socs − RSocsUnbind×RactSocs
P2 + ROS → P2ox	koxPTP×P2×ROS
P2ox → P2	kredPTP×P2ox
P1 + ROS → P1ox	koxPTP×P1×ROS
P1ox → P1	kredPTP×P1ox
Ract → null	kintRAct×Ract
null ↔ Stat	ksynthStat − kdegStat×Stat
Socs → null	kdegSocs×Socs
RactSocs + P2 ↔ RactSocsP2	kPTPBind×RactSocs×P2 − kPTPUnbind×RactSocsP2
RactSocsP2 → RL + P2 + Socs	kcatPTP×RactSocsP2
StatpNuc + P1n ↔ P1nStatpNuc	kPTPBind×StatpNuc×P1n − kPTPUnbind×P1nStatpNuc
P1nStatpNuc → StatNuc + P1n	kcatPTP×P1nStatpNuc
StatpNuc ↔ StatActNuc	kStatDimerize×StatpNuc×StatpNuc − kStatDissoc×StatActNuc
P1 ↔ P1n	kcyt2nuc×P1 − knuc2cyt×P1n
P1ox ↔ P1nox	kcyt2nuc×P1ox − knuc2cyt×P1nox
P1nox → P1n	kredPTP×P1nox

B.2.1 Optimized Parameters

Concentrations and rate constants were estimated to fit the model to experimental data. Because MG132 and CHX are both pharmacological inhibitors that affect protein degradation and synthesis in the cell, some initial values had to be recalibrated for MG132 and/or CHX pretreatment. Recalibrated values are shown in columns 3 and 4 of the tables below. If these columns are blank, no re-estimation of parameters was necessary. The values are in units of nM.

Table 15: Optimized non-zero initial values of the model

Molecule	IL4	MG132 + IL4	CHX + IL4
R	40.5		
Total STAT6	1016	882.5	
pSTAT6	304.8	364.0	
SOCS	18.5	1.5	2.4
P2	84		
P1	990.5		

The estimated values of rate constants are shown in the table below. MG132 inhibited the rate of protein degradation by a factor of "mgFac" and CHX slowed down the rate of protein synthesis by a factor of "chxFac". First order rate constants are in min^{-1} and second order in $nM^{-1}s^{-1}$.

Table 16: Optimized parameter values of the IL-4 model across different experimental conditions

Rate constant	IL4	MG132 + IL4	CHX + IL4
mgFac	99		
chxFac	15		
kPTPBind	0.98		
kPTPUnbind	6		
kcatPTP	0.6		
vmTrans	0.13		0.13/chxFac
KmTrans	4.2		
RSocsBind	3.31		

Continued on next page

Table16 – continued from previous page

Rate constant	IL4	MG132 + IL4	CHX + IL4
RSocsUnbind	4.76		
koxPTP	0.002		
kredPTP	0.0016		
ksynthStat	0.9		0.9/chxFac
kdegSTAT	0.02	0.02/mgFac	
kRLBind	1.17		
kRLUnbind	2.65		
kRact	1.27		
kStatRBind	0.48		
kStatRUnbind	1.11		
kStatPhos	23.5		
kStatDimerize	0.759		
kStatDissoc	11.92		
kcyt2nuc	0.024		
knuc2cyt	0.06		
kintRAct	0.001		
kdegSocs	0.067	0.067/mgFactor	
rosBaseline	82		
rosScale	73.6667		

B.2.2 Normalization of model output

Simulated total concentrations of STAT6, pSTAT6 and SOCS were calculated by summing together the time courses of all molecular complexes containing these species. Stoichiometry of dimeric form of pSTAT6 was accounted for as shown in the equations below. The variable names on the RHS correspond to names used in the equations in Table 14.

$$\begin{aligned}
\text{pSTAT}_{\text{total}} &= 2 \times \text{StatAct} + 2 \times \text{StatActNuc} + \text{Statp} + 2 \times \text{StatActPTP1B} + \text{StatpPTP1B} \\
&\quad + 2 \times \text{TCPTPStatActNuc} + \text{StatpNuc} + \text{TCPTPStatpNuc} \\
\text{STAT}_{\text{total}} &= \text{Stat} + \text{Statp} + 2 \times \text{StatAct} + 2 \times \text{StatActNuc} + \text{StatNuc} + 2 \times \text{StatActPTP1B} \\
&\quad + \text{StatpPTP1B} + 2 \times \text{TCPTPStatActNuc} + \text{StatRact} + \text{StatpNuc} \\
&\quad + \text{TCPTPStatpNuc} \\
\text{SOCS}_{\text{total}} &= \text{Socs} + \text{RactSocs} + \text{RactSocsCD45}
\end{aligned}$$

To compare model output with experimentally measured protein fluorescence, all model output was normalized using an equation of the form $y(t) = a \times x(t) + b$, where $x(t)$ is the simulated time course and a and b are molecule specific, optimized constants. Values of a and b for all three experimentally measured species are given in the table below.

Table 17: Normalization factors for simulation output

Molecule	***a***	***b***
Total STAT	.001	.063
SOCS3	.0133	1.0372
pSTAT6	0.0033	0

B.2.3 ROS input to the model

Experimentally measured intracellular oxidation of Jurkat cells under IL-4 stimulation was used as a direct input to the model. $h(t)$, the time derivative of Hill equation fitted to CM-H_2DCFDA oxidation data (Fig. 7) is given by

$$h(t) = \frac{1.25 \times 10^6 \times t^{1.5}}{(4725 + t^{2.5})^2} \tag{3}$$

To reflect the basal oxidation state of the cell and to scale the numerical value of curve to a reasonable level, the, intracellular ROS were assumed to follow the equation

$$\mathrm{ROS}(t) = \mathrm{rosBaseline} + \mathrm{rosScale} \times h(t)$$

These parameters rosBaseline and rosScale were optimized to values shown in Table 16. The curve corresponding to the DPI pretreated cells is given by

$$h_{\mathrm{DPI}}(t) = \frac{8.3 \times 10^5 \times t^{1.5}}{(8738 + t^{2.5})^2}$$

When validating the model with DPI data, rosBaseline was assumed to be 0 and rosScaleDPI was chosen to be a tenth of rosScale. These numbers were chosen to reflect the highly reduced state of the cell under DPI treatment. Also, since the initial phosphorylation of STAT6 was drastically reduced under the influence of DPI, to simulate DPI prereatment, low initial phosphorylation of STAT6 (5% of total STAT6) was assumed.

To simulate exogenous addition of H_2O_2 together with IL-4 stimulation, an exponentially decaying curve was added to Eq. (3). The rate of decay was adjusted so that ROS were brought back to baseline level in approximately 20 min. The following equation was used to simulate the combined effect of H_2O_2 and IL-4:

$$\mathrm{ROS}(t) = \mathrm{rosBaseline} + \mathrm{rosScale} \times (h(t) + 1000 \times \exp(-0.3 * t))$$

B.3 Optimization of cell concentration and serum starvation period

The cell concentration and serum starvation period to be used in the experiments for measuring STAT6 phosphorylation were optimized to maximize the pSTAT6 signal. The serum starvation condition was first optimized by testing a range of values and 4 hours of serum starvation was found to be nearly optimal for maximizing pSTAT6 (Fig. 24). Cell concentration of 16×10^6 cells/ml was used for the experiments performed to optimize the starvation period. Next, the optimal cell concentration was determined by testing a number of cell concentrations with 4 hours of serum starvation, and a concentration of 4×10^6 was found to be nearly optimal (Fig. 25).

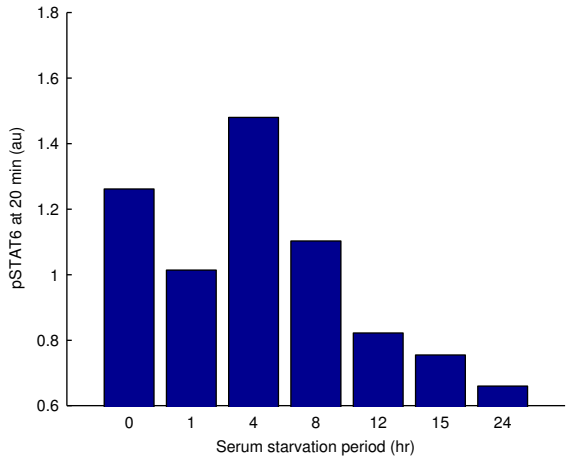

Figure 24: Optimization of serum starvation period. Jurkat cells were serum starved by culturing them at 16×10^6 cells/ml in Jurkat media with 0.5% FBS for a range of time periods. The serum starved cells were stimulated with 100 ng/ml IL-4 for 20 min and pSTAT6 was quantified using flow cytometry.

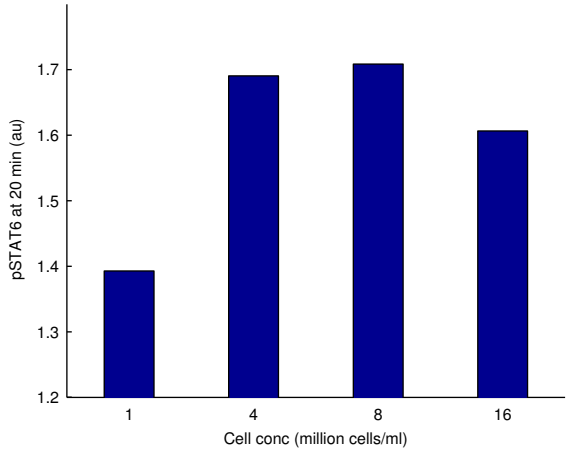

Figure 25: Optimization of cell concentration. Jurkat cells at different concentrations were serum starved for 4 hours. The serum starved cells were stimulated with 100 ng/ml IL-4 for 20 min and pSTAT6 was quantified using flow cytometry.

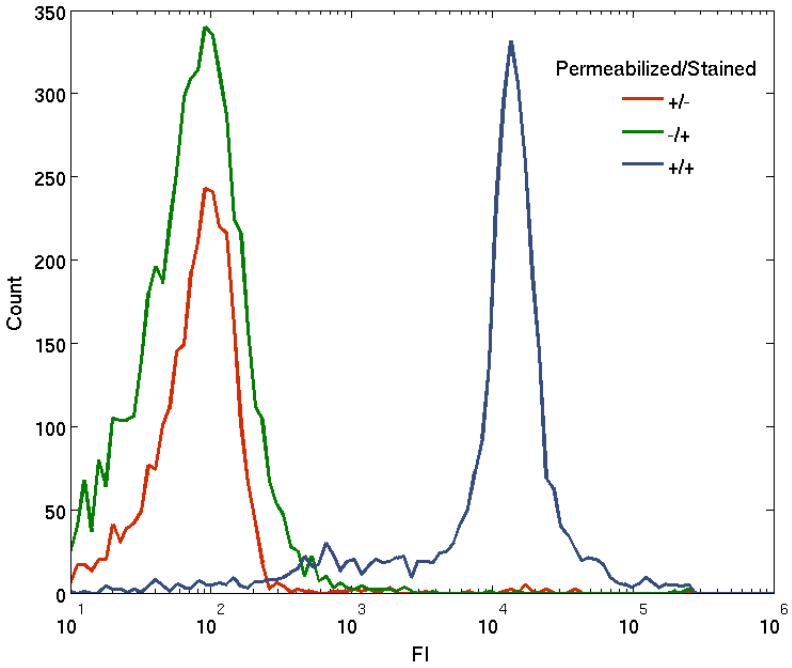

Figure 26: Histone staining in permeabilized Jurkat cells. Jurkat cells were permeabilized or not and stained for the nuclear protein histone. Permeabilized and stained cells (blue histogram) showed signal well above background (red) suggesting that the permeabilization protocol made the intra-nuclear space accessible to the staining antibodies.

B.4 Experimentally measured pSTAT6 represents whole cell value

We have based much of our analysis of the IL-4 pathway on our ability to measure total pSTAT6 levels in the cell. To verify that we were indeed measuring whole cell pSTAT6 through our flow cytometry protocol, we performed two separate experiments.

B.4.1 Histone staining to verify that the nuclear compartment is accessible

Jurkat cells were serum starved like in other experiments (see Methods in Chapter 3). Serum starved cells were either fixed, and then permeabilized or not. Cells were then stained for the nuclear protein, histone. Only cells that were permeabilized showed a positive signal above background. Representative data are shown in Fig. 26. This suggests that the permeabilization protocol was sufficient to allow antibodies access to the nucleus.

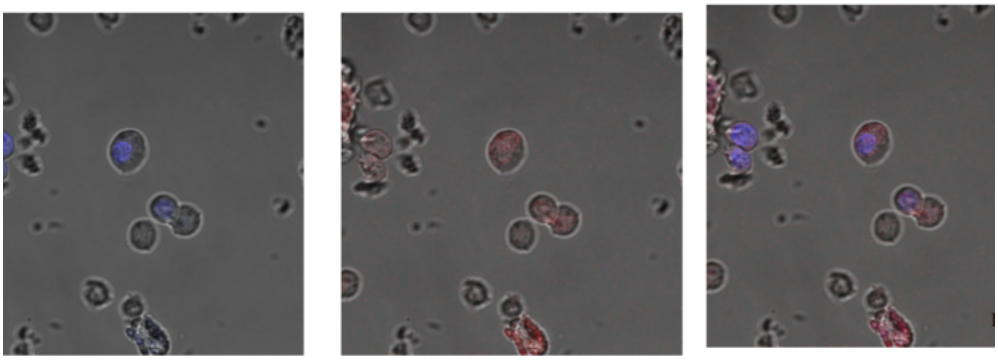

Figure 27: Confocal microscope images confirm whole cell distribution of pSTAT6. Jurkat cells permeabilized and statined for pSTAT6 were counterstained with DAPI. pSTAT6 was found to be distributed throught the intracellular space.

B.4.2 Confocal microsocopy of pSTAT6 stained cells

Jurkat cells were permeabilized and stained for pSTAT6 following the protocol used in other experiments (Methods in Chapter 3). The nucleus was costained with DAPI. Cells were observed under a confocal microscope and it was found that DAPI stain localized to the nucleus whereas pSTAT6 could be detected in both the nuclear and cytosolic compartments Fig. 27

B.5 J45.01 cells to validate the IL-4 model

We attempted to validate the model using data from the J45.01 cell line, which is derived from Jurkat cells by exposing them to gamma irradiation and selecting CD45 deficient cells. Since CD45 is a phosphatase involved in regulation of IL-4 signaling, we hypothesized that signaling characteristics of Jurkat and J45.01 should be different, and these differences should be determined by the differential expression of CD45 between the two cell lines. If this hypothesis is correct, the behavior of J45.01 cells could be simulated in the systems model of IL-4 pathway by assuming reduced concentration of membrane bound PTP, providing a way to further validate the model. We performed experiments using the J45.01 cell line with a view to acquire data that could be used to validate the model.

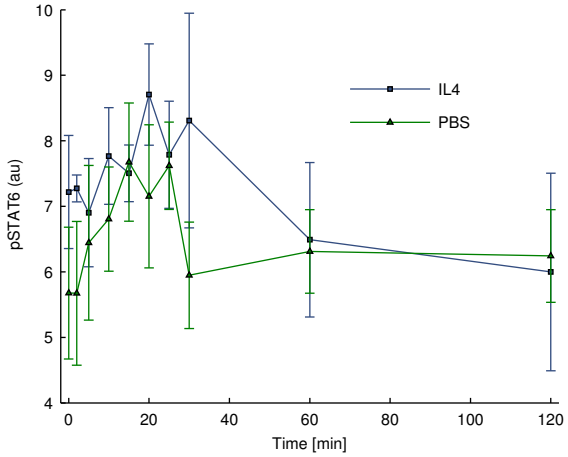

Figure 28: STAT6 phosphorylation following IL-4 stimulation of J45.01 cells. J45.01 cells were serum starved for 4 hours and stimulated with 100 ng/ml IL-4. pSTAT6 was quantified using flow cytometry. Mean and standard errors are shown; n = 4.

B.5.1 J45.01 cells do not respond to IL-4 stimulation

We measured STAT6 phosphorylation in J45.01 cells following IL-4 stimulation and found that basal level of pSTAT6 in this cell line was more than 5 fold higher than that observed in Jurkat cells (compare Fig. 28 with Fig. 7). Furthermore, IL-4 stimulation did not alter pSTAT6 level significantly compared to baseline (Fig. 28). When the J45.01 cells were treated with DPI, STAT6 phosphorylation steadily decreased over time but even under this condition, IL-4 did not elicit any increase in pSTAT6 as compared to cells untreated with IL-4 (Fig. 29).

We hypothesized that the non-responsiveness of J45.01 cells to IL-4 could be linked to altered dynamics of ROS production in these cells as compared to Jurkat cells. To test this hypothesis we measured oxidation of CM-H_2DCFDA in J45.01 following IL-4 stimulation. In a manner similar to pSTAT6, the oxidation of CM-H_2DCFDA did not change significantly when J45.01 cells were stimulated with IL-4 (Fig. 30); however, unlike pSTAT6, the basal oxidation CM-H_2DCFDA observed in J45.01 cells was very similar to that found in Jurkat cells. This suggests that high basal level of STAT6 phosphorylation in J45.01 cells is probably not linked to cellular oxidation state.

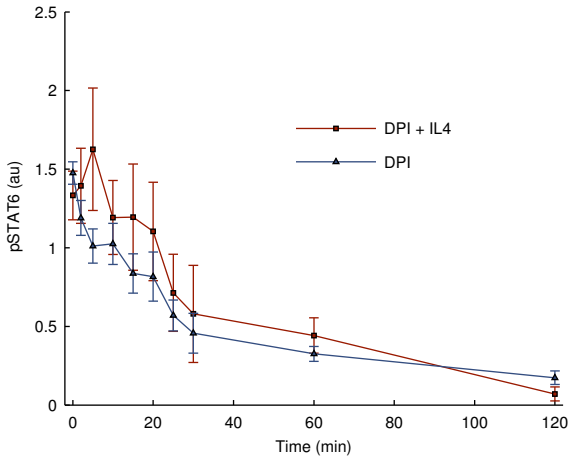

Figure 29: Effect of DPI on IL-4 signaling in J45.01 cells. J45.01 cells were serum starved for 4 hours and treated with DPI for 1 hour before being stimulated with 100 ng/ml IL-4. pSTAT6 was quantified using flow cytometry. Mean and standard errors are shown; n = 4.

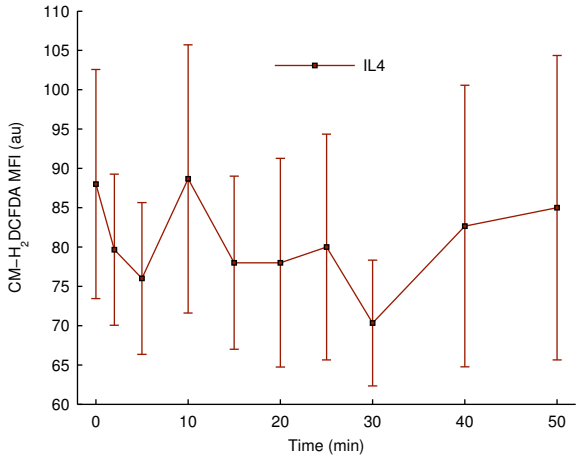

Figure 30: Intracellular oxidation in J45.01 cells following IL-4 stimulation. J45.01 cells were incubated with CM-H_2DCFDA for 30 minutes prior to IL-4 stimulation and oxidation of CM-H_2DCFDA was measured using flow cytometry. Mean and standard errors are shown; n = 3.

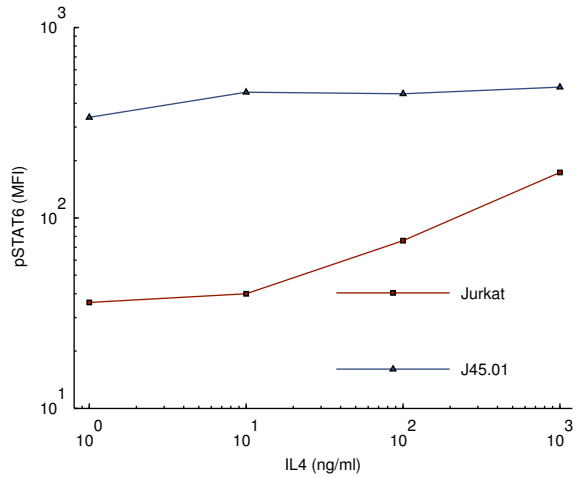

Figure 31: Dose-response of Jurkat and J45.01 cells to IL-4. Jurkat and J45.01 cells were serum starved for 4 hours separately and treated with different concentrations of IL-4 for 15 minutes. STAT6 phosphorylation was measured using flow cytometry.

One of the possible reasons for the lack of response to IL-4 could be that J45.01 cells require stronger IL-4 stimulation than Jurkat cells. To rule out the possibility that the IL-4 concentration was too low for J45.01 cells, we measured the dose responsiveness of J45.01 and Jurkat cells. We found that while STAT6 phosphorylation in Jurkats increased with increasing IL-4, the dose-response curve for J45.01 cells was flat, indicating that J45.01 cells failed to respond to IL-4 over a wide range of doses (Fig. 31).

The lack of responsiveness of J45.01 cells over a wide range of IL-4 doses is indicative of missing components of the IL-4 signaling pathway. We tested J45.01 cells for the presence of IL-4 receptor alpha and found that the expression was comparable between Jurkat and J45.01 cells (Fig. 32).

B.5.2 Expression of multiple proteins could be perturbed in J45.01 cells

We next hypothesized that the difference in pSTAT6 levels between Jurkat and J45.01 cells could be linked to different total STAT6 levels in the two cell lines. We quantified total STAT6 in both cell lines and observed that the basal expression of total STAT6 was nearly 1.6 times greater in J45.01 cells (Fig. 33). The greater levels of pSTAT6 in J45.01 cells could, therefore, be partially explained by increased level of total STAT6 in these cells.

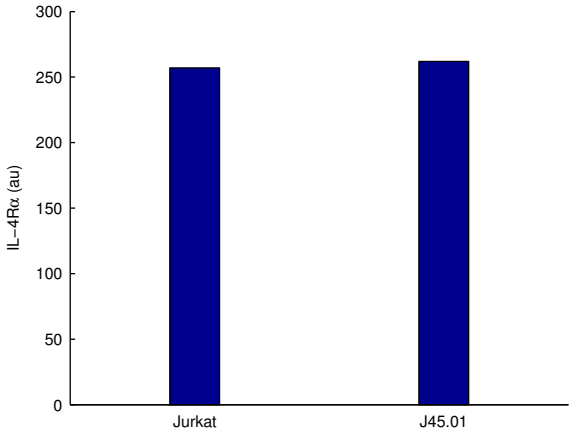

Figure 32: Expression of IL-4 receptor alpha in Jurkat and J45.01 cells. Cells were serum starved for 4 hours and expression of cell surface IL-4R4α was measured using flow cytometry.

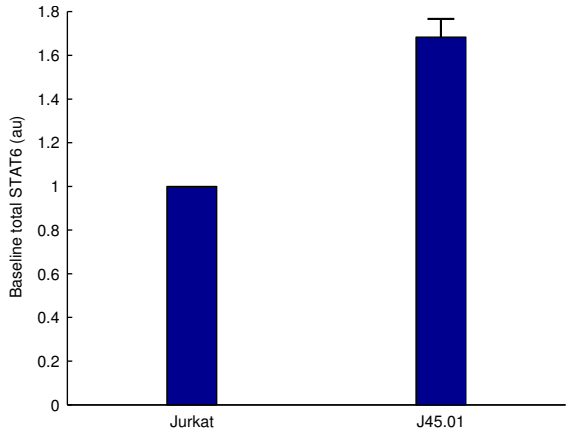

Figure 33: J45.01 cells express more STAT6 than Jurkat cells. J45.01 and Jurkat cells were separately serum starved for 4 hours and the basal expression of total STAT6 was measured using flow cytometry. Data were normalized to get the MFI in Jurkat cells equal to 1. Mean and standard errors are shown; n = 3.

However, as compared to Jurkat cells, the basal STAT6 phosphorylation was more than 5 times greater in J45.01 cells, which is not proportional to the increase observed in total STAT6 levels. The higher level of total STAT6 in J45.01 cells also indicates that CD45 is not the only protein to be expressed differentially between the two cell lines. It is possible that several other proteins have altered expression levels in J45.01 cells, which could affect the dynamics of IL-4 signaling in unpredictable ways. Quantifying all such differences and simulating them in our model of IL-4 signaling is a very difficult proposition. We therefore decided not to use J45.01 cells to validate our model.

APPENDIX C

ES-HM IMPLEMENTATION AND TESTING DETAILS

C.1 Test functions

The test functions used to evaluate the performance of the algorithms are described below. The functions were selected from the test suites of CEC 2008 [140] and BBOB 2009 [47].

C.1.1 Sphere function

$$f_1(\boldsymbol{x}) = \sum_{i=1}^{n} x_i^2 \tag{4}$$

- Unimodal, separable
- $\boldsymbol{x} \in [-100, 100]^n$

C.1.2 Schwefel's problem 2.21

$$f_2(\boldsymbol{x}) = \max\{|x_i|, 1 \leq i \leq n\} \tag{5}$$

- Unimodal, non-separable
- $\boldsymbol{x} \in [-100, 100]^n$

C.1.3 Rastrigin function

$$f_3(\boldsymbol{x}) = \sum_{i=1}^{n} \left(x_i^2 - 10\cos(2\pi x_i) + 10\right) \tag{6}$$

- Multimodal, separable
- $\boldsymbol{x} \in [-5, 5]^n$

C.1.4 Ackley function

$$f_4(\boldsymbol{x}) = -20\exp\left(-0.2\sqrt{\frac{1}{n}\sum_{i=1}^{n}x_i^2}\right) - \exp\left(\frac{1}{n}\sum_{i=1}^{n}\cos(2\pi x_i)\right) + 20 + e \tag{7}$$

- Multimodal, separable
- $\boldsymbol{x} \in [-32, 32]^n$

C.1.5 Rosenbrock function

$$f_5(\boldsymbol{x}) = \sum_{i=1}^{n}\left(100(x_i^2 - x_{i+1})^2 + (x_i - 1)^2\right) \tag{8}$$

- Multimodal, non-separable
- $\boldsymbol{x} \in [-100, 100]^n$

C.1.6 Griewank function

$$f_6(\boldsymbol{x}) = \frac{1}{4000}\sum_{i=1}^{n}x_i^2 - \prod_{i=1}^{n}\cos\left(\frac{x_i}{\sqrt{i}}\right) + 1 \tag{9}$$

- Multimodal, non-separable
- $\boldsymbol{x} \in [-600, 600]^n$

C.1.7 Gallgher's Gaussian 21-peak function

$$f_7(\boldsymbol{x}) = \left(10 - \max_{i=1}^{n} w_i \exp\left(\frac{-1}{2n}(\boldsymbol{x} - \boldsymbol{y_i})^T \boldsymbol{R}^T \boldsymbol{C}_i \boldsymbol{R}(\boldsymbol{x} - \boldsymbol{y}_i)\right)\right)^2 \tag{10}$$

- $w_i = \begin{cases} 1.1 + 8 \times \dfrac{i-2}{19} & , i = 2, \ldots 21 \\ 10 & , i = 1 \end{cases}$
- $\boldsymbol{C}_i = \boldsymbol{\Lambda}^{\alpha_i}/\alpha_i^{1/4}$, where $\boldsymbol{\Lambda}^{\alpha_i}$ is a diagonal matrix with elements first defined as $\lambda_{ii} = \alpha_i^{\frac{i-1}{2(n-1)}}$ and then randomly permuted. α_is are in turn drawn with uniform random chance from the set $\{1000^{2j/19} \mid j = 0, \ldots, 19\}$ without replacement for $i = 1, \ldots, 21$, and $\alpha_1 = 1000^2$.

- $\boldsymbol{R}$ is an orthonormal (rotation) matrix. It was generated from a matrix with standard normally distributed entries by QR decomposition using the Matlab function qr.
- For each run of f_7, a new set of $\boldsymbol{C}_i$ and $\boldsymbol{R}$ was generated.
- $\boldsymbol{y}_i$ are local optima chosen by uniform random sampling from $[-4.9, 4.9]^n$ for $i = 2, \ldots, 21$. The global optimum $\boldsymbol{y}_1$ was uniformly randomly sampled in $[-4, 4]^n$.
- f_7 is multimodal with 21 optima with random sizes and positions.
- $\boldsymbol{x} \in [-5, 5]^n$

C.1.8 Rotated Weierstrass function

$$f_8(\boldsymbol{x}) = 10\left(\frac{1}{n}\sum_{i=1}^{n}\sum_{k=0}^{11}\frac{1}{2^k}\cos\left(2\pi 3^k z_i\right) - f_o\right)^3 \tag{11}$$

- $\boldsymbol{z} = \boldsymbol{R}\boldsymbol{x}$, where $\boldsymbol{R}$ is a rotation matrix as defined in C.1.7
- $f_0 = \sum_{k=0}^{11}\frac{1}{2^k}\cos(\pi 3^k)$
- Multimodal, non-separable
- Rugged landscape with non-unique global optimum
- $\boldsymbol{x} \in [-5, 5]^n$

C.1.9 Rotated Lunacek bi-Rastrigin function

$$f_9(\boldsymbol{x}) = \min\left(\sum_{i=1}^{n}(x_i - \mu_0)^2, dD + s\sum_{i=1}^{n}(x_i - \mu_1)^2\right) + 10\left(D - \sum_{i=1}^{n}\cos(2\pi z_i)\right) \tag{12}$$

- $\boldsymbol{z} = \boldsymbol{R}\boldsymbol{x}$, where $\boldsymbol{R}$ is a rotation matrix as defined in C.1.7
- $\mu_0 = 2.5, \mu_1 = -\sqrt{\frac{\mu_0^2 - d}{s}}, s = 1 - \frac{1}{2\sqrt{n+20} - 8.2}, d = 1.$
- Multimodal, non-separable
- Very rugged landscape superimposed on two larger valleys around μ_0 and μ_1. The global optimum is at μ_0.

- $\boldsymbol{x} \in [-5, 5]^n$

C.2 Settings used in the ES algorithms

This section describes the details of the internal settings used in the implementation of the evolutionary strategy algorithms. All the variants of ES used in the present work (ES, ES with naive restart, ES-IPOP, ES-HM) were implemented by adding metaheuristics on top of the same implementation of ES; therefore, the settings described here were common to all algorithms. The symbols used are μ, the number of parents; λ, the number of offspring; $\boldsymbol{x}_i$, object parameter vectors; and $\boldsymbol{\sigma}_i$ are the strategy parameters.

Initial population: Initial population was generated by uniform random sampling on linear scale in the search range for all the test functions. For the ODE model, since the parameter ranges spanned several order of magnitude, the initial population was sampled uniformly on a log scale.

Initial step size: Initial step size for each parameter was set at 0.1 times the width of the search range for the parameter.

Recombination: Global uniform recombination was used [125] to recombine the object parameters as well as strategy parameters. For example, in a population of μ parents, there are μ values of x_i, the i^{th} component of the object parameter vector , $i = 1, \ldots, n$. To generate a child using global uniform recombination, one of these μ different values of x_i is picked randomly for each i. This process is repeated λ times to get the offspring population. The same process is applied to the strategy parameters.

Mutation: Mutation was applied to both object and strategy parameters using the following equations for $i = 1, \ldots, \lambda$ and $j = 1, \ldots, n$ [163].

$$\sigma'_{ij} = \sigma_{ij} \exp\left(\tau' N(0,1) + \tau N_j(0,1)\right) \tag{13}$$

$$x'_{ij} = x_{ij} + \sigma'_{ij} N_j(0,1) \tag{14}$$

where, x_{ij} and σ_{ij} are j^{th} components of of the vectors $\boldsymbol{x}_i$ and $\boldsymbol{\sigma}_i$, respectively. The primed symbols indicate the mutated values. The mutated step size is used to mutate the object

parameters. $N(0,1)$ represents a normally distributed scalar with mean 0 and standard deviation 1. $N_j(0,1)$ implies that a new number is generated for each j. τ and τ' were set to $\left(\sqrt{2\sqrt{n}}\right)^{-1}$ and $\left(\sqrt{2n}\right)^{-1}$.

Stopping criteria: A stopping criterion was deemed to be satisfied if any of the following became true. b denotes fitness score of the fittest individual in the current generation and w, the worst fitness score.

- $|w - b| <$ absTolFitness

  $|w - b| <$ relTolFitness $\times \widehat{\text{fitness}}$, where $\widehat{\text{fitness}}$ is the average fitness of the population

- $\sigma_{ij} <$ absTolStepSize for all i, j

- $\sigma_{ij} <$ relTolStepSize $\times x_{ij}$ for all i, j

The default values used for the tolerances were absTolFitness = 10^{-3}, relTolFitness = 10^{-6}, absTolStepSize = 10^{-3}, and relTolStepSize = 10^{-6}.

C.3 A model of the IL-4 pathway

C.3.1 Major assumptions of the model

This model is not the same as the systems model of IL-4 signaling proposed in Chapter 3. This is instead a simplified model of the IL-4 pathway that was used only to test the performance of the optimization algorithm.

The IL-4 receptor uses the kinase activity of JAK1 and JAK3 proteins for downstream phosphorylation. As JAK1 and JAK3 have been shown to be constitutively associated with the cytoplasmic chains of the IL-4 receptor [45], we did not explicitly model the JAK proteins and treated the IL-4 receptor/JAK complex as a single molecule. Furthermore, we ignored the multimeric nature of the IL-4 receptor and assumed that IL-4 activates the receptor in a single step [77].

STAT6 is thought to homodimerize after it is phosphorylated [113]. We ignored the dimerization in our model and assumed that monomeric pSTAT6 represents the entire

pSTAT6 pool. We further assumed that the IL-4 receptor and STAT6 have distinct phosphatases. However, a single phosphatase can possibly act on multiple substrates and the assumption of one substrate-one phosphatase is a simplification [120].

We assumed that total concentration of all the modeled molecules, except IL-4 and ROS, remains constant over time. We assigned a first order removal term to IL-4 to simulate receptor mediated internalization and degradation. ROS time course was simulated using explicit functions of time and provided as input to the model (Fig. 34).

C.3.2 ODE system and simulation settings

The ODE system shown below was used to model the IL-4 pathway assuming mass action kinetics. Meanings of the symbols and values of the parameters are given in Tables 18 and 19. We ran the model from time $t = -1500$ min to $t = 0$ min to allow the system to reach a steady state (equilibration process). During this equilibration, ROS levels were fixed to a constant baseline value shown in the table. DPI pre-treatment was simulated by setting the ROS baseline value to 1 to reflect depleted intracellular ROS. Our experimental data showed noticeable phosphorylation of STAT6 even without any IL-4 stimulation. In order to capture this effect in the model, we assumed the presence of a constant weak activating signal throughoutt the equilibration process. This was simulated by fixing IL-4 concentration to 0.005 nM from time $t = -1500$ min to $t = 0$ min (value fitted by hand). At time $t = 0$ min, IL-4 concentration was increased to 5.8 nM (corresponding to 100 ng/mL IL-4 used in the experiments) and first order decay of IL-4 was allowed (as shown in Fig. 19). ROS time course was simulated using the profiles shown in Fig. 34.

The experimental data used to optimize the model represent normalized fluorescence intensities corresponding to total phosphorylated STAT6 in Jurkat cells. To compare the simulated time courses with the experimental data, the simulated values of cytosolic and nuclear pSTAT6 were summed and then transformed using the equation $y = ax + b$, where y is the transformed value, x is the total pSTAT6 concentration returned by the model and a

and b are constants. The values of a and b were determined by mapping the lowest value of x to the lowest experimental data point and the highest value of x to the largest data point, when both the simulation and the experimental data were taken from the IL-4 stimulation condition (i.e., with no DPI pre-treatment). The same transformation was also applied to scale the simulation results for DPI + IL-4 treatment. It should be noted that the values of a and b change depending on the parameters of the ODE system.

$$
\begin{aligned}
\frac{dx_1}{dt} &= -k_1 x_1 x_3 + k_2 x_2 x_8 \\
\frac{dx_2}{dt} &= +k_1 x_1 x_3 - k_2 x_2 x_8 \\
\frac{dx_3}{dt} &= -k_3 x_3 \\
\frac{dx_4}{dt} &= -k_4 x_4 x_2 + k_5 x_5 x_{10} + k_7 x_7 \\
\frac{dx_5}{dt} &= +k_4 x_4 x_2 - k_5 x_5 x_{10} - k_6 x_5 \\
\frac{dx_6}{dt} &= +k_6 x_5 - k_5 x_6 x_{12} \\
\frac{dx_7}{dt} &= +k_5 x_6 x_{12} - k_7 x_7 \\
\frac{dx_8}{dt} &= -k_8 x_8 ros + k_9 x_9 \\
\frac{dx_9}{dt} &= +k_8 x_8 ros - k_9 x_9 \\
\frac{dx_{10}}{dt} &= -k_{10} x_{10} x_{14} + k_{11} x_{11} \\
\frac{dx_{11}}{dt} &= +k_{10} x_{10} x_{14} - k_{11} x_{11} \\
\frac{dx_{12}}{dt} &= -k_{10} x_{12} x_{15} + k_{12} x_{13} \\
\frac{dx_{13}}{dt} &= +k_{10} x_{12} x_{15} - k_{12} x_{13}
\end{aligned}
$$

C.3.3 Parameter values

Even though different members of the JAK-STAT family are activated by different interleukins, the core structure of JAK-STAT pathway is very similar across many types of cytokines, such as IL-1 and IL-4. Because of this similarity, we used the parameter set of a previously published model of IL-1 signaling as the basis for parameter estimation of JAK-STAT core of the IL-4 pathway [161]. Starting from these values, we adjusted them by hand to obtain reasonable fits to the data as determined by visual inspection (column *Initial estimate* in Tables 18 and 19). The optimization algorithms were executed to estimate parameters within fixed bounds around these initial estimates. The optimized parameter values corresponding to the median fitness scores found by ES and ES-HM are presented in Tables 18 and 19.

C.4 Tables and Figures

Table 18: Initial values. Symbols used in the equations and the molecular species they represent according to Fig. 19. Hand-fitted values used as first guess for optimization are shown in the column *Initial estimate*. Parameter estimates corresponding to the median scores found by ES-HM and ES when the search range was fixed 5-fold above and below the first estimate values are shown under the columns *ES-HM* and *ES*, respectively. All concentrations are in units of nM.

Symbol	**Molecular species**	**Initial estimate**	**Optimized value**	
			ES-HM	**ES**
x_1	IL4R	4.51	10.9	1.23

Continued on next page

Table18 – continued from previous page

Symbol	Molecular species	Initial estimate	Optimized value	
			ES-HM	ES
x_2	IL4R*	0	0	0
x_3	IL4	0.005[a]	-	-
x_4	STAT6	168	209	243
x_5	pSTAT6	0	0	0
x_6	pSTAT6$_n$	0	0	0
x_7	STAT6$_n$	0	0	0
x_8	P1$_{red}$	41.1	24	25.1
x_9	P1$_{ox}$	0	0	0
x_{10}	P2$_{red}$	117	572	162
x_{11}	P2$_{ox}$	0	0	0
x_{12}	P2n$_{red}$	0.094	0.45	0.195
x_{13}	P2n$_{ox}$	0	0	0
x_{14}	ROS (basal)	1.9e3[b]	792	633
x_{15}	ROSn (basal)	1.9e2[c]	79.2	63.3

[a] IL-4 was set to a low initial value to simulate a small activating signal during equilibration (see subsection C.3.2). The same value was used in all simulations. To simulate addition of 100 ng/mL IL-4 (the experimental concentration used), IL-4 was changed to 5.8 nM.

[b] ROS level was fixed to this value during equilibration. Afterwards, curves shown in Fig. 34 were used. To simulate DPI pre-treatment, the baseline ROS level was set to 1.

[c] Nuclear ROS was assumed to be one-tenth of cytosolic ROS throughout all conditions and time points in order to reflect the relatively more reduced environment of the nucleus.

Table 19: Rate constants. Symbols used in the equations and the rate constants they represent according to Fig. 19 in the main text are indicated. The hand-fitted values used as the first guess for optimization are shown in the column *Initial estimate*. Parameter values corresponding to the median scores found by ES-HM and ES when the search range was fixed 5-fold above and below the first estimate values are shown under the columns *ES-HM* and *ES*, respectively. First order rate constants are in units of min^{-1} and second order rate constants in $nM^{-1}min^{-1}$.

Symbol	Rate constant	Initial estimate	Optimized value	
			ES-HM	ES
k_1	kract	0.0254	0.113	0.0903
k_2	krinact	0.0048	0.0087	0.0019
k_3	kintil4	0.0795	0.162	0.303
k_4	konstat	12	31.2	4.81
k_5	koffstat	3.5	11.3	5.63
k_6	kc2n	0.266	0.598	0.865
k_7	kn2c	0.334	0.87	0.622
k_8	k1ox	0.00361	0.00774	0.0102
k_9	k1red	0.178	0.281	0.489
k_{10}	k2ox	0.00633	0.0268	0.027
k_{11}	k2red	0.0886	0.114	0.0303
k_{12}	k2redn	7.22	36	35.6

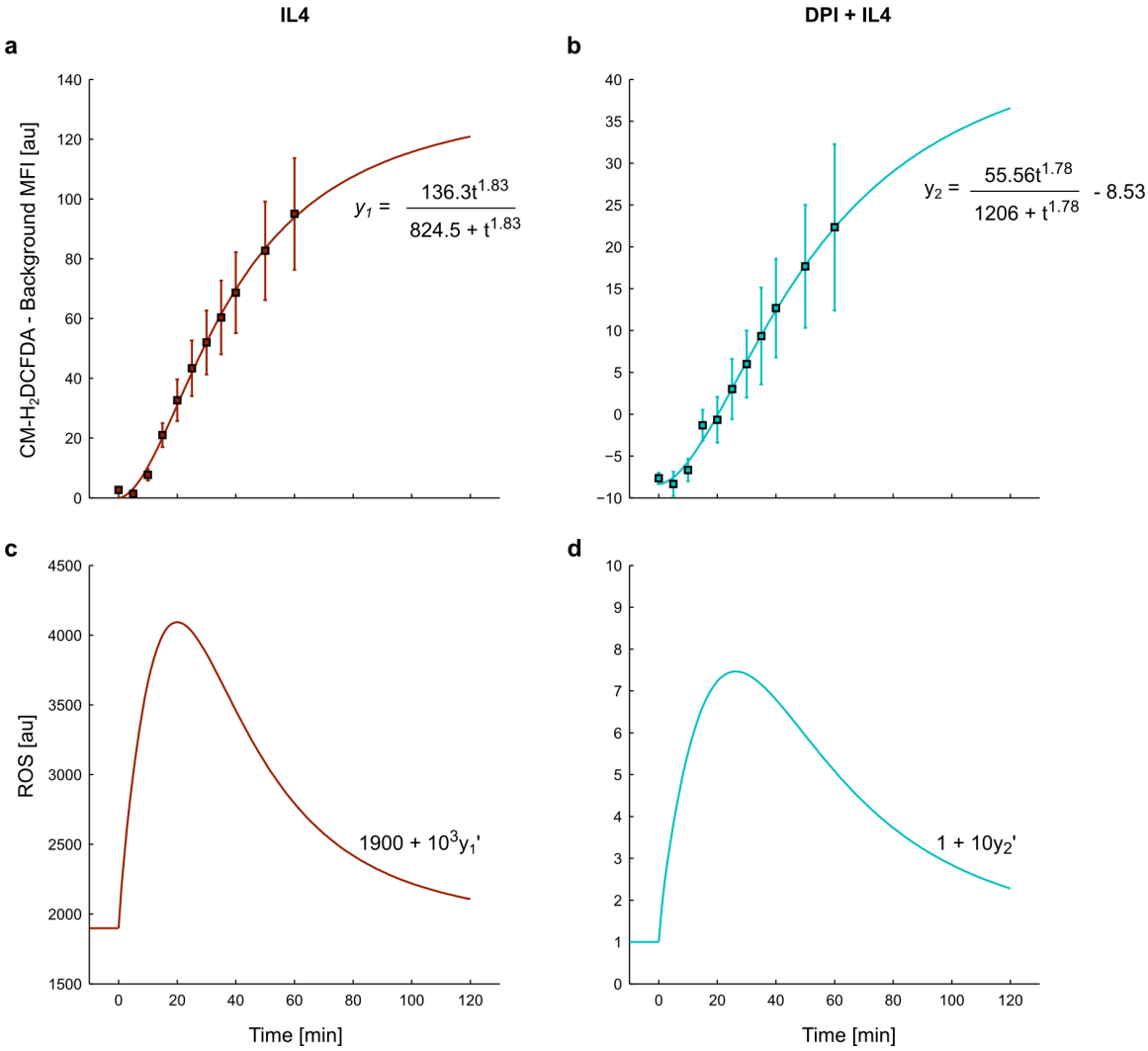

Figure 34: ROS profiles. Oxidation of CM-H_2DCFDA was measured for 60 min following stimulation with IL-4 without (a) or with (b) DPI pre-treatment for 1 hour (data points show mean ± standard error of the mean from 3 independent runs after background subtraction). Hill curves were fitted (lines in a and b) to the means and extrapolated to 120 min. Since the oxidation of CM-H_2DCFDA is irreversible, the oxidation time courses show cumulative oxidation of the dye over time. To estimate instantaneous ROS levels, derivatives of the Hill curves were calculated, scaled by a constant and shifted on the y-axis to represent baseline ROS concentration. In the IL-4 treatement condition, the scaling factor was estimated to be 1000 and the baseline value was estimated at 1900 by manual fitting (c). For the DPI-pretreated condition, the values were 10 and 1 respectively (d).

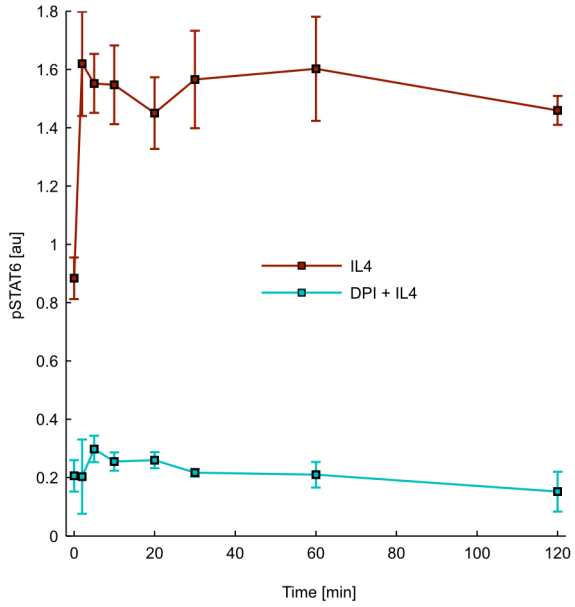

Figure 35: STAT6 phosphorylation time course. Jurkat cells pre-treated or not with DPI were treated with 100 ng/mL IL-4 and STAT6 phosphorylation time courses were measured over a 2 hour time period. Background signal was subtracted from the mean fluorescence intensity values obtained using flow cytometry; the background subtracted values were divided by the fluorescence intensity of cells stained for pSTAT6 without DPI and IL-4 treatment to obtain normalized MFI values. Data points show mean ± standard error of the mean from 3 independent experiments.

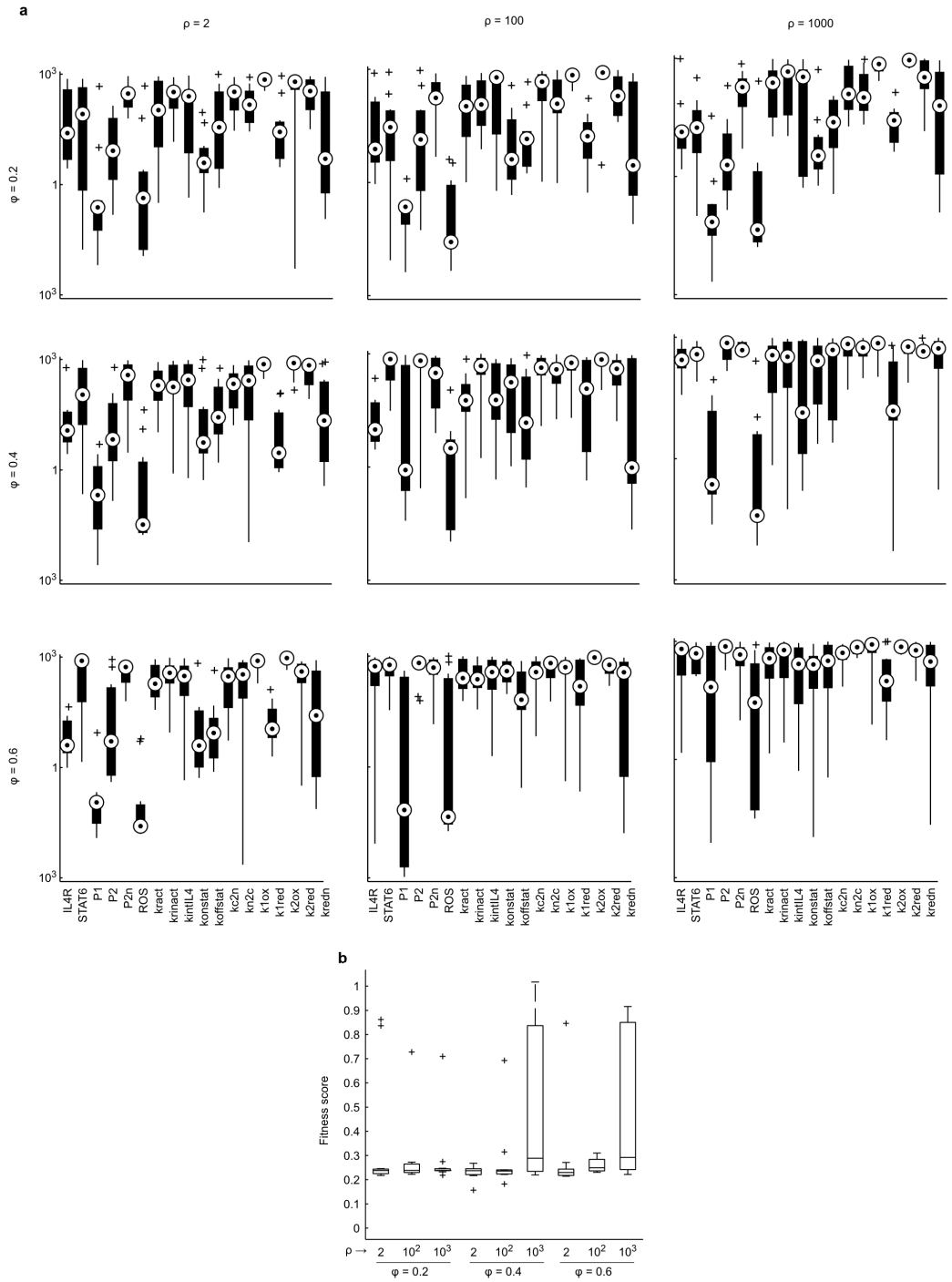

Figure 36: Parameter and score distribution. ES-HM algorithm was run using 9 pairs of (ϕ, ρ) values to optimize the parameters of the IL-4 model. Parameter bounds were set at 1000-fold above and below the first estimate and 10 runs were executed for each (ϕ, ρ) pair. Box plots showing distributions of all the parameters (a) and scores (b) corresponding to all the pairs are shown. The parameter values have been scaled by dividing them by the corresponding first estimate values.

APPENDIX D

DETAILS OF IL-4–EPO CROSSTALK MODEL

Details of models used in Chapter 5 to study ROS mediated crosstalk between IL-4 and Epo pathways are provided here.

The network shown in Fig. 37 was coded into an ODE system assuming mass action kinetics(Eq. (15)). The parameters of the model were optimized to get a reasonable fit to data available from the literature (Fig. 38). The model without crosstalk (Fig. 23b) was obtained by setting the rate constants k8, k11, k13 and k14 to 0. The hypothetical redundant model (Fig. 23c) was obtained by making the following modifications to the model shown in Fig. 37: i) JAK3* catalyzed phosphorylation of STAT5 was added (k = 0.8); ii) JAK2* catalyzed phosphorylation of STAT6 was added (k = 0.8); iii) PTP1B catalyzed dephosphorylation of STAT6 was turned off; iv) PTP1B catalyzed dephosphorylation of JAK3* was added (k = 1.2).

ODE system used to model the network in Fig. 37:

$$
\begin{aligned}
\dot{x}1 &= k18 - k1 \times x1 + k3 \times x2 \\
\dot{x}2 &= k1 \times x1 - k19 \times x2 - k3 \times x2 \\
\dot{x}3 &= k18 - k2 \times x3 + k4 \times x4 \\
\dot{x}4 &= k2 \times x3 - k20 \times x4 - k4 \times x4 \\
\dot{x}5 &= -k5 \times x5 \times x2 + k7 \times x6 \\
\dot{x}6 &= k5 \times x5 \times x2 - k7 \times x6 \\
\dot{x}7 &= -k6 \times x7 \times x4 + k8 \times x8 \times x9 \\
\dot{x}8 &= k6 \times x7 \times x4 - k8 \times x8 \times x9 \\
\dot{x}9 &= -k16 \times x9 \times x15 + k17 \times x10 \\
\dot{x}10 &= k16 \times x9 \times x15 - k17 \times x10 \\
\dot{x}11 &= -k9 \times x11 \times x6 + k11 \times x12 \times x9 + k18 \\
\dot{x}12 &= k9 \times x11 \times x6 - k11 \times x12 \times x9 - k21 \times x12 \\
\dot{x}13 &= k18 + k12 \times x14 - k10 \times x13 \times x8 \\
\dot{x}14 &= -k22 \times x14 - k12 \times x14 + k10 \times x13 \times x8 \\
\dot{x}15 &= k13 \times x2 + k14 \times x4 - k15 \times x15 - k16 \times x9 \times x15
\end{aligned}
\tag{15}
$$

Table 20: List of species in the model and their initial values.

Species	Symbol	Initial value
IL4R	x1	12
IL4R*	x2	0
EpoR	x3	12
EpoR*	x4	0
JAK3	x5	12

Continued on next page

Table20 – continued from previous page

Species	Symbol	Initial value
JAK3*	x6	0
JAK2	x7	12
JAK2*	x8	0
PTP1Bred	x9	50
PTP1Box	x10	0
STAT6	x11	1000
STAT6*	x12	0
STAT5	x13	1000
STAT5*	x14	0
ROS	x15	0

Table 21: Optimized values of rate constants. Edges associated with the constants are indicated in Fig. 37. First order rate constants are in min^{-1} and second order rate constants in $nM^{-1}min^{-1}$.

Parameter	Value
k1	0.4
k2	0.4
k3	1
k4	1
k5	0.1
k6	0.5
k7	1

Continued on next page

Table21 – continued from previous page

Parameter	Value
k8	1.2
k9	0.8
k10	0.8
k11	0.01
k12	0.05
k13	10
k14	10
k15	0.06
k16	0.5
k17	0.02
k18	0.005
k19	1
k20	1
k22	0.0005
k23	0.0005

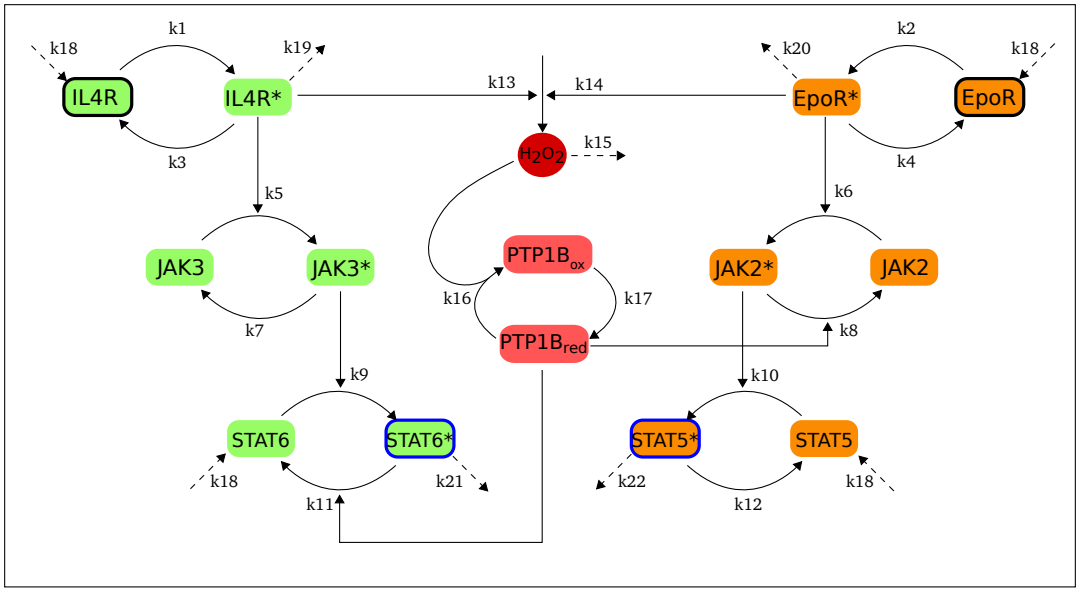

Figure 37: Model of the IL4R and EpoR signaling cross-talk. The signaling system was modeled by ODEs shown in Eq. (15). The parameters in Table 21 correspond to edges indicated in the figure.

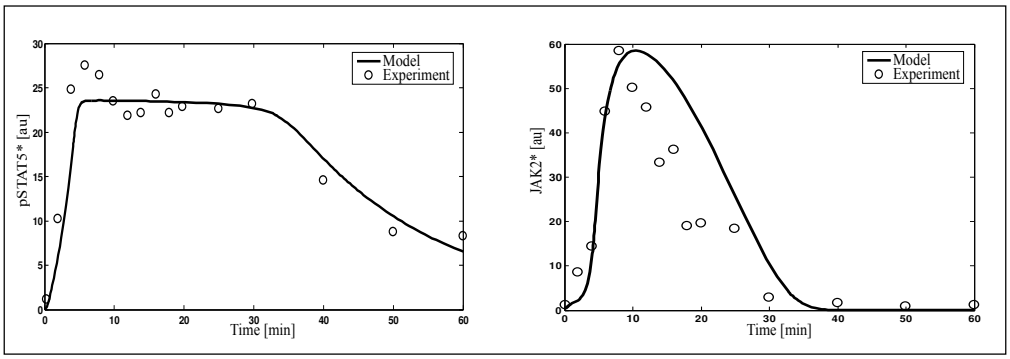

Figure 38: Approximate fitting of the model to experimental data. The parameters in Table 21 were optimized to generate reasonable fits to STAT5 and JAK2 phosphorylation data obtained from [139].

APPENDIX E

LISTING OF MATLAB IMPLEMENTATION OF ES-HM

E.1 ES-HM in MATLAB

A MATLAB implementation of the ES-HM algorithm is presented here.

```
% Author: Gaurav Dwivedi (g.dwivedi@gatech.edu)
% Date: October 22, 2013

function [optimParam, funEvalCount, bestScores, ↓
→    worstScores] = es(fitnessFn, nvar, lb, ub, ↓
→    userOptions)
%ES uses evolutionary strategies to find the minimum of a given function.
%Hypermutation can be optionally turned on to use the ES-HM algorithm. If
%a worker pool has been started using matlabpool, ES uses parfor to
%parallelize objective function evaluation.
%
%The ES algorithm was implemented as described by 'Evolution and Optimum
%Seeking' by Hans-Paul Schwefel (1995) and 'Evolutionary Computation' by
%Xin Yao, Ch. 2 in Evolutionary Optimization, editors, Ruhul Sarker, Masoud
%Mohammadian & Xin Yao (2002).
%
%The hyper-mutation (HM) algorithm was developed by Gaurav Dwivedi and
%Melissa L. Kemp.
%
%    [OPTIMPARAM, FUNEVALCOUNT, BESTSCORES, WORSTSCORES] = ES(FITNESSFN, NVAR, LB, ↓
→    UB,
%    USEROPTIONS)
%
%    Output:
%    -------
%    OPTIMPARAM = Optimized parameter values. This is the parameter vector
%——————→corresponding to the fittest individual in the last generation.
%    FUNEVALCOUNT = Number of function evaluations.
%    BESTSCORES = Vector containing best fitness score for each generation.
%    WORSTSCORES = Vector containing worst fitness score for each generation.
%
%    Required input parameters:
```

```
%    --------------------------
%    FITNESSFN = Handle to fitness scoring function. Should return a scalar
%        (fitness score) when a vector of length NVAR is passed. If parallel is
%        set to 1 in USEROPTIONS, it should accept an MxNVAR matrix, where each
%        row is a parameter vector and return a vector of scores of length M, with
%        each element being the fitness score corresponding to a row of the input ↓
→       matrix.
%    NVAR = Problem dimension (i.e., number of object parameters to be
%    optimized).
%
%    Optional input parameters:
%    --------------------------
%    LB = Lower bound of parameters. If scalar, same lower bound is used for all
%    ———————→dimensions. A vector of length NVAR can be used to specifiy different
%    ———————→lower bounds for each dimension. {Default = -Inf}
%    UB = Upper bound of parameters. If scalar, same upper bound is used for all
%    ———————→dimensions. A vector of length NVAR can be used to specifiy different
%    ———————→upper bounds for each dimension. {Default = +Inf}
%    USEROPTIONS = Structure containing fields to specify settings of the ES
%    ———————→algorithm. The following fields can be optionally specified. Values in
%    ———————→curly braces indicate defalut values used.
%          MU = Number of parents {7}
%          LAMBDA = Number of  children {50}
%          MAXITER = Maximum number of iterations or generations. {50}
%          INITSTEP = Determines step size of the first generation using the
%    ————→       equation STEPSIZE = INITSTEP*(UB-LB)
%          LOGSPACE = Solve the problem in log space instead of linear? {false}
%          ABSTOLSCORE = Absolute tolerance for score: stop if |best -worst| <
%                ABSTOLSCORE {1e-3}
%          RELTOLSCORE = Relative tolerance for score: stop if |best - worst| <
%                RELTOLSCORE*mean(score) {1e-6}
%          ABSTOLSTEPSIZE = Absolute tolerance for step size: stop if each step size↓
→       <
%              ABSTOLSTEPSIZE {1e-3}
%          RELTOLSTEPSIZE = Relative tolerance for step size: stop if (step
%                size)/(parameter value) < RELTOLSTEPSIZE for each step size {1e-6}
%          MAXMUTATIONATTEMPT = Maximum number of attempts to mutate object ↓
→       parameter.
%                See function mutate for detailed description. {30}
%          PARALLEL = Can FITNESSFN evaluate candidates in parallel? Use if ↓
→       FITNESSFN
%                is parallelized or a speed up is expected {false}
%          FUNEVALLIM = Maximum number of objective function evaluations allowed
%                {NVAR*1e4}
%          DISPLAY = Show progress in command window {false}
```

```
71  %          USEHM = Use the hyper-mutation partial restart strategy? {false}
    %          ** The following options are meaningful only if USEHM is true **
    %          HMFREQUENCY = Frequency of occurrence of hypermutants (parameter phi in ↓
→       the
    %                manuscript). HMFREQUENCY fraction of step-sizes (randomly selected)↓
→        are
    %                increased by factor HMSTRENGTH {0.4}
76  %          HMSTRENGH = Strength of hyper mutation (parameter rho in the manuscript).
    %                Step-sizes of randomly selected parameters are multiplied by ↓
→       HMSTRENGTH.
    %   ———→ HMSTRENGTH should be greater than 1. {10}
    %          STAGNATIONGENHISTORY = Number of generations to monitor to determine if
    %                evolution has stagnated. If the relative percent change in the best↓
→        score is
81  %                less than STAGNATIONTHRESHOLD over the last STAGNATIONGENHISTORY
    %                generations, evolution is assumed to have stagnated. {NVAR}
    %          STAGNATIONTHRESHOLD = If relative percent difference between scores of
    %                successive generations is less than STAGNATIONTHRESHOLD for
    %   ———→ STAGNATIONGENHISTORY generations, evolution is assumed to have
86  %                stagnated. {1}
    %          RESTARTLIM = Maximum number of hypermutation rounds allowed. {10}
    %          RESTARTNOIMPROVELIM = Maximum number of successive restarts withour
    %                improving the score. If the score does not improve in ↓
→       RESTARTNOIMPROVELIM
    %                successive restarts, the algorithm stops. {3}
91

    %% Check validity of the input arguments and update optimization settings
    if nargin < 2
        error('Too␣few␣arguments:␣fitnessFn␣and␣nvar␣are␣↓
→           required');
    end
96

    if ~isa(fitnessFn, 'function_handle')
        error('Argument␣1␣(fitnessFn)␣should␣be␣a␣function␣↓
→           handle');
    end

101 if ~isscalar(nvar)
        error('Argument␣2␣(nvar)␣should␣be␣a␣scalar');
    end

    options = defaultOptions(nvar); %get default options
106


    % Check if options specified by user match the allowed names.
```

```
    if nargin > 4    %one or more fields of options struct are specified by the ↓
→       user
        if ~isstruct(userOptions)
            error('Incorrect␣data␣type:␣userOptions␣should␣↓
→               be␣a␣structure\n');
        end
        names = fieldnames(userOptions);
        for i = 1:length(names)
            if ~isfield(options, names{i})
                error('%s␣is␣not␣a␣valid␣option.␣Check␣↓
→                   userOptions␣structure', names{i});
            else
                options.(names{i}) = userOptions.(names{i});
            end
        end
    end

    if options.logSpace
        options.logInit = true; % if search is in log space, initialize ↓
→           generation 0 in log space
    end

    if options.hmStrength < 1
        warning('Hyper-mutation␣strength␣is␣less␣than␣1.␣↓
→           Values␣greater␣than␣1␣are␣recommended');
    end

    % Check the bounds
    if nargin > 3    % ub has been passed
        if ~isnumeric(ub)
            error('Incorrect␣data␣type:␣ub␣should␣be␣numeric↓
→               ');
        end
        if isempty(ub)   % no limit specified
            ub = ones(1, nvar)*Inf;      % set to +inf
        elseif length(ub) == 1   % one number specied. Use this ub for all ↓
→           params
            ub = ub*ones(1, nvar);
        elseif length(ub) ~= nvar
            error('Vector␣size␣mismatch:␣ub␣should␣be␣a␣↓
→               scalar␣or␣a␣vector␣of␣length␣nvar');
        end
    else     %ub not specified
        ub = ones(1, nvar)*Inf;      % set to +inf
    end
```

```
146
    if nargin > 2    %lb has been passed
        if ~isnumeric(lb)
            error('Incorrect␣data␣type:␣lb␣should␣be␣numeric↓
→               ');
        end
151     if isempty(lb)  % no limit specified
            lb = -ones(1, nvar)*Inf;     % set to -inf
        elseif length(lb) == 1  % one number specied. Use this lb for all ↓
→           params
            lb = lb*ones(1, nvar);
        elseif length(lb) ~= nvar
156         error('Vector␣size␣mismatch:␣lb␣should␣be␣a␣↓
→               scalar␣or␣a␣vector␣of␣length␣nvar');
        end
    else     %lb not passed
        lb = -ones(1, nvar)*Inf;     % set to -inf
    end
161
    if any(ub <= lb)
        error('Error:␣ub␣should␣be␣greater␣than␣lb');
    end


166 % Start ES
    %% Initialize data to be used for optimization
    [params, stdDev] = ...
        gen0(nvar, lb, ub, options.mu, options.logInit, ↓
→           options.logSpace, options.initStep);
    [scoreParents, funEvalCount] = scoreVectors(params, ↓
→       fitnessFn, options.parallel, options.logSpace, 1);
171
    %% Let the system evolve until stopping criteria are met
    iter = 1;    % iteration or generation number
    numRescales = 0;     % number of times strategy parameter hypermutation has↓
→       been used
    lastRestartTime = -Inf; % iteration number at which the last restart was↓
→       applied.
176                                 % At the beginning of the run, this time was inf↓
→                                       generations ago (i.e., no restart yet)
    bestScoreBeforeHM = zeros(options.restartLim, 1);    % ↓
→       vector of best scores just before the HMs are applied
```

```
                                                                    % Used↓
→                                                                     ↓
→                                                                   to↓
→                                                                     ↓
→                                                                   monitor↓
→                                                                     ↓
→                                                                   if↓
→                                                                     ↓
→                                                                   HM↓
→                                                                     ↓
→                                                                   is↓
→                                                                     ↓
→                                                                   improving↓
→                                                                     ↓
→                                                                   score↓
→                                                                   .
    bestScores = zeros(options.maxIter, 1); bestScores(1) = ↓
→      min(scoreParents);
    worstScores = zeros(options.maxIter, 1); worstScores(1) ↓
→      = max(scoreParents);
181
    while 1

        if options.display && mod(iter, 1) == 0
            fprintf(1, 'Iteration␣%d,␣best␣score␣=␣%g,␣worst↓
→              ␣score␣=␣%g\n', ...
186             iter, min(scoreParents), max(scoreParents));
        end

        %%% Store the best and worst stores
        bestScores(iter) = min(scoreParents);
191     worstScores(iter) = max(scoreParents);

        %%% Check if max iteration is reached
        if iter > options.maxIter
            if options.display
196             fprintf('Maximum␣number␣of␣iterations␣↓
→                  exceeded\n');
            end
            break;
        end

201     if funEvalCount > options.funEvalLim
            if options.display
```

```
            fprintf('Maximum number of objective function evaluations exceeded\n');
        end
        break;
    end

    %%% If hypermutation is not requested and stopping criteria are met,
    %%% exit evolution loop.
    stopCriteria = stop(scoreParents, params, stdDev, options.absTolScore, options.relTolScore, options.absTolStepSize, options.relTolStepSize, options.display);
    if ~options.useHM && stopCriteria
        break;
    end

    %%% If hypermutation is requested, then rescale the standard deviations
    %%% if scores are stagnating or stopping criteria are met. Stop if
    %%% score is not improving despite several restarts.
    if options.useHM && ...
            ( stopCriteria || (iter - lastRestartTime >= options.stagnationGenHistory && scoresStagnant(options, bestScores, iter)) )
                                    % (line above) check for stagnation
                                        only if sufficient time has passed
                                        since last restart,
                                    % otherwise restarts can possibly occur
                                         too close to each other

        % If scores have not improved after several restarts, then stop.
        if numRescales > options.restartNoImproveLim
            indicesOfLastFew = (numRescales - options.restartNoImproveLim):numRescales;
            if all(diff(bestScoreBeforeHM(indicesOfLastFew)) >= 0)
                if options.display, fprintf(1, 'Stopping: Too many restarts without improving\n'); end
                break;
            end
        end

        % Introduce HMs or stop if maximum no. of restarts exceeded
```

```
            if numRescales >= options.restartLim     %maximum ↓
→               rounds of hypermutation are done
                if options.display, fprintf(1, 'Maximum␣↓
→                   number␣of␣restarts␣reached\n'); end
                break;
            else      %not at max rounds of hypermutation
                % Rescale
                if options.display, fprintf(1, 'Rescaling␣at↓
→                   ␣iteration␣%d\n', iter); end
                stdDev = hyperMutation(stdDev, options.↓
→                   hmFrequency, options.hmStrength);
                numRescales = numRescales + 1;
                lastRestartTime = iter; % update time of latest ↓
→                   restart
                bestScoreBeforeHM(numRescales) = bestScores(↓
→                   iter);  % the best score just before the hypermutants take↓
→                    effect
            end
        end


        %%% Recombine to produce children
        [paramsChild, stdDevChild] = recombine(params, ↓
→           stdDev, options.lambda);

        %%% Mutation of individuals
        [paramsChild, stdDevChild] = ...
            mutate(paramsChild, stdDevChild, lb, ub, options↓
→               .maxMutationAttempt);

        %%% Scoring the individuals
        [scoreChildren, funEvalCount] = scoreVectors(↓
→           paramsChild, fitnessFn, options.parallel, options↓
→           .logSpace);

        %%% Select the next generation of parents
        [params, stdDev, scoreParents] = ...
            select(paramsChild, stdDevChild, scoreChildren, ↓
→               options.mu);

        iter = iter + 1;

    end
```

```
%%% Trim the storage vectors if required
if iter < options.maxIter
    bestScores = bestScores(1:iter);
    worstScores = worstScores(1:iter);
end

optimParamIdx = find(scoreParents == bestScores(end), 1,↓
    'first');  %index of the best solution
optimParam = params(optimParamIdx, :); %the best parameter set in↓
    the last generation
if options.logSpace      %params were tranformed to log10. Change them ↓
    back
    optimParam = 10.^optimParam;
end
%---

function stopFlag = ...
    stop(score, param, stdDev, absTolScore, relTolScore,↓
        absTolStepSize, relTolStepSize, out)
% Check if the evolving system meets any of the following stopping criteria
% absTolScore = absolute tolerance for score: |best -worst| < absTolScore
% relTolScore = relative tol for score: |b - w| < relTolScore*mean(score)
% absTolStepSize = abs tol for step size: Each step size < absTolStepSize
% relTolStepSize = rel tol for step size: step size/paramValue <
%    relTolStepSize for each step size
% Display stopping decision if out is true.

stopFlag = false;
best = min(score);
worst = max(score);

if abs(worst - best) < absTolScore
    stopFlag = true;
    if out
        fprintf('Absolute␣tolerance␣satisfied.␣Best␣↓
            score␣=␣%g,␣worst␣score␣=␣%g\n', best, worst)↓
            ;
    end
    return;
end

if abs(worst - best) < mean(score)*relTolScore
    stopFlag = true;
    if out
```

```
            fprintf('Relative tolerance satisfied. Best ↓
→               score = %g, worst score = %g\n', best, worst)↓
→               ;
        end
        return;
    end

    if all(all(stdDev < absTolStepSize))
        stopFlag = true;
        if out
            fprintf('Step size absolute tolerance satisfied.↓
→               Best score = %g, worst score = %g\n', best, ↓
→               worst);
        end
        return;
    end

    if all(all(stdDev./param < relTolStepSize))
        stopFlag = true;
        if out
            fprintf('Step size relative tolerance satisfied.↓
→               Best score = %g, worst score = %g\n', best, ↓
→               worst);
        end
        return;
    end
    %---


    function [paramsParent, stdDevParent, scoreParent] = ...
        select(paramsChild, stdDevChild, scoreChildren, ↓
→           numParents)
    % Select the best scoring children and assign them as parents for the next
    % generation. Return the scores of the individuals retained

    [~, idx] = sort(scoreChildren); %get the indices of sorted ↓
→       individuals

    paramsParent = paramsChild(idx(1:numParents), :);
    stdDevParent = stdDevChild(idx(1:numParents), :);
    scoreParent = scoreChildren(idx(1:numParents));
    %---
```

```
function [params, stdDev] = mutate(params, stdDev, lb, ↓
→    ub, maxMutationAttempt)
% Mutate the strategy parameters (s) and then mutate the object params (x) using
% the following equations:
% s'(k, i) = s(k, i)*exp(tao'*N(0, 1) + tao*Ni(0, 1))
% x'(k, i) = x(k, i) + s'(k, i)*Ni(0, 1)
%    k = individual #; i = ith component of the vector
%    N(0, 1) = for the whole vector; Ni(0, 1) = for each ith component
%
%    tao   = 1/sqrt(2*sqrt(n))
%    tao' = 1/sqrt(2*n)
%
% Ref: Xin Yao, Evolutionary computation (2002). Ch 2 in Evolutionary
% Optimization, R. Sarker, M. Mohammadian, X. Yao (Eds.).

[popSize, numParam] = size(params);    %number of individuals and ↓
→    number of parameters per individual

%% update the strategy parameters using the expression in function comments
taoIndivid = 1/sqrt(2*sqrt(popSize));
taoCommon = 1/sqrt(2*popSize);
nCommon = randn(popSize, 1);     %one common N(0,1) for each ↓
→    individual
nIndivid = randn(popSize, numParam);     %individual and ↓
→    parameter specific variate
stdDev = stdDev.*exp(bsxfun(@plus, taoCommon*nCommon, ↓
→    taoIndivid*nIndivid));

%% update the optimization parameters
% Element-wise operation is used to mutate each object parameter and check
% if it is within upper and lower bounds. If not, a new mutation is
% attempted. This is until a valid number is found. If no value is
% determined in maxMutationAttemp attempts, the previous value is kept.
for j = 1:numParam  %traverse along columns
    for i = 1:popSize
        failCount = 0;
        while 1
            temp = params(i, j) + stdDev(i, j).*randn;
            if temp > lb(j) && temp < ub(j) %loop till a ↓
→                number within limits is found
                params(i, j) = temp;
                break
            else
                failCount = failCount + 1;
```

```
                    if failCount > maxMutationAttempt %if an ↓
→                       acceptable number cannot be found, keep the previous ↓
→                       number
                        break;
                    end
381             end
            end
        end
    end

386 %---


    function [paramsChild, stdDevChild] = recombine(params, ↓
→       stdDev, numChild)
    % Recombine the parents to create the next generation of children.
391
    [numParent, numParam] = size(params);

    paramsChild = zeros(numChild, numParam);
    stdDevChild = zeros(numChild, numParam);
396
    % Recombine using global uniform recombination
    parentIndex = floor(rand(numChild, numParam)*numParent) ↓
→       + 1;     %random indices of parents
    for i = 1:numParam
        paramsChild(:, i) = params(parentIndex(:, i), i);
401     stdDevChild(:, i) = stdDev(parentIndex(:, i), i);
    end
    %---

    function stagnate = scoresStagnant(opt, scoreHistory, ↓
→       iteration)
406 % Return true if the scores have changed by < thredshold% over successive
    % genHistory generations.

    threshold = opt.stagnationThreshold;
    genHistory = opt.stagnationGenHistory;
411
    stagnate = 0;

    if iteration > genHistory
        temp = scoreHistory(iteration-genHistory:iteration);↓
→               % last genHistory+1 scores
416
```

```
        if all(abs(diff(temp))./temp(1:end-1)*100 < ↓
→           threshold) % if all changes are less than threshold %
             stagnate = 1;    % scores are stagnant
        end
    end
421 %---


    function stdDev = hyperMutation(stdDev, hmFrequency, ↓
→       hmStrength)
    % A fraction of strategy parameters are randomly chosen based on user
426 % speciied options and are increased in value to produce hypermutants

    r = rand(size(stdDev));
    r = r < hmFrequency;
    stdDev = stdDev.* (hmStrength*r);
431

    return;
    %---


436 function [score, funEval] = scoreVectors(params, ↓
→       fitnessFn, parallel, logSpace, reset)
    % Calculate the scores of all the individuals in the population using
    % fitnessFn. Each row in params represents one individual.
    % If fitnessFn is parallelized (parallel = 1), pass the params
    % matrix as such, otherwise, evaluate one parameter vector at a time using
441 % parfor.
    % Transform back to linear space if the searching in logSpace.
    % The reset argument is used to reset the funEvalCount variable. this
    % variable keeps track of how many times the objective function has been
    % evaluated.
446

    if nargin < 5    %if reset is not passed, do not reset funEvalCount
        reset = 0;
    end

451 persistent funEvalCount;     %number of times the scoring function is ↓
→       called

    if reset || isempty(funEvalCount)
        funEvalCount = 0;
    end
456

    if logSpace      %searchin in log space
```

```
        params = 10.^params;      % transform objective parameters back to ↓
→           linear space before passing to scoring fn
    end

461 score = zeros(1, size(params, 1));
    if parallel
        score = fitnessFn(params);
    else
        parfor i = 1:length(score)
466         score(i) = fitnessFn(params(i, :));
        end
    end

    % increment funEvalCount
471 funEvalCount = funEvalCount + size(params, 1);   % the ↓
→       scoring function has been called this many times

    % Warn if the score vector has NaN or Inf
    if any(isnan(score)) || any(isinf(score))
        fprintf(1, 'Warning: The score vector contains Inf ↓
→           or NaN\n');
476 end

    funEval = funEvalCount; %copy persistent variable to return value
    %---

481 function [params, stdDev] = gen0(nvar, lb, ub, mu, ↓
→       logInit, logSpace, initStep)
    % Create an intial population of parents with lower (lb) and upper (ub)
    % bounds. The individuals are generated by uniform random sampling in
    % linear (if logInit == false) or log (if logInit == true) space.
    % See defaultOption fn for meaning of initStep.
486
    % replace +/- Inf with real small/large numbers. These bounds are only used
    % here and do not apply to rest of the search. Changing Inf to real numbers
    % is required because the sampling method used requires calculation of the
    % difference between upper and lower bounds, which should be real.
491 index = (lb == Inf); lb(index) = 1e12;
    index = (lb == -Inf); lb(index) = -1e12;

    index = (ub == Inf); ub(index) = 1e12;
    index = (ub == -Inf); ub(index) = -1e12;
496
    % transform lb and ub to log10 space and use the limits to sample
    if logInit
```

```
        if any(lb <= 0) || any(ub <= 0)
            error('Cannot use log space with non-positive upper or lower bounds');
        else
            lb = log10(lb); ub = log10(ub);
        end
    end

    % Generate initial population
    % r = a + rand*(b-a) => sampling b/w a and b
    a = zeros(1, nvar); b = zeros(1, nvar);
    a(:) = lb(:); b(:) = ub(:); %this preserves the shape of a. We want a, b as row vectors
    a = repmat(a, mu, 1);
    b = repmat(b, mu, 1);
    params = a + rand(mu, nvar).*(b-a);    %each row is one individual; in (0, 1)

    % Generate variances of the individuals
    stdDev = initStep.*(b-a);

    if logInit && ~logSpace %change back to linear-space if log initialize was used but search is in linear space
        params = 10.^params;
        stdDev = 10.^stdDev;
    end
    %---


    function options = defaultOptions(nvar)
    % Populate the options structure of the optimization algo with the
    % following defaults
    %    MU = Number of parents {7}
    %    LAMBDA = Number of  children {50}
    %    MAXITER = Maximum number of iterations or generations. {50}
    %    INITSTEP = Determines step size of the first generation using the
    %----------->      equation STEPSIZE = INITSTEP*(UB-LB)
    %    LOGINIT = Sample in the log space (instead of linear) to initialize
    %          first generation of objective parameters and step sizes. {false}
    %    LOGSPACE = Solve the problem in log space instead of linear? If LOGSPACE
    %          is true, LOGINIT is also switched to true. {false}
    %    ABSTOLSCORE = Absolute tolerance for score: stop if |best -worst| <
    %          ABSTOLSCORE {1e-3}
    %    RELTOLSCORE = Relative tolerance for score: stop if |best - worst| <
    %          RELTOLSCORE*mean(score) {1e-6}
```

```
%    ABSTOLSTEPSIZE = Absolute tolerance for step size: stop if each step size <
%          ABSTOLSTEPSIZE {1e-3}
%    RELTOLSTEPSIZE = Relative tolerance for step size: stop if (step
%          size)/(parameter value) < RELTOLSTEPSIZE for each step size {1e-6}
%    MAXMUTATIONATTEMPT = Maximum number of attempts to mutate object parameter.
%          See function mutate for detailed description. {30}
%    PARALLEL = Can FITNESSFN evaluate candidates in parallel? Use if FITNESSFN
%          is parallelized or a speed up is expected {false}
%    FUNEVALLIM = Maximum number of objective function evaluations allowed
%          {nvar*1e4}
%    DISPLAY = Show progress in command window {false}
%    USEHM = Use the hyper-mutation partial restart strategy? {false}
%    ** The following options are meaningful only if USEHM is true **
%    HMFREQUENCY = Frequency of occurrence of hypermutants (parameter phi in the
%          manuscript). HMFREQUENCY fraction of step-sizes (randomly selected) are
%          increased by factor HMSTRENGTH {0.4}
%    HMSTRENGH = Strength of hyper mutation (parameter rho in the manuscript).
%          Step-sizes of randomly selected parameters are multiplied by HMSTRENGTH.
%          HMSTRENGTH should be greater than 1. {10}
%    STAGNATIONGENHISTORY = Number of generations to monitor to determine if
%         evolution has stagnated. If the relative percent change in the best score ↓
→       is
%          less than STAGNATIONTHRESHOLD over the last STAGNATIONGENHISTORY
%          generations, evolution is assumed to have stagnated. {nvar}
%    STAGNATIONTHRESHOLD = If relative percent difference between scores of
%          successive generations is less than STAGNATIONTHRESHOLD for
%————————→STAGNATIONGENHISTORY generations, evolution is assumed to have
%          stagnated. {1}
%    RESTARTLIM = Maximum number of hypermutation rounds allowed. {10}
%    RESTARTNOIMPROVELIM = Maximum number of successive restarts withour
%          improving the score. If the score does not improve in RESTARTNOIMPROVELIM
%          successive restarts, the algorithm stops. {3}

options.mu = 7;
options.lambda = 50;
options.maxIter = 50;
options.initStep = 0.10;
options.logInit = false;
options.logSpace = false;
options.absTolScore = 1e-3;
options.relTolScore = 1e-6;
options.absTolStepSize = 1e-3;
options.relTolStepSize = 1e-6;
options.maxMutationAttempt = 30;
options.parallel = false;
```

```
options.useHM = false;
options.hmStrength = 10;
options.hmFrequency = 0.4;
options.stagnationThreshold = 1;
options.stagnationGenHistory = nvar;
options.restartLim = 10;
options.restartNoImproveLim = 3;
options.funEvalLim = nvar*1e4;
options.display = 0;
%---
```

Listing 1: (ES-HM.m) The ES-Hm algorithm in MATLAB

REFERENCES

[1] Adimora, N. J., Jones, D. P., and Kemp, M. L., "A model of redox kinetics implicates the thiol proteome in cellular hydrogen peroxide responses," *Antioxidants & Redox Signaling*, vol. 13, no. 6, pp. 731–743, 2010. 1.2, 3.2.3, 3.4

[2] Alon, U., *An introduction to systems biology: design principles of biological circuits*. CRC press, 2006. 1.2

[3] Anagnostopoulos, A., Michel, L., Van Hentenryck, P., and Vergados, Y., "A simulated annealing approach to the traveling tournament problem," *Journal of Scheduling*, vol. 9, no. 2, pp. 177–193, 2006. 4.6

[4] Andrews, R. P., Ericksen, M. B., Cunningham, C. M., Daines, M. O., and Hershey, G. K. K., "Analysis of the life cycle of stat6 continuous cycling of stat6 is required for IL-4 signaling," *Journal of Biological Chemistry*, vol. 277, no. 39, pp. 36563–36569, 2002. 3.1, 3.4

[5] Aon, M. A., Stanley, B. A., Sivakumaran, V., Kembro, J. M., O'Rourke, B., Paolocci, N., and Cortassa, S., "Glutathione/thioredoxin systems modulate mitochondrial h2o2 emission: an experimental-computational study," *The Journal of General Physiology*, vol. 139, no. 6, pp. 479–491, 2012. 3.4

[6] Ashyraliyev, M., Fomekong-Nanfack, Y., Kaandorp, J. A., and Blom, J. G., "Systems biology: parameter estimation for biochemical models," *FEBS Journal*, vol. 276, no. 4, pp. 886–902, 2009. 4.1

[7] Auger, A. and Hansen, N., "Performance evaluation of an advanced local search evolutionary algorithm," in *Evolutionary Computation, 2005. The 2005 IEEE Congress on*, vol. 2, pp. 1777–1784, IEEE, 2005. 4.6

[8] Auger, A. and Hansen, N., "A restart CMA evolution strategy with increasing population size," in *Evolutionary Computation, 2005. The 2005 IEEE Congress on*, vol. 2, pp. 1769–1776, IEEE, 2005. 4.4

[9] Babon, J. J., Kershaw, N. J., Murphy, J. M., Varghese, L. N., Laktyushin, A., Young, S. N., Lucet, I. S., Norton, R. S., and Nicola, N. A., "Suppression of cytokine signaling by SOCS3: characterization of the mode of inhibition and the basis of its specificity," *Immunity*, vol. 36, no. 2, pp. 239–250, 2012. 3.3.4

[10] Berndt, C., Lillig, C. H., and Holmgren, A., "Thiol-based mechanisms of the thioredoxin and glutaredoxin systems: implications for diseases in the cardiovascular system," *American Journal of Physiology - Heart and Circulatory Physiology*, vol. 292, no. 3, pp. H1227–H1236, 2007. 1.3

[11] Beyer, H.-G. and Schwefel, H.-P., "Evolution strategies–A comprehensive introduction," *Natural Computing*, vol. 1, no. 1, pp. 3–52, 2002. 1.7

[12] Bjelakovic, G., Nikolova, D., and Gluud, C., "Antioxidant supplements to prevent mortality," *JAMA*, vol. 310, no. 11, pp. 1178–1179, 2013. 1.2

[13] Buul, J. v., Fernandez-Borja, M., Anthony, E., and Hordijk, P., "Expression and localization of NOX2 and NOX4 in primary human endothelial cells," *Antioxidants & Redox Signaling*, vol. 7, no. 3-4, pp. 308–317, 2005. 3.4

[14] Chao-Wei Chen, K., Zhou, Y., Xing, K., Krysan, K., and Lou, M. F., "Platelet derived growth factor (PDGF)-induced reactive oxygen species in the lens epithelial cells: the redox signaling," *Experimental Eye Research*, vol. 78, no. 6, pp. 1057–1067, 2004. 2.2, 2, 2.2, 2.7

[15] Chen, C.-Y., Willard, D., and Rudolph, J., "Redox regulation of SH2-domain-containing protein tyrosine phosphatases by two backdoor cysteines," *Biochemistry*, vol. 48, no. 6, pp. 1399–1409, 2009. 2.2, 3.1

[16] Chen, H.-C. and Reich, N. C., "Live cell imaging reveals continuous STAT6 nuclear trafficking," *The Journal of Immunology*, vol. 185, no. 1, pp. 64–70, 2010. 3.1, 3.4

[17] Chen, K., Kirber, M. T., Xiao, H., Yang, Y., and Keaney, J. F., "Regulation of ROS signal transduction by NADPH oxidase 4 localization," *The Journal of Cell Biology*, vol. 181, no. 7, pp. 1129–1139, 2008. 1.3

[18] Cheng, G., Diebold, B. A., Hughes, Y., and Lambeth, J. D., "Nox1-dependent reactive oxygen generation is regulated by Rac1," *Journal of Biological Chemistry*, vol. 281, no. 26, pp. 17718–17726, 2006. 1.3

[19] Chou, I.-C. and Voit, E. O., "Recent developments in parameter estimation and structure identification of biochemical and genomic systems," *Mathematical Biosciences*, vol. 219, no. 2, p. 57, 2009. 1.2

[20] Cooney, R. N., "Suppressors of cytokine signaling (SOCS): inhibitors of the JAK/STAT pathway," *Shock*, vol. 17, no. 2, pp. 83–90, 2002. 3.1

[21] Czech, M. P., Lawrence, J. C., and Lynn, W. S., "Evidence for electron transfer reactions involved in the Cu^{2+}-dependent thiol activation of fat cell glucose utilization," *Journal of Biological Chemistry*, vol. 249, no. 4, pp. 1001–1006, 1974. 1.3

[22] Czech, M. P., Lawrence, J. C., and Lynn, W. S., "Evidence for the involvement of sulfhydryl oxidation in the regulation of fat cell hexose transport by insulin," *Proceedings of the National Academy of Sciences*, vol. 71, no. 10, pp. 4173–4177, 1974. 1.3

[23] Datta, K., Sinha, S., Chattopadhyay, P., and others, "Reactive oxygen species in health and disease," *National Medical Journal of India*, vol. 13, no. 6, pp. 304–310, 2000. 1, 1.2

[24] den Hertog, J., Groen, A., and van der Wijk, T., "Redox regulation of protein-tyrosine phosphatases," *Archives of Biochemistry and Biophysics*, vol. 434, no. 1, pp. 11–15, 2005. 2.2

[25] Denu, J. M. and Tanner, K. G., "Specific and reversible inactivation of protein tyrosine phosphatases by hydrogen peroxide: evidence for a sulfenic acid intermediate and implications for redox regulation," *Biochemistry*, vol. 37, no. 16, pp. 5633–5642, 1998. 1.4

[26] Devadas, S., Zaritskaya, L., Rhee, S. G., Oberley, L., and Williams, M. S., "Discrete generation of superoxide and hydrogen peroxide by t cell receptor stimulation selective regulation of mitogen-activated protein kinase activation and fas ligand expression," *The Journal of Experimental Medicine*, vol. 195, no. 1, pp. 59–70, 2002. 1.2, 1.3

[27] DeYulia Jr, G. J. and Cárcamo, J. M., "EGF receptor–ligand interaction generates extracellular hydrogen peroxide that inhibits EGFR-associated protein tyrosine phosphatases," *Biochemical and Biophysical Research Communications*, vol. 334, no. 1, pp. 38–42, 2005. 1.3, 2.5, 3.1

[28] Duhé, R. J., Evans, G. A., Erwin, R. A., Kirken, R. A., Cox, G. W., and Farrar, W. L., "Nitric oxide and thiol redox regulation of Janus kinase activity," *Proceedings of the National Academy of Sciences*, vol. 95, no. 1, pp. 126–131, 1998. 3.1

[29] Ďuračková, Z., "Some current insights into oxidative stress," *Physiological Research*, vol. 59, no. 4, 2010. 1.2

[30] Dwivedi, G. and Kemp, M. L., "Systemic redox regulation of cellular information processing," *Antioxidants & Redox Signaling*, vol. 16, no. 4, pp. 374–380, 2012. 1.1, 1, 3.1

[31] Edelman, G. M. and Gally, J. A., "Degeneracy and complexity in biological systems," *Proceedings of the National Academy of Sciences*, vol. 98, no. 24, pp. 13763–13768, 2001. 5.1, 5.2.2

[32] Finkel, T., "Signal transduction by reactive oxygen species," *The Journal of Cell Biology*, vol. 194, no. 1, pp. 7–15, 2011. 1.3, 3.1

[33] Finkel, T., "From sulfenylation to sulfhydration: what a thiolate needs to tolerate," *Science Signaling*, vol. 5, no. 215, p. pe10, 2012. 3.1

[34] Foley, T. D., Armstrong, J. J., and Kupchak, B. R., "Identification and H_2O_2 sensitivity of the major constitutive MAPK phosphatase from rat brain," *Biochemical and Biophysical Research Communications*, vol. 315, no. 3, pp. 568–574, 2004. 1.4

[35] Foley, T. D. and Kintner, M. E., "Brain PP2A is modified by thiol-disulfide exchange and intermolecular disulfide formation," *Biochemical and Biophysical Research Communications*, vol. 330, no. 4, pp. 1224–1229, 2005. 2.2

[36] Frei, B., "Reactive oxygen species and antioxidant vitamins: mechanisms of action," *The American Journal of Medicine*, vol. 97, no. 3, pp. S5–S13, 1994. 1.2

[37] Gey, K. F., Moser, U., Jordan, P., Stähelin, H., Eichholzer, M., and Lüdin, E., "Increased risk of cardiovascular disease at suboptimal plasma concentrations of essential antioxidants: an epidemiological update with special attention to carotene and vitamin c," *The American Journal of Clinical Nutrition*, vol. 57, no. 5, pp. 787S–797S, 1993. 1.2

[38] Goel, G., Chou, I.-C., and Voit, E. O., "Biological systems modeling and analysis: a biomolecular technique of the twenty-first century," *Journal of Biomolecular Techniques: JBT*, vol. 17, no. 4, p. 252, 2006. 1.2

[39] Gough, D. and Cotter, T., "Hydrogen peroxide: a Jekyll and Hyde signalling molecule," *Cell Death & Disease*, vol. 2, no. 10, p. e213, 2011. 1.2

[40] Griendling, K. K., Minieri, C. A., Ollerenshaw, J. D., and Alexander, R. W., "Angiotensin ii stimulates nadh and nadph oxidase activity in cultured vascular smooth muscle cells," *Circulation Research*, vol. 74, no. 6, pp. 1141–1148, 1994. 1.3

[41] Groen, A., Lemeer, S., van der Wijk, T., Overvoorde, J., Heck, A. J., Ostman, A., Barford, D., Slijper, M., and den Hertog, J., "Differential oxidation of protein-tyrosine phosphatases," *Journal of Biological Chemistry*, vol. 280, no. 11, pp. 10298–10304, 2005. 2.2

[42] Guo, Z., Kozlov, S., Lavin, M. F., Person, M. D., and Paull, T. T., "Atm activation by oxidative stress," *Science*, vol. 330, no. 6003, pp. 517–521, 2010. 1.3

[43] Gupta, V. and Carroll, K., "Sulfenic acid chemistry, detection and cellular lifetime," *Biochimica et Biophysica Acta*, vol. 1840, no. 2, p. 847, 2014. 1, 1.2, 3.1

[44] Gutscher, M., Sobotta, M. C., Wabnitz, G. H., Ballikaya, S., Meyer, A. J., Samstag, Y., and Dick, T. P., "Proximity-based protein thiol oxidation by H_2O_2-scavenging peroxidases," *Journal of Biological Chemistry*, vol. 284, no. 46, pp. 31532–31540, 2009. 6.5.2

[45] Haan, C., Kreis, S., Margue, C., and Behrmann, I., "Jaks and cytokine receptorsâĂŤan intimate relationship," *Biochemical Pharmacology*, vol. 72, no. 11, pp. 1538–1546, 2006. C.3.1

[46] Hansen, J. M., Go, Y.-M., and Jones, D. P., "Nuclear and mitochondrial compartmentation of oxidative stress and redox signaling," *Annual Review of Pharmacology and Toxicology*, vol. 46, pp. 215–234, 2006. 2.3

[47] Hansen, N., Finck, S., Ros, R., Auger, A., and others, "Real-parameter black-box optimization benchmarking 2009: Noiseless functions definitions (Report No. RR-6829)," tech. rep., INRIA, 2009. 4.2, C.1

[48] Hansen, N. and Ostermeier, A., "Completely derandomized self-adaptation in evolution strategies," *Evolutionary Computation*, vol. 9, no. 2, pp. 159–195, 2001. 4.1

[49] Hanson, E., Dickensheets, H., Qu, C., Donnelly, R., and Keegan, A., "Regulation of the dephosphorylation of Stat6. Participation of Tyr-713 in the interleukin-4 receptor alpha, the tyrosine phosphatase SHP-1, and the proteasome," *Journal of Biological Chemistry*, vol. 278, no. 6, pp. 3903–3911, 2003. 3.1, 3.4

[50] Haque, S. J., Harbor, P., Tabrizi, M., Yi, T., and Williams, B. R., "Protein-tyrosine phosphatase Shp-1 is a negative regulator of IL-4-and IL-13-dependent signal transduction," *Journal of Biological Chemistry*, vol. 273, no. 51, pp. 33893–33896, 1998. 3.1

[51] Hartwell, L. H., Hopfield, J. J., Leibler, S., and Murray, A. W., "From molecular to modular cell biology," *Nature*, vol. 402, pp. C47–C52, 1999. 5.1, 5.3

[52] Hatakeyama, M., Kimura, S., Naka, T., Kawasaki, T., Yumoto, N., Ichikawa, M., Kim, J., Saito, K., Saeki, M., Shirouzu, M., and others, "A computational model on the modulation of mitogen-activated protein kinase (MAPK) and Akt pathways in heregulin-induced ErbB signalling," *Biochemical Journal*, vol. 373, pp. 451–463, 2003. 2.5, 6, A.5

[53] Heo, J. and Campbell, S. L., "Ras regulation by reactive oxygen and nitrogen species," *Biochemistry*, vol. 45, no. 7, pp. 2200–2210, 2006. 1.3

[54] Hertog, M. G., Feskens, E. J., Kromhout, D., Hertog, M., Hollman, P., Hertog, M., and Katan, M., "Dietary antioxidant flavonoids and risk of coronary heart disease: the zutphen elderly study," *The Lancet*, vol. 342, no. 8878, pp. 1007–1011, 1993. 1.2

[55] Hooke, R. and Jeeves, T. A., ""direct search" solution of numerical and statistical problems," *Journal of the ACM (JACM)*, vol. 8, no. 2, pp. 212–229, 1961. 4.1

[56] Hornberg, J. J., Bruggeman, F. J., Binder, B., Geest, C. R., De Vaate, A., Lankelma, J., Heinrich, R., and Westerhoff, H. V., "Principles behind the multifarious control of signal transduction," *FEBS Journal*, vol. 272, no. 1, pp. 244–258, 2005. 2.2

[57] Irie-Sasaki, J., Sasaki, T., Matsumoto, W., Opavsky, A., Cheng, M., Welstead, G., Griffiths, E., Krawczyk, C., Richardson, C. D., Aitken, K., and others, "CD45 is a JAK phosphatase and negatively regulates cytokine receptor signalling," *Nature*, vol. 409, no. 6818, pp. 349–354, 2001. 3.1, 3.3.4

[58] Jansen, T., *On the analysis of dynamic restart strategies for evolutionary algorithms*. Springer, 2002. 4.1, 4.4

[59] Johnson, G. L. and Lapadat, R., "Mitogen-activated protein kinase pathways mediated by ERK, JNK, and p38 protein kinases," *Science*, vol. 298, no. 5600, pp. 1911–1912, 2002. 1.2, 1.4

[60] Jomova, K., Vondrakova, D., Lawson, M., and Valko, M., "Metals, oxidative stress and neurodegenerative disorders," *Molecular and Cellular Biochemistry*, vol. 345, no. 1-2, pp. 91–104, 2010. 1.2

[61] Jones, D. P., "Radical-free biology of oxidative stress," *American Journal of Physiology - Cell Physiology*, vol. 295, no. 4, pp. C849–C868, 2008. 3.4

[62] Jones, D. P., "Redox sensing: orthogonal control in cell cycle and apoptosis signalling," *Journal of Internal Medicine*, vol. 268, no. 5, pp. 432–448, 2010. 1, 2.3

[63] Kalyanaraman, B., "Teaching the basics of redox biology to medical and graduate students: oxidants, antioxidants and disease mechanisms," *Redox Biology*, vol. 1, no. 1, pp. 244–257, 2013. 1.2

[64] Karisch, R. and Neel, B. G., "Methods to monitor classical protein-tyrosine phosphatase oxidation," *FEBS Journal*, vol. 280, no. 2, pp. 459–475, 2013. 1.2

[65] Kelly-Welch, A., Hanson, E. M., and Keegan, A. D., "Interleukin-4 (IL-4) pathway," *Science Signaling*, vol. 2005, no. 293, p. cm9, 2005. 1.5, 3.1, 3.3.4

[66] Kelly-Welch, A. E., Hanson, E. M., Boothby, M. R., and Keegan, A. D., "Interleukin-4 and interleukin-13 signaling connections maps," *Science*, vol. 300, no. 5625, pp. 1527–1528, 2003. 1.2

[67] Kemp, M., Go, Y.-M., and Jones, D. P., "Nonequilibrium thermodynamics of thiol/disulfide redox systems: a perspective on redox systems biology," *Free Radical Biology and Medicine*, vol. 44, no. 6, pp. 921–937, 2008. 3.3.4

[68] Kholodenko, B., Yaffe, M. B., and Kolch, W., "Computational approaches for analyzing information flow in biological networks," *Science Signaling*, vol. 5, no. 220, p. re1, 2012. 3.1

[69] Kirkpatrick, S., Gelatt Jr, C., Vecchi, M., and McCoy, A., "Optimization by simulated annealing," *Science*, vol. 220, no. 4598, pp. 671–679, 1983. 4.1

[70] Kitano, H., "Towards a theory of biological robustness," *Molecular Systems Biology*, vol. 3, no. 1, 2007. 5.1

[71] Kris-Etherton, P. M., Lichtenstein, A. H., Howard, B. V., Steinberg, D., Witztum, J. L., and others, "Antioxidant vitamin supplements and cardiovascular disease," *Circulation*, vol. 110, no. 5, pp. 637–641, 2004. 1.2

[72] Kurdi, M. and Booz, G. W., "Evidence that IL-6-type cytokine signaling in cardiomyocytes is inhibited by oxidative stress: Parthenolide targets jak1 activation by generating ros," *Journal of Cellular Physiology*, vol. 212, no. 2, pp. 424–431, 2007. 3.1

[73] Kwon, J., Devadas, S., and Williams, M., "T cell receptor-stimulated generation of hydrogen peroxide inhibits mek-erk activation and lck serine phosphorylation," *Free Radical Biology and Medicine*, vol. 35, no. 4, pp. 406–417, 2003. 1.3

[74] Lam, M. H., Michell, B. J., Fodero-Tavoletti, M. T., Kemp, B. E., Tonks, N. K., and Tiganis, T., "Cellular stress regulates the nucleocytoplasmic distribution of the protein-tyrosine phosphatase TCPTP," *Journal of Biological Chemistry*, vol. 276, no. 40, pp. 37700–37707, 2001. 1.5, 3.1

[75] Lambeth, J. D., "Nox enzymes and the biology of reactive oxygen," *Nature Reviews Immunology*, vol. 4, no. 3, pp. 181–189, 2004. 1.2, 1.3

[76] Lambeth, J. D., Kawahara, T., and Diebold, B., "Regulation of Nox and Duox enzymatic activity and expression," *Free Radical Biology and Medicine*, vol. 43, no. 3, pp. 319–331, 2007. 1.3

[77] LaPorte, S. L., Juo, Z. S., Vaclavikova, J., Colf, L. A., Qi, X., Heller, N. M., Keegan, A. D., and Garcia, K. C., "Molecular and structural basis of cytokine receptor pleiotropy in the interleukin-4/13 system," *Cell*, vol. 132, no. 2, pp. 259–272, 2008. C.3.1

[78] Li, Y., Dwivedi, G., Huang, W., Kemp, M. L., and Yi, Y., "Quantification of degeneracy in biological systems for characterization of functional interactions between modules," *Journal of Theoretical Biology*, vol. 302, pp. 29–38, 2012. 1.1, 1.6, 1, 5.1, 5.2.1, 5.2.2, 5.3, 6.3

[79] Losman, J., Chen, X., Hilton, D., and Rothman, P., "Cutting edge: SOCS-1 is a potent inhibitor of IL-4 signal transduction," *The Journal of Immunology*, vol. 162, no. 7, pp. 3770–3774, 1999. 3.1, 3.3.3, 3.4

[80] Lu, X., Chen, J., Sasmono, R. T., Hsi, E. D., Sarosiek, K. A., Tiganis, T., and Lossos, I. S., "T-cell protein tyrosine phosphatase, distinctively expressed in activated-B-cell-like diffuse large B-cell lymphomas, is the nuclear phosphatase of STAT6," *Molecular and Cellular Biology*, vol. 27, no. 6, pp. 2166–2179, 2007. 3.1, 3.3.4

[81] Lu, X., Malumbres, R., Shields, B., Jiang, X., Sarosiek, K. A., Natkunam, Y., Tiganis, T., and Lossos, I. S., "PTP1B is a negative regulator of interleukin 4–induced STAT6 signaling," *Blood*, vol. 112, no. 10, pp. 4098–4108, 2008. 3.1, 3.3.4, 5.2.2

[82] Lukosz, M., Jakob, S., Büchner, N., Zschauer, T.-C., Altschmied, J., and Haendeler, J., "Nuclear redox signaling," *Antioxidants & Redox Signaling*, vol. 12, no. 6, pp. 713–742, 2010. 3.3.4

[83] Mahadev, K., Zilbering, A., Zhu, L., and Goldstein, B. J., "Insulin-stimulated hydrogen peroxide reversibly inhibits protein-tyrosine phosphatase 1b in vivo and enhances the early insulin action cascade," *Journal of Biological Chemistry*, vol. 276, no. 24, pp. 21938–21942, 2001. 3.1

[84] Mangan, S. and Alon, U., "Structure and function of the feed-forward loop network motif," *Proceedings of the National Academy of Sciences*, vol. 100, no. 21, pp. 11980–11985, 2003. 3.4

[85] Maraldi, T., Prata, C., Caliceti, C., Vieceli Dalla Sega, F., Zambonin, L., Fiorentini, D., and Hakim, G., "VEGF-induced ROS generation from NAD(P)H oxidases protects human leukemic cells from apoptosis," *International Journal of Oncology*, vol. 36, no. 6, pp. 1581–1589, 2010. 1.3

[86] Meier, B., Radeke, H., Selle, S., Younes, M., Sies, H., Resch, K., and Habermehl, G., "Human fibroblasts release reactive oxygen species in response to interleukin-1 or tumour necrosis factor-alpha," *Biochemical Journal*, vol. 263, pp. 539–545, 1989. 1.3

[87] Mendes, P. and Kell, D., "Non-linear optimization of biochemical pathways: applications to metabolic engineering and parameter estimation," *Bioinformatics*, vol. 14, no. 10, pp. 869–883, 1998. 4.1

[88] Meng, T.-C., Buckley, D. A., Galic, S., Tiganis, T., and Tonks, N. K., "Regulation of insulin signaling through reversible oxidation of the protein-tyrosine phosphatases tc45 and ptp1b," *Journal of Biological Chemistry*, vol. 279, no. 36, pp. 37716–37725, 2004. 1.2, 1.3, 3.1

[89] Meng, T.-C., Fukada, T., and Tonks, N. K., "Reversible oxidation and inactivation of protein tyrosine phosphatases in vivo," *Molecular Cell*, vol. 9, no. 2, pp. 387–399, 2002. 1.4

[90] Mittler, R., Vanderauwera, S., Suzuki, N., Miller, G., Tognetti, V. B., Vandepoele, K., Gollery, M., Shulaev, V., and Van Breusegem, F., "Ros signaling: the new wave?," *Trends in Plant Science*, vol. 16, no. 6, pp. 300–309, 2011. 5.3

[91] Moles, C. G., Mendes, P., and Banga, J. R., "Parameter estimation in biochemical pathways: a comparison of global optimization methods," *Genome Research*, vol. 13, no. 11, pp. 2467–2474, 2003. 4.1

[92] Münzel, T., Gori, T., Bruno, R. M., and Taddei, S., "Is oxidative stress a therapeutic target in cardiovascular disease?," *European Heart Journal*, vol. 31, no. 22, pp. 2741–2748, 2010. 1.2

[93] Myers, M. P., Andersen, J. N., Cheng, A., Tremblay, M. L., Horvath, C. M., Parisien, J.-P., Salmeen, A., Barford, D., and Tonks, N. K., "TYK2 and JAK2 are substrates of protein-tyrosine phosphatase 1B," *Journal of Biological Chemistry*, vol. 276, no. 51, pp. 47771–47774, 2001. 5.2.2

[94] Nakano, H., Nakajima, A., Sakon-Komazawa, S., Piao, J., Xue, X., and Okumura, K., "Reactive oxygen species mediate crosstalk between NF-κB and JNK," *Cell Death & Differentiation*, vol. 13, no. 5, pp. 730–737, 2006. 1.6, 5.3

[95] Nam, H.-J., Park, Y.-Y., Yoon, G., Cho, H., and Lee, J.-H., "Co-treatment with hepatocyte growth factor and tgf-β1 enhances migration of hacat cells through nadph oxidase-dependent ros generation," *Experimental & Molecular Medicine*, vol. 42, no. 4, pp. 270–279, 2010. 1.3

[96] Nelder, J. A. and Mead, R., "A simplex method for function minimization," *Computer Journal*, vol. 7, no. 4, pp. 308–313, 1965. 4.1

[97] Nelms, K., Keegan, A. D., Zamorano, J., Ryan, J. J., and Paul, W. E., "The IL-4 receptor: signaling mechanisms and biologic functions," *Annual Review of Immunology*, vol. 17, no. 1, pp. 701–738, 1999. 1, 1.5, 3.1

[98] Oda, K., Matsuoka, Y., Funahashi, A., and Kitano, H., "A comprehensive pathway map of epidermal growth factor receptor signaling," *Molecular Systems Biology*, vol. 1, no. 1, 2005. 1.2

[99] Ohba, M., Shibanuma, M., Kuroki, T., and Nose, K., "Production of hydrogen peroxide by transforming growth factor-beta 1 and its involvement in induction of egr-1 in mouse osteoblastic cells," *The Journal of Cell Biology*, vol. 126, no. 4, pp. 1079–1088, 1994. 1.3

[100] O'Shea, J. J., Gadina, M., and Schreiber, R. D., "Cytokine signaling in 2002: new surprises in the jak/stat pathway," *Cell*, vol. 109, no. 2, pp. S121–S131, 2002. 1.2

[101] Osman, I. H., "Metastrategy simulated annealing and tabu search algorithms for the vehicle routing problem," *Annals of Operations Research*, vol. 41, no. 4, pp. 421–451, 1993. 4.6

[102] Ostermeier, A., Gawelczyk, A., and Hansen, N., "A derandomized approach to self-adaptation of evolution strategies," *Evolutionary Computation*, vol. 2, no. 4, pp. 369–380, 1994. 4.1

[103] Östman, A., Frijhoff, J., Sandin, Å., and Böhmer, F.-D., "Regulation of protein tyrosine phosphatases by reversible oxidation," *Journal of Biochemistry*, vol. 150, no. 4, pp. 345–356, 2011. 1.5, 3.1

[104] Paulsen, C. E., Truong, T. H., Garcia, F. J., Homann, A., Gupta, V., Leonard, S. E., and Carroll, K. S., "Peroxide-dependent sulfenylation of the EGFR catalytic site enhances kinase activity," *Nature Chemical Biology*, vol. 8, no. 1, pp. 57–64, 2012. 1, 1.3, 6.5.1

[105] Persson, C., Kappert, K., Engström, U., Östman, A., and Sjöblom, T., "An antibody-based method for monitoring in vivo oxidation of protein tyrosine phosphatases," *Methods*, vol. 35, no. 1, pp. 37–43, 2005. 2.2

[106] Peters, G. H., Frimurer, T. M., and Olsen, O. H., "Electrostatic evaluation of the signature motif (H/V) CX5R (S/T) in protein-tyrosine phosphatases," *Biochemistry*, vol. 37, no. 16, pp. 5383–5393, 1998. 3.1

[107] Piessevaux, J., Lavens, D., Peelman, F., and Tavernier, J., "The many faces of the SOCS box," *Cytokine & Growth Factor Reviews*, vol. 19, no. 5, pp. 371–381, 2008. 3.1

[108] Poole, L. B., Klomsiri, C., Knaggs, S. A., Furdui, C. M., Nelson, K. J., Thomas, M. J., Fetrow, J. S., Daniel, L. W., and King, S. B., "Fluorescent and affinity-based tools to detect cysteine sulfenic acid formation in proteins," *Bioconjugate Chemistry*, vol. 18, no. 6, pp. 2004–2017, 2007. 2.6

[109] Qi, M. and Elion, E. A., "MAP kinase pathways," *Journal of Cell Science*, vol. 118, no. 16, pp. 3569–3572, 2005. 1.4

[110] Rahaman, S. O., Sharma, P., Harbor, P. C., Aman, M. J., Vogelbaum, M. A., and Haque, S. J., "IL-13rα2, a decoy receptor for IL-13 acts as an inhibitor of IL-4-dependent signal transduction in glioblastoma cells," *Cancer Research*, vol. 62, no. 4, pp. 1103–1109, 2002. 3.1

[111] Ray, P. D., Huang, B.-W., and Tsuji, Y., "Reactive oxygen species (ros) homeostasis and redox regulation in cellular signaling," *Cellular Signalling*, vol. 24, no. 5, pp. 981–990, 2012. 1, 1.2

[112] Reddie, K. G., Seo, Y. H., Muse Iii, W. B., Leonard, S. E., and Carroll, K. S., "A chemical approach for detecting sulfenic acid-modified proteins in living cells," *Molecular BioSystems*, vol. 4, no. 6, pp. 521–531, 2008. 2.6

[113] Reich, N. C. and Liu, L., "Tracking STAT nuclear traffic," *Nature Reviews Immunology*, vol. 6, no. 8, pp. 602–612, 2006. C.3.1

[114] Reuter, S., Gupta, S. C., Chaturvedi, M. M., and Aggarwal, B. B., "Oxidative stress, inflammation, and cancer: how are they linked?," *Free Radical Biology and Medicine*, vol. 49, no. 11, pp. 1603–1616, 2010. 1.2

[115] Rhee, S. G., "H_2O_2, a necessary evil for cell signaling," *Science*, vol. 312, no. 5782, pp. 1882–1883, 2006. 1.2, 3.1

[116] Richmond, T. D., Chohan, M., and Barber, D. L., "Turning cells red: signal transduction mediated by erythropoietin," *Trends in Cell Biology*, vol. 15, no. 3, pp. 146–155, 2005. 5.2.2

[117] Rider, D. A., Sinclair, A. J., and Young, S. P., "Oxidative inactivation of CD45 protein tyrosine phosphatase may contribute to T lymphocyte dysfunction in the elderly," *Mechanisms of Ageing and Development*, vol. 124, no. 2, pp. 191–198, 2003. 3.1

[118] Rizk, A., Batt, G., Fages, F., and Soliman, S., "A general computational method for robustness analysis with applications to synthetic gene networks," *Bioinformatics*, vol. 25, no. 12, pp. i169–i178, 2009. 5.1

[119] Ross, S. H., Lindsay, Y., Safrany, S. T., Lorenzo, O., Villa, F., Toth, R., Clague, M. J., Downes, C. P., and Leslie, N. R., "Differential redox regulation within the PTP superfamily," *Cellular Signalling*, vol. 19, no. 7, pp. 1521–1530, 2007. 2.2

[120] Sacco, F., Gherardini, P. F., Paoluzi, S., Saez-Rodriguez, J., Helmer-Citterich, M., Ragnini-Wilson, A., Castagnoli, L., and Cesareni, G., "Mapping the human phosphatome on growth pathways," *Molecular Systems Biology*, vol. 8, no. 1, 2012. C.3.1

[121] Salmeen, A., Andersen, J. N., Myers, M. P., Meng, T.-C., Hinks, J. A., Tonks, N. K., and Barford, D., "Redox regulation of protein tyrosine phosphatase 1b involves a sulphenyl-amide intermediate," *Nature*, vol. 423, no. 6941, pp. 769–773, 2003. 3.1

[122] San José, G., Bidegain, J., Robador, P. A., Díez, J., Fortuño, A., and Zalba, G., "Insulin-induced NADPH oxidase activation promotes proliferation and matrix metalloproteinase activation in monocytes/macrophages," *Free Radical Biology and Medicine*, vol. 46, no. 8, pp. 1058–1067, 2009. 1.3

[123] Sasagawa, S., Ozaki, Y.-i., Fujita, K., and Kuroda, S., "Prediction and validation of the distinct dynamics of transient and sustained ERK activation," *Nature Cell Biology*, vol. 7, no. 4, pp. 365–373, 2005. 1.2

[124] Schoeberl, B., Eichler-Jonsson, C., Gilles, E. D., and Müller, G., "Computational modeling of the dynamics of the MAP kinase cascade activated by surface and internalized EGF receptors," *Nature Biotechnology*, vol. 20, no. 4, pp. 370–375, 2002. 1.2, 2.2, 2.7, A.1

[125] Schwefel, H., *Evolution and optimum seeking. Sixth-generation computer technology series*. John Wiley & Sons, Inc., 1995. 4.1, 4.3.1, 4.4, C.2

[126] Seo, Y. H. and Carroll, K. S., "Profiling protein thiol oxidation in tumor cells using sulfenic acid-specific antibodies," *Proceedings of the National Academy of Sciences*, vol. 106, no. 38, pp. 16163–16168, 2009. 2.6

[127] Seth, D. and Rudolph, J., "Redox regulation of MAP kinase phosphatase 3," *Biochemistry*, vol. 45, no. 28, pp. 8476–8487, 2006. 1.3

[128] Shankaran, H., Chrisler, W. B., Sontag, R. L., and Weber, T. J., "Inhibition of ERK oscillations by ionizing radiation and reactive oxygen species," *Molecular Carcinogenesis*, vol. 50, no. 6, pp. 424–432, 2011. 2.3

[129] Shankaran, H., Ippolito, D. L., Chrisler, W. B., Resat, H., Bollinger, N., Opresko, L. K., and Wiley, H. S., "Rapid and sustained nuclear–cytoplasmic ERK oscillations induced by epidermal growth factor," *Molecular Systems Biology*, vol. 5, no. 1, 2009. 2.3

[130] Sharma, P., Chakraborty, R., Wang, L., Min, B., Tremblay, M. L., Kawahara, T., Lambeth, J. D., and Haque, S. J., "Redox regulation of interleukin-4 signaling," *Immunity*, vol. 29, no. 4, pp. 551–564, 2008. 1, 1.2, 1.5, 1.6, 3.1, 3.4, 5.2.2, 5.3

[131] Shuai, K. and Liu, B., "Regulation of JAK–STAT signalling in the immune system," *Nature Reviews Immunology*, vol. 3, no. 11, pp. 900–911, 2003. 1.5, 3.1

[132] Singh, D. K., Kumar, D., Siddiqui, Z., Basu, S. K., Kumar, V., and Rao, K. V., "The strength of receptor signaling is centrally controlled through a cooperative loop between Ca^{2+} and an oxidant signal," *Cell*, vol. 121, no. 2, pp. 281–293, 2005. 1.3

[133] Smith, J. K., Patil, C. N., Patlolla, S., Gunter, B. W., Booz, G. W., and Duhé, R. J., "Identification of a redox-sensitive switch within the JAK2 catalytic domain," *Free Radical Biology and Medicine*, vol. 52, no. 6, pp. 1101–1110, 2012. 1.5, 3.1

[134] Sommer, D., Coleman, S., Swanson, S. A., and Stemmer, P. M., "Differential susceptibilities of serine/threonine phosphatases to oxidative and nitrosative stress," *Archives of Biochemistry and Biophysics*, vol. 404, no. 2, pp. 271–278, 2002. 2.2

[135] Stone, J. R. and Yang, S., "Hydrogen peroxide: a signaling messenger," *Antioxidants & Redox Signaling*, vol. 8, no. 3-4, pp. 243–270, 2006. 3.4

[136] Sundaresan, M., Yu, Z., Ferrans, V., Sulciner, D., Gutkind, J., Irani, K., Goldschmidt-Clermont, P., and Finkel, T., "Regulation of reactive-oxygen-species generation in fibroblasts by Rac1," *Biochemical Journal*, vol. 318, pp. 379–382, 1996. 1.3

[137] Sundaresan, M., Yu, Z.-X., Ferrans, V. J., Irani, K., and Finkel, T., "Requirement for generation of H_2O_2 for platelet-derived growth factor signal transduction," *Science*, vol. 270, no. 5234, pp. 296–299, 1995. 1.2, 1.3, 1.4, 3.1

[138] Suzuki, K., Nakajima, H., Kagami, S.-i., Suto, A., Ikeda, K., Hirose, K., Hiwasa, T., Takeda, K., Saito, Y., Akira, S., and others, "Proteolytic processing of stat6 signaling in mast cells as a negative regulatory mechanism," *The Journal of Experimental Medicine*, vol. 196, no. 1, pp. 27–38, 2002. 3.4

[139] Swameye, I., Müller, T., Timmer, J. t., Sandra, O., and Klingmüller, U., "Identification of nucleocytoplasmic cycling as a remote sensor in cellular signaling by databased modeling," *Proceedings of the National Academy of Sciences*, vol. 100, no. 3, pp. 1028–1033, 2003. 3.1, 3.4, 38

[140] Tang, K., Yáo, X., Suganthan, P. N., MacNish, C., Chen, Y.-P., Chen, C.-M., and Yang, Z., "Benchmark functions for the CECâĂŹ2008 special session and competition on large scale global optimization," *Nature Inspired Computation and Applications Laboratory, USTC, China*, 2007. 4.2, C.1

[141] Tanner, J. J., Parsons, Z. D., Cummings, A. H., Zhou, H., and Gates, K. S., "Redox regulation of protein tyrosine phosphatases: structural and chemical aspects," *Antioxidants & Redox Signaling*, vol. 15, no. 1, pp. 77–97, 2011. 1.3, 3.1, 3.4

[142] Templeton, D. J., Aye, M.-S., Rady, J., Xu, F., and Cross, J. V., "Purification of reversibly oxidized proteins (PROP) reveals a redox switch controlling p38 MAP kinase activity," *PloS One*, vol. 5, no. 11, p. e15012, 2010. 2.4

[143] Tonks, N. K., "Redox redux: revisiting PTPs and the control of cell signaling," *Cell*, vol. 121, no. 5, pp. 667–670, 2005. 1.5

[144] Tononi, G., Sporns, O., and Edelman, G. M., "A measure for brain complexity: relating functional segregation and integration in the nervous system," *Proceedings of the National Academy of Sciences*, vol. 91, no. 11, pp. 5033–5037, 1994. 5.1

[145] Tononi, G., Sporns, O., and Edelman, G. M., "Measures of degeneracy and redundancy in biological networks," *Proceedings of the National Academy of Sciences*, vol. 96, no. 6, pp. 3257–3262, 1999. 5.1, 5.3

[146] Turrens, J. F., "Mitochondrial formation of reactive oxygen species," *The Journal of Physiology*, vol. 552, no. 2, pp. 335–344, 2003. 1.2

[147] van Montfort, R. L., Congreve, M., Tisi, D., Carr, R., and Jhoti, H., "Oxidation state of the active-site cysteine in protein tyrosine phosphatase 1B," *Nature*, vol. 423, no. 6941, pp. 773–777, 2003. 3.1

[148] Vivekananthan, D. P., Penn, M. S., Sapp, S. K., Hsu, A., and Topol, E. J., "Use of antioxidant vitamins for the prevention of cardiovascular disease: meta-analysis of randomised trials," *The Lancet*, vol. 361, no. 9374, pp. 2017–2023, 2003. 1.2

[149] Voit, E. O., Marino, S., and Lall, R., "Challenges for the identification of biological systems from in vivo time series data," *In Silico Biology*, vol. 5, no. 2, pp. 83–92, 2005. 1.2

[150] Wang, D., Moriggl, R., Stravopodis, D., Carpino, N., Marine, J.-C., Teglund, S., Feng, J., and Ihle, J. N., "A small amphipathic α-helical region is required for transcriptional activities and proteasome-dependent turnover of the tyrosine-phosphorylated Stat5," *The EMBO Journal*, vol. 19, no. 3, pp. 392–399, 2000. 3.1, 3.4

[151] Watanabe, Y., Suzuki, O., Haruyama, T., and Akaike, T., "Interferon-γ induces reactive oxygen species and endoplasmic reticulum stress at the hepatic apoptosis," *Journal of Cellular Biochemistry*, vol. 89, no. 2, pp. 244–253, 2003. 1.2, 1.3

[152] Weber, T. J., Shankaran, H., Wiley, H. S., Opresko, L. K., Chrisler, W. B., and Quesenberry, R. D., "Basic fibroblast growth factor regulates persistent ERK oscillations in premalignant but not malignant JB6 cells," *Journal of Investigative Dermatology*, vol. 130, no. 5, pp. 1444–1456, 2010. 2.3

[153] Weibrecht, I., Böhmer, S.-A., Dagnell, M., Kappert, K., Östman, A., and Böhmer, F.-D., "Oxidation sensitivity of the catalytic cysteine of the protein-tyrosine phosphatases SHP-1 and SHP-2," *Free Radical Biology and Medicine*, vol. 43, no. 1, pp. 100–110, 2007. 3.1

[154] Wentworth, C. C., Alam, A., Jones, R. M., Nusrat, A., and Neish, A. S., "Enteric commensal bacteria induce extracellular signal-regulated kinase pathway signaling via formyl peptide receptor-dependent redox modulation of dual specific phosphatase 3," *Journal of Biological Chemistry*, vol. 286, no. 44, pp. 38448–38455, 2011. 1.4

[155] Whitacre, J. and Bender, A., "Degeneracy: a design principle for achieving robustness and evolvability," *Journal of Theoretical Biology*, vol. 263, no. 1, pp. 143–153, 2010. 5.3

[156] Whitacre, J. M., "Degeneracy: a link between evolvability, robustness and complexity in biological systems," *Theoretical Biology and Medical Modelling*, vol. 7, no. 1, p. 6, 2010. 5.3

[157] Wills-Karp, M. and Finkelman, F. D., "Untangling the complex web of IL-4-and IL-13-mediated signaling pathways," *Science Signaling*, vol. 1, no. 51, p. pe55, 2008. 3.1

[158] Winterbourn, C. C. and Hampton, M. B., "Thiol chemistry and specificity in redox signaling," *Free Radical Biology and Medicine*, vol. 45, no. 5, pp. 549–561, 2008. 1.3, 6.5.2

[159] Woo, C.-H., Eom, Y.-W., Yoo, M.-H., You, H.-J., Han, H. J., Song, W. K., Yoo, Y. J., Chun, J.-S., and Kim, J.-H., "Tumor necrosis factor-α generates reactive oxygen species via a cytosolic phospholipase a2-linked cascade," *Journal of Biological Chemistry*, vol. 275, no. 41, pp. 32357–32362, 2000. 1.3

[160] Wruck, C. J., Fragoulis, A., Gurzynski, A., Brandenburg, L.-O., Kan, Y. W., Chan, K., Hassenpflug, J., Freitag-Wolf, S., Varoga, D., Lippross, S., and others, "Role of oxidative stress in rheumatoid arthritis: insights from the Nrf2-knockout mice," *Annals of the Rheumatic Diseases*, vol. 70, no. 5, pp. 844–850, 2011. 1.2

[161] Yamada, S., Shiono, S., Joo, A., and Yoshimura, A., "Control mechanism of JAK/STAT signal transduction pathway," *FEBS Letters*, vol. 534, no. 1, pp. 190–196, 2003. 3.2.3, 3.4, C.3.3

[162] Yamada, T., Zhu, D., Saxon, A., and Zhang, K., "CD45 controls interleukin-4-mediated IgE class switch recombination in human B cells through its function as a janus kinase phosphatase," *Journal of Biological Chemistry*, vol. 277, no. 32, pp. 28830–28835, 2002. 3.1

[163] Yao, X., "Evolutionary computation: A gentle introduction," in *Evolutionary optimization* (Sarker, R., Mohammadian, M., and Yao, X., eds.), pp. 27–53, Springer, 2002. 4.1, C.2

[164] Yin, W., *The role and regulatory mechanisms of Nox1 in vascular systems*. PhD thesis, Georgia Institute of Technology, 2012. 1.3

[165] Yin, W. and Vort, E. O., "Function and design of the Nox1 system in vascular smooth muscle cells," *BMC Systems Biology*, vol. 7, no. 1, p. 20, 2013. 1.3

[166] Ying, J., Clavreul, N., Sethuraman, M., Adachi, T., and Cohen, R. A., "Thiol oxidation in signaling and response to stress: detection and quantification of physiological and pathophysiological thiol modifications," *Free Radical Biology and Medicine*, vol. 43, no. 8, pp. 1099–1108, 2007. 1, 1.3

[167] Yu, J., Ustach, C., Kim, H.-R. C., and others, "Platelet-derived growth factor signaling and human cancer," *Journal of Biochemistry and Molecular Biology*, vol. 36, no. 1, pp. 49–59, 2003. 1.4